NASA TECHNICAL MEMORANDUM

NASA TM X-2572

NASA TM X-2572

HYPERSONIC RESEARCH ENGINE PROJECT - TECHNOLOGICAL STATUS 1971 [U]

by

Staff of the Langley Research Center

and

AiResearch Manufacturing Co., The Garrett Corp.

NATIONAL AERONAUTICS AND SPACE ADMINISTRATION • WASHINGTON, D. C. • SEPTEMBER 1972

C 7 2 72384

[redacted]CONFIDENTIAL

1. Report No.	2. Government Accession No.	3. Recipient's Catalog No.
NASA TM X-2572		

4. Title and Subtitle	5. Report Date
HYPERSONIC RESEARCH ENGINE PROJECT TECHNOLOGICAL STATUS 1971 (U)	September 1972
	6. Performing Organization Code
7. Author(s)	8. Performing Organization Report No.
Staff of Langley Research Center and AiResearch Manufacturing Co., The Garrett Corp.	L-8396
	10. Work Unit No.
9. Performing Organization Name and Address	501-24-16-00
NASA Langley Research Center Hampton, Va. 23365	11. Contract or Grant No. NAS 1-6666
	13. Type of Report and Period Covered
12. Sponsoring Agency Name and Address	Technical Memorandum
National Aeronautics and Space Administration Washington, D.C. 20546	14. Sponsoring Agency Code

15. Supplementary Notes

16. Abstract

The National Aeronautics and Space Administration's Hypersonic Research Engine Project (HREP) is reviewed; the review includes the program evolution and accomplishments to date in the development of a hypersonic scramjet research engine designed to operate from Mach 3 to Mach 8, fueled and regeneratively cooled by liquid hydrogen. The four primary parts of this report deal with: (1) a summary of the overall project results to date and contributions to airbreathing propulsion technology to be expected from scheduled aerothermodynamic research tests on hypersonic engines; (2) a summary of project developmental research data in the area of supersonic mixing and combustion; (3) a discussion of the design of flightweight regeneratively cooled hypersonic research engine structures; and (4) a description of and results from Mach 7 tests of a full-scale structural assembly model of HRE in the Langley 8-foot high-temperature structures tunnel.

[redacted]
BY [redacted] CLASSIFIED
SUBJECT TO GENERAL DECLASSIFICATION SCHEDULE OF
EXECUTIVE ORDER 11652. AUTOMATICALLY DOWNGRADED
AT TWO-YEAR INTERVALS AND DECLASSIFIED ON DECEM-
BER 31, 1978.

17. Key Words (Suggested by Author(s))	18. Distribution Statement
Hypersonic research engine Scramjet Ramjet Regeneratively cooled structure	[redacted] – Available to U.S. Government [redacted]

19. Security Classif. (of this report)	20. Security Classif. (of this page)	21. No. of Pages	22. Price
[redacted]	Unclassified	120	

[redacted]
This material contains information affecting the national defense of the United States within the meaning of the espionage laws, Title 18, U.S.C. Secs. 793 and 794, the transmission or revelation of which in any manner to an unauthorized person is prohibited by law.
CONFIDENTIAL

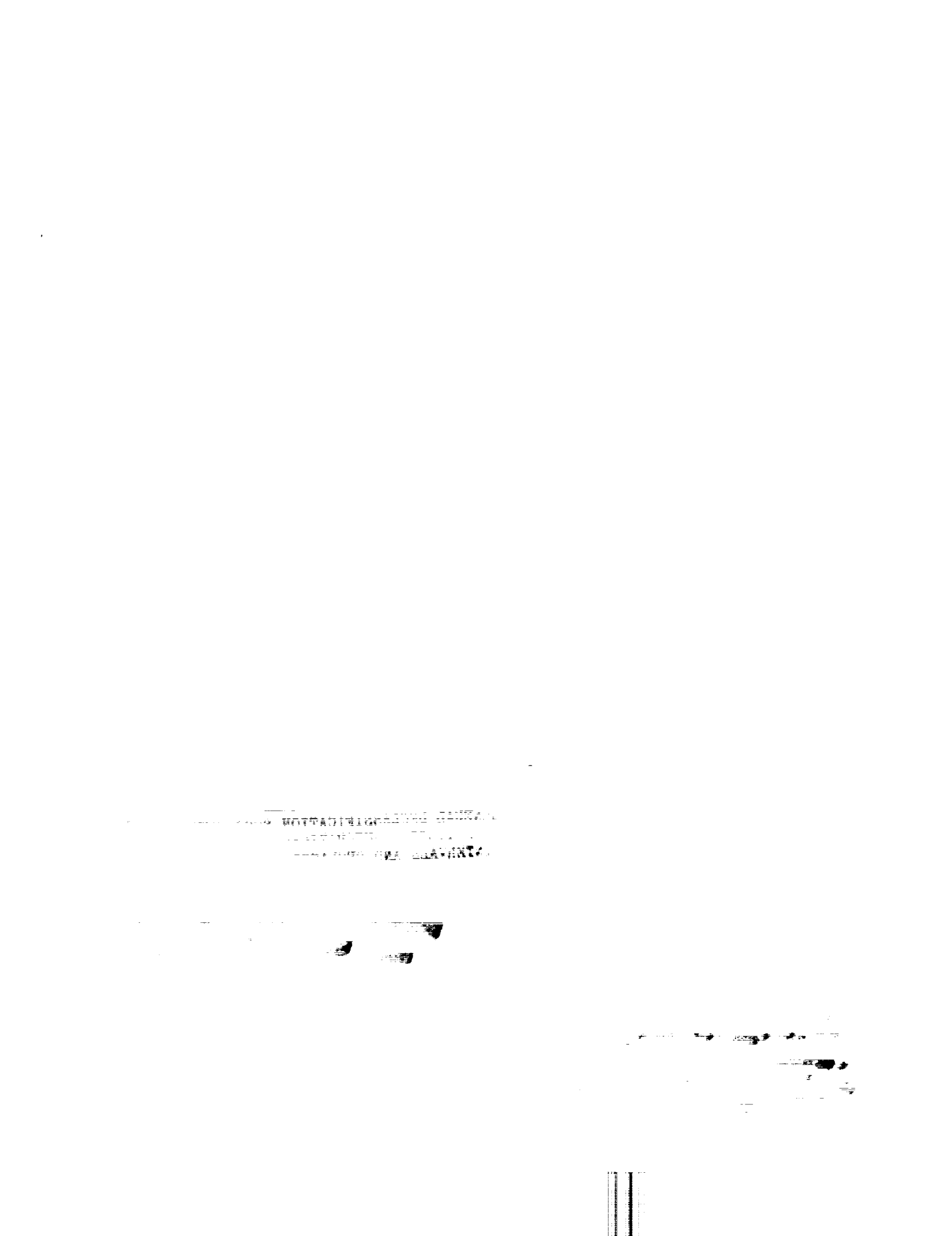

FOREWORD

This report is a compilation of papers which summarizes the technological status of the Hypersonic Research Engine Project (HREP) as of the latter part of 1971. Its four main papers comprise a general overview of the project technology, including disciplines previously well reported and anticipated results from data yet to be obtained, a discussion of the supersonic combustor design development, a review of the design and development of the flight-type regeneratively cooled engine structure, and presentation of results of tests from Langley 8-foot high-temperature structures tunnel tests on a full-scale, hydrogen-cooled flight-type structural model of the HRE. Most of the information in the four main papers of this compilation was presented in June 1971 at the 7th Propulsion Specialists Meeting of the American Institute of Aeronautics and Astronautics in Salt Lake City, Utah. Additional information, in the form of an added paper, on the Hypersonic Research Engine Project background and engine requirements has been placed at the front of this compilation to provide a more orderly and complete picture of the project status.

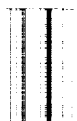

[redacted]

CONTENTS

[redacted]

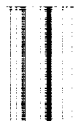

BACKGROUND AND ENGINE REQUIREMENTS

By Ernest A. Mackley
Langley Research Center

BACKGROUND

In order to accelerate the technical progress of hypersonic airbreathing propulsion, the National Aeronautics and Space Administration in 1964 established the Hypersonic Research Engine Project with the project management at Langley Research Center and with participation by Lewis Research Center, Flight Research Center, and Ames Research Center.

This research effort was to provide realistic data on hypersonic airbreathing engine performance, a definition of engine design and research problem areas and their relative importance, a focal point for further research, and an evaluation of the usefulness of existing hypersonic research and development techniques and facilities.

Project concept.- The NASA approach to meet the objectives has been to undertake the design, development, construction, and testing of a hypersonic research ramjet engine for high performance over the speed range from Mach 3 to 8. It should be emphasized that from the beginning the design was specified to be a research ramjet engine for the conduct of meaningful experiments and was in no sense intended to be a small-scale prototype of a propulsion system for any particular mission.

Project plan.- The plan for this project was devised to utilize the best technical capabilities of the United States to the greatest extent compatible with reasonable cost. The original project plan comprises three principal phases. In phase I, in May 1965, from among several proposing contractors three were given 9-month parallel contracts for creating a concept, developing a preliminary design, and planning the follow-on development of the actual hardware. From among the three concepts created (refs. 1 to 7) the one which was most suited to the overall needs of NASA was selected for phase II development. Phase II, as originally planned, was to cover the research and development for the engine concept, fabrication, test, and qualification for flight use on the man-carrying vehicle. Phase III was planned as a flight experimentation program in which the engine, airborne on the X-15-2 research airplane, would be tested in actual flight at Mach 8.

Contract work on phase II began in February 1967. About a year later the X-15 program was phased out; as a result, adjustments to the project plan and scope were

necessitated, which were, however, effected without detriment to achievement of the basic project objectives. The main features of these adjustments are described in the papers that follow.

SYMBOLS

$C_{t,i}$ internal thrust coefficient equal to internal thrust T_i divided by product of free-stream dynamic pressure and reference capture area, 0.1635 meter^2 (1.76 feet^2)

h geometric altitude, meters (feet)

$I_{s,i}$ internal specific impulse equal to internal thrust T_i divided by weight rate of fuel flow, seconds

q dynamic pressure, atmospheres (1 atmosphere = 101.325 kN/m^2)

T_i net sum, in a direction parallel with engine center line and opposed to that of entering airstream, of absolute pressure forces and frictional forces on physical parts of engine as imposed by fluids passing through engine

ENGINE REQUIREMENTS

Detailed, definitive specifications governing the concept and engine development are documented in the statements of work for the phase I and phase II contracts. These documents are not generally available; however, the design constraints which they established are to be found in relevant discussion in the phase I reports (refs. 1 to 7). The requirements to be outlined here will be general in nature.

To keep the project within a reasonable scope, it was necessary to establish areas of primary emphasis. The choice was for a liquid-hydrogen fueled engine that minimized but not necessarily eliminated variable geometry, operating from Mach 3 to 8 with an altitude variation capability within the flight envelope of the X-15-2. The line in figure 1 for a dynamic pressure q of 0.85 atmosphere (1800 psf) represents the design altitude flight profile at which the flights during the phase III flight experiments were planned.

External aerodynamics, structural refinement, and cooling system development were areas of technology which, although of recognized importance, were originally to be subordinated to the primary purpose of the engine, namely, to study the internal performance aspects of the hypersonic ramjet.

Operation and Performance

The research ramjet engine was required to operate with supersonic combustion for free-stream Mach numbers of 6 to 8, but the combustion mode between Mach 3 and 6 was optional as long as the engine performance requirements were met. The specified engine internal thrust coefficient and specific impulse guidelines as functions of flight Mach number are shown in figure 2. The lower line in each figure represents the minimum specified values. Points on the upper line are considered to be realizable only in engines optimized for a particular Mach number; the object sought is a close approach to this line over the speed range from Mach 4 to Mach 8.

Structure

All engine surfaces wetted by the internal stream were required to be regeneratively cooled; efficient use of the hydrogen coolant fuel was required because of space and weight limitations on the X-15-2 airplane. The original engine mass requirements were related to the X-15-2 mass at launch and landings. Only a 362-kilogram increase in X-15-2 mass could be allowed for the complete hypersonic research engine plus instrumentation, fuel, plumbing, and mounting strut (less the original X-15 ventral-fin stub mass). During the phase I design study, it was found that the requirements including that of compatibility with the capabilities of the X-15-2 research airplane necessitated use of lightweight regeneratively cooled structures for all interior parts of the engine. Aft of the cowling leading edge, on the outside where gases or particles from ablation could not enter the engine, ablation cooling was feasible and preferred for the flight-test application. The engine mass predictions were then about 250 to 270 kilograms.

The structural design loads for the research ramjet engine were primarily determined by the X-15-2 flight conditions and the internal heat loads, air pressure, and hydrogen coolant pressures. The material limit stress for the primary structure was limited to two-thirds of ultimate strength, the ultimate strength being defined by the combined stresses required for either buckling or failure (whichever was critical) at the operating temperature. Material limit stress in excess of the yield strength (0.2-percent offset) was permitted in the design of the engine components and primary structure only if the resulting distortions did not degrade engine performance and life below minimum acceptable limits.

The primary structure was defined as that surface and supporting structure needed to withstand the required loads. Thermal protection surfaces which were not required as part of the primary structure did not have these limitations. Such surfaces were to be designed to provide the required life and resistance to flutter. Distortions of these surfaces were not to degrade performance of the engine below the minimum specified limits.

Where it was advantageous, the use of a thermal protection surface to stabilize the primary structure was permitted.

The engine design life requirements were specified as follows: "The research ramjet engine shall be designed to withstand 100 operational cycles at conditions which produce the highest plastic strains. The engine shall be designed to withstand 10 hours of hot operation, of which 3 hours shall be at Mach numbers 7 to 8 on the design Mach number altitude profile of figure 1."

Development

In order to insure that the highest possible engine performance would be attained, aerothermodynamic development programs were specified for the inlet, combustor, and nozzle components. Combining these developed components into a final engine configuration would then accomplish, through experimental tests, the integration of components and the attainable engine performance levels. The engine structural concept and fabrication techniques were developed under a specified program of element, component, subassembly, and assembly development in order to insure that the structure would be built to meet the specified constraints.

Subsystems required for the original concept of X-15-2 experiments also required development. The hydrogen coolant and fuel, the engine control, and the instrumentation subsystems were sufficiently developed to feasibility under the original requirements before the cancellation of the X-15 program.

REFERENCES

1. Staff: Hypersonic Ramjet Experiment Project. Phase I. Conceptual Design Study Report. Vol. I. AP-66-0167-1 (Contract NAS 1-5116), AiResearch Manufacturing Co., The Garrett Corp., 1966. (Available as NASA CR-66221.)

2. Staff: Hypersonic Ramjet Experiment Project. Phase I. Conceptual Design Study Report. Vol. II, Appendix A. AP-66-0167-2 (Contract NAS 1-5116), AiResearch Manufacturing Co., The Garrett Corp., 1966. (Available as NASA CR-66222.)

3. Staff: Hypersonic Ramjet Experiment Project. Phase I. Conceptual Design Study Report. Vol. III, Appendix B. AP-66-0167-3 (Contract No. NAS 1-5116), AiResearch Manufacturing Co., The Garrett Corp., 1966. (Available as NASA CR-66223.)

4. Staff: Hypersonic Ramjet Experiment Project. Phase I. Preliminary Design Report – Vol. I. AP-66-0168-1 (Contract NAS 1-5116), AiResearch Manufacturing Co., The Garrett Corp., 1966. (Available as NASA CR-66224.)

5. Staff: Hypersonic Ramjet Experiment Project. Phase I, Appendix A. Preliminary Design Report – Vol. II. AP-66-0168-2 (Contract NAS 1-5116), AiResearch Manufacturing Co., The Garrett Corp., 1966. (Available as NASA CR-66225.)

6. Staff: Hypersonic Ramjet Experiment Project. Phase I, Appendix B. Preliminary Design Report – Vol. III. AP-66-0168-3 (Contract NAS 1-5116), AiResearch Manufacturing Co., The Garrett Corp., 1966. (Available as NASA CR-66226.)

7. Staff: Hypersonic Ramjet Experiment Project. Phase I, Appendix C. Preliminary Design Drawings. Preliminary Design Report – Vol. IV. AP-66-0168-4 (Contract NAS 1-5116), AiResearch Manufacturing Co., The Garrett Corp., 1966. (Available as NASA CR-66227.)

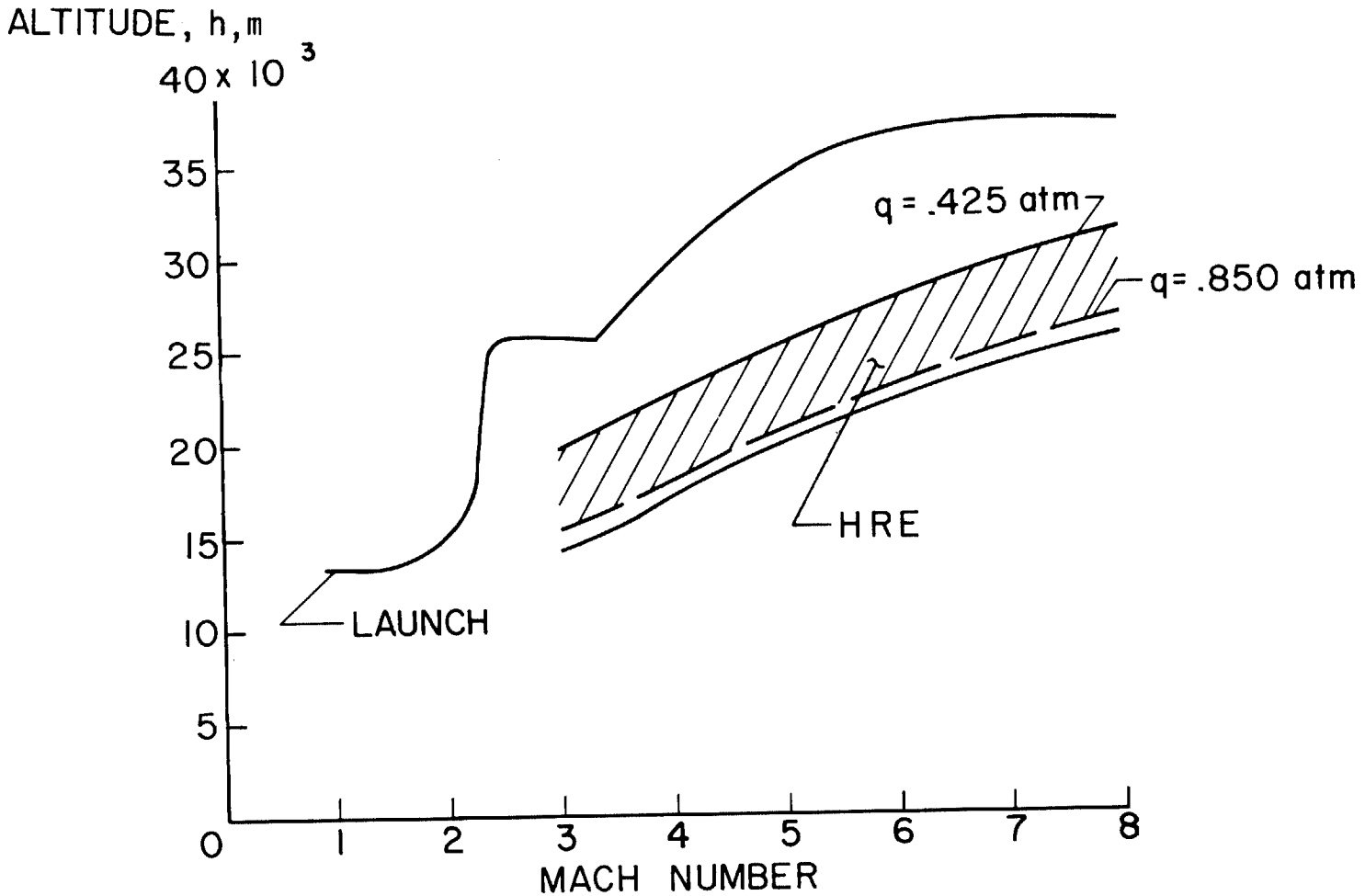

Figure 1.- Mach number and altitude profile envelope of the X-15-2 airplane.

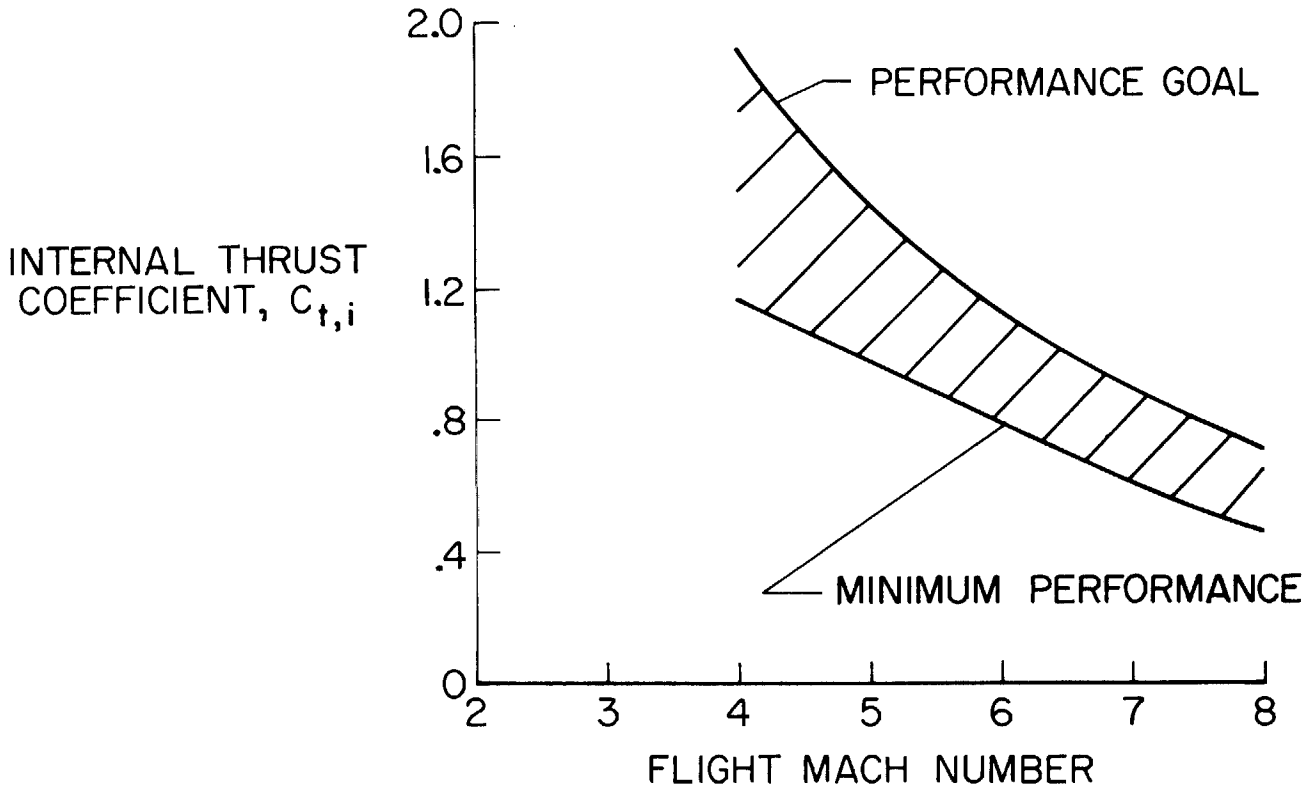

(a) Thrust coefficient.

Figure 2.- Internal performance with engine outside X-15-2 flow field.

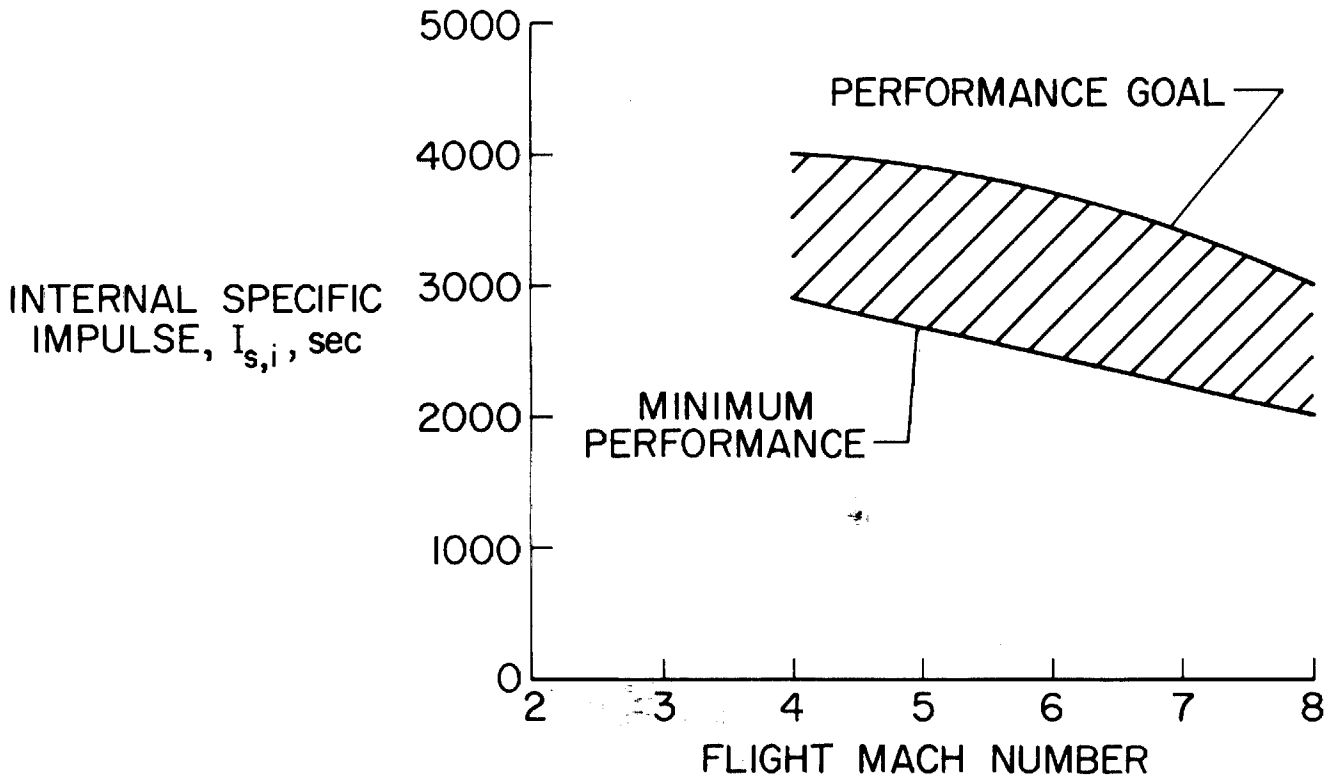

(b) Specific impulse.

Figure 2.- Concluded.

PROGRESS AND STATUS OF THE NASA HYPERSONIC RESEARCH ENGINE PROJECT

Kennedy F. Rubert
Langley Research Center

and

Henry J. Lopez
AiResearch Manufacturing Co., The Garrett Corp.

INTRODUCTION

This paper provides an overview of the NASA Hypersonic Research Engine Project, describes the engine concept which was evolved, summarizes the accomplishments to date, and closes with current status and plans. A modest amount of detail as to the aerothermodynamic integration investigation will be given; adequate coverage of other aspects of the subject is to be found in the referenced papers and other parts of this compilation.

The National Aeronautics and Space Administration undertook the Hypersonic Research Engine Project (HREP) as an in-depth program of hypersonic airbreathing propulsion research to provide essential inputs to future prototype engine development and decision making. An airbreathing liquid-hydrogen-fueled research-oriented scramjet was to be developed to the performance goals shown in the first paper of this compilation and tested in flight from Mach 3 to Mach 8 on the X-15 airplane (fig. 1) as well as in ground-based facilities. The work was many faceted, required aerodynamic design evaluation, structures development, and required development of all flight systems such as the fuel and control system, but the prime objective was investigation of the internal aerothermodynamics of the propulsion system. In view of the severe constraints inherent in the use of the flight vehicle, aerodynamic refinement with respect to external flow about the engine was required only to the extent necessary to insure acceptable execution of the airborne tests. At flight speeds below Mach 6, the combustion mode was to be at the contractor's option; above Mach 6, supersonic combustion was specified.

SYMBOLS

C_S	ratio of measured to ideal nozzle stream thrust
M_∞	free-stream Mach number
M^*	Mach number at the combustor "thermal throat" (exit); equal to unity for subsonic combustion
p_t	total pressure, atmospheres
T_t	total temperature, K
$\dot{w}_A$	air mass flow rate, kg/sec
$\dot{w}_{H_2}$	hydrogen mass flow rate, kg/sec
$\dot{w}_{H_2O}$	water mass flow rate, kg/sec
η_r	total pressure recovery
ϕ	fuel equivalence ratio; ratio of fuel flow to stoichiometric fuel flow

Subscript:

max	maximum

RESEARCH ENGINE CONCEPT

To meet these requirements, an axisymmetric dual-combustion mode design illustrated in figure 2 was selected. The axisymmetric configuration was necessary in order to obtain maximum capture area, within weight limitations imposed by the X-15, with a view to avoiding undesired scale effects. The capture diameter is 0.457 meter (18 in.), the area of the exit nozzle is twice the capture area, and the overall length with the translating spike in the full-forward closed position is 2.13 meters (84 in.). Employment of the external-internal compression inlet having a significant degree of external compression minimized inlet wetted surface and associated cooling load. Translation of the inlet spike provides for advantageous adjustment of the internal area contraction at higher flight speeds and minimization of inlet spillage at lower flight speeds.

Subsonic combustion was preferred for best performance at flight speeds up to Mach 6. In order to accommodate stoichiometric heat release in the supersonic combustion mode at Mach 6 while minimizing total-pressure loss, the combustor exit area must exceed that at the combustor inlet. For minimum loss of total pressure with increasing flight speed, the combustor exit area must diminish. This desirable variation in combustor area ratio is to be obtained in a fixed geometry by staging fuel injection along a continuously diverging combustor in such a manner that total combustion is effected at various distances from the point of initial fuel injection.

PROGRAM EVOLUTION

At its inception the hypersonic research engine project plan provided for aerothermodynamic development, first at the subscale component level, followed by component integration and engine performance at full scale for a concurrent development of structures and subsystems, and then, finally, after marrying the products of these several disciplinary efforts, for airborne experiments which would be the culmination of the program. This program was subsequently restructured to accommodate retirement of the flight test vehicle and deactivation of an intended ground-based facility. These program changes redirected structural evaluation toward Mach 7 true-temperature testing in the Langley 8-foot high-temperature structures tunnel of an assembly of the structural components (the structures assembly model, SAM) as the final act in structural development. The restructured program retained aerothermodynamic development essentially unchanged except for deletion of the final step, that of building and flight testing the unified product of the separate subsystems, structures, and aerothermodynamic development efforts. Flight system development, having already reached a point where feasibility was insured, was discontinued.

SUBSYSTEMS

The hydrogen system, a schematic of which is given in figure 3, consists of a number of circuits supplied by the turbine-driven pump and regulated by special-purpose valves all under command of a digital computer which provides overall control of the system. The pump capacity is 1.37 kilograms (3 lb) of liquid hydrogen per second at a discharge pressure of 74.7 atm (1100 psia). Four high-pressure cryogenic valves distribute the hydrogen among the engine cooling passages and three high-temperature valves of 922 K (1200° F design) redistribute the collected hot jacket effluent to the fuel injectors. In addition, a turbine control valve regulates the flow of hot hydrogen to the pump drive, and a waste (dump) valve permits operating the system when desired at engine fuel-consumption values below coolant requirements. The computer provides all logic and

control signals necessary for (1) operating the translating inlet spike, (2) operating the combustor fuel feed and distribution as required by speed and altitude for programed equivalence ratios, (3) regulating the coolant flows in the several circuits to maintain desired skin temperatures, and (4) performing numerous safety and self-checking functions.

Building the turbopump and valves, breadboarding the computer to the dynamic characteristics of the elements of the system, and making preliminary analog studies demonstrating the feasibility and merit of the flight system completed this work. (See refs. 1 and 2.) Specimens of the flight system hardware are shown in figure 4.

STRUCTURES

In order that the structures development might proceed concurrently with the aerothermodynamic and system developments, the flightweight engine structure was developed (ref. 3) to an aerodynamic configuration from the earlier phase I "Concept Development" contract. This earlier configuration differs from the later and improved configuration in several aerodynamically significant respects, but structurally the differences are trivial and the earlier configuration is entirely satisfactory for evaluating structural aspects of the engine development.

The basic structural element of the shell shown in figure 5 is a brazed plate-fin sandwich of Hastelloy-X through which the hydrogen coolant flows between the relatively thin (0.0381-cm or 0.015-in.) hot skin and the usually thicker (0.0381- to 0.1523-cm or 0.015- to 0.060-in.) primary load-bearing cold skin. Fins range in thickness from 6 to 12 per cm (16 to 28 per in.) and in height from 0.05 to 0.388 cm (0.020 to 0.153 in.) according to the requirements of operating temperature, heat flux, and other geometry.

The SAM configuration is the culmination of the structures research and development effort and reflects the design concepts evolved for the flight engine. The configuration is a plate-fin monocoque structure with local stiffening as required to resist buckling. The stiffening rings (fig. 5) double as fuel-injection manifolds or fuel collector manifolds. (See refs. 3 and 4.) The SAM is hydrogen cooled except for a water-cooled cowling outer surface which is part of the wind-tunnel installation. A hydraulic actuator has been incorporated in the design to provide for positioning of the variable-geometry inlet. Details of the structure will be described by Buchmann and Flieder subsequently.

Inasmuch as the vitiation-heated SAM test facility lacked the oxygen replenishment required for testing with combustion, the SAM was fitted with only the first of the several rows of fuel injectors which would be fitted to an operational engine. This model has now been tested successfully at a nominal Mach 7 true temperature and altitude in the Langley 8-foot high-temperature structures tunnel, as will be described by Kelly and Vuigner

subsequently. To the best of our knowledge, the SAM tests are at the highest temperature and pressure of any engine structural tests to date. In the SAM, as in a complete engine, are reproduced the aerodynamic interferences which cause uneven heating and the thermal expansions which give rise to structural interactions. (See ref. 5.) The SAM investigation has, beyond doubt, demonstrated the capability by appropriate design to cope with nonlinearities and other peculiarities inherent in a total engine structure.

THERMODYNAMIC COMPONENT DEVELOPMENT

Aerodynamic development at the component level was done at reduced scale with a view to arriving at preferred component characteristics, and experimental verification thereof, at minimum time and cost. Through the use of sophisticated computer programs, the aerodynamic performance of inlet and nozzle components as a function of component configuration was calculated and then the actual performance of the configurations selected on the basis of superior predicted performance characteristics was validated by experiment at reduced scale. Figure 6 shows a comparison of the inlet performance, as predicted, with the results measured on a 2/3-scale cryogenically cooled model in tests made at AEDC (refs. 6 and 7) through courtesy of the Air Force. As can be seen, the pressure-recovery requirements were achieved. Figure 7 is a breakdown summary of nozzle performance. Testing (refs. 8 and 9) was with unheated air in order to permit thrust measurement with a high accuracy dynamometer; however, heat transfer was provided through cooling of the nozzle walls in key parts of the test program. The nozzle performance also was up to expectations.

Combustion studies (ref. 10) were made by using a quasi-two-dimensional variable-geometry combustion rig provided with separately heated test stream (vitiated and replenished) and gaseous hydrogen fuel. Subsonic and supersonic combustion modes were investigated in this rig. The subsonic combustion mode results were reported at the AIAA Fifth Joint Propulsion Specialists Conference (ref. 11 and a subsequent paper in this compilation by Y. Sun and W. Sanio). Combustion efficiencies in excess of 95 percent were shown to be quite attainable, and an initial investigation of the complex interrelated problems of staged injection in diverging supersonic combustors was made. This investigation showed a need for further research at full scale and with better simulation, as could be done with the aerothermodynamic integration model.

FULL-SCALE PERFORMANCE ENGINE

The aerothermodynamic integration model (AIM) is the "proof of the pudding" for the aerothermodynamic design of the engine. The important design features of this model are covered in modest detail because they are not covered in subsequent parts of this

compilation. The engine configuration reflects the aerodynamic contours established in the subscale component program. (See refs. 7 to 13.) The engine is constructed from nickel and is water cooled. Heavy duty, nonflight, laboratory models such as the AIM are commonly referred to as "boilerplate" models, a somewhat misleading term. The thick-plate construction at high heat fluxes necessitates a very sophisticated structural design and places unusually severe demands on the fabrication technology. For example, zirconium copper was required to form the tip of the cowl leading edge, where the thermal conductivity and high-temperature strength requirements exceeded the capability of nickel 200. Because of stress and dimensional stability requirements, explosive bonding was used for attaching the copper tip to the nickel. Water cooling was elected as a matter of convenience in testing; temperature gradients through the thick nickel plates will be such that proper simulation of the temperature of the hydrogen-cooled flightweight wall will be obtained at points where this is important, such as at the inlet to the combustor. Heated hydrogen will be used to simulate properly the flight engine combustion and ignition characteristic in the burner. In addition, the effect of nonregenerative cooling on engine performance will be minimized since the separately heated hydrogen fuel partially compensates for the heat removed by the separate coolant. The AIM without the external cowl and leg fairings is shown in figure 8. The sophistication of the design and the extensive instrumentation provided is evident in the figure. The design has provisions for 266 pressure measurements, for 138 temperature measurements, and for 5 gas sampling probes. The complete model, as it will be installed in the Plum Brook Facility at NASA Lewis Research Center, is shown in figure 9. To minimize the corrections on the direct thrust measurement, the external cowl and leg fairings are supported separately from the model.

Highlights of the AIM design are as follows:

Operating envelope:

Mach number	3.0 to 8.0
$p_{t,max}$	68 atm
$T_{t,max}$	2055 K (3700° R)

Heat flux:

Stagnation point	7.37 MW/m^2 (650 Btu/sec-ft^2)
Combustor	3.4 MW/m^2 (300 Btu/sec-ft^2)

Flows:

$(\dot{w}_A)_{max}$	15.4 kg/sec (34 lb/sec)
$(\dot{w}_{H_2})_{max}$ at 810 K	0.68 kg/sec (1.5 lb/sec)
$(\dot{w}_{H_2O})_{max}$	77 kg/sec (170 lb/sec)
Mass	1042 kg (2300 lb)

The engine is designed for operation between Mach 3 and 8 and is to be tested at the Plum Brook Facility at Mach 5, 6, and 7. The Lewis Plum Brook hypersonic test facility is capable of providing nonvitiated, true temperature simulation over this Mach range up to a total pressure of 81.5 atm (1200 psia).

A comprehensive 34-week test program is planned for the AIM. The test program may be divided into four broad categories, namely, (1) component performance evaluation, (2) fuel-injection optimization, (3) inlet-combustor investigation, and (4) overall engine performance.

The HRE-AIM test objectives are as follows:

(1) Inlet-combustor integration effects
(2) Staged fuel injection in diverging combustor
(3) Performance over a Mach number range of 5, 6, and 7
(4) Subsonic combustion mode evaluation
(5) Performance over altitude, angle of attack, and fuel-air ratio ranges
(6) Combustor-nozzle integration effects
(7) Evaluation of engine design techniques
(8) Evaluation of facility and testing techniques
(9) Heat transfer with combustion

Features (2), (3), and (5) are unique to the AIM. Accomplishment of these objectives will result in major contributions to airbreathing propulsion technology. All engine concepts will derive benefit from these data. Sufficient instrumentation has been included in the model to permit determining individual component performance. As will be discussed later by Y. H. Sun and W. C. Sanio, sufficient versatility has been designed into the AIM combustor to permit tuning of the fuel injection system in order to optimize the heat released along the combustor. This versatility will also permit investigation of the inlet-combustor stability. Finally, engine thrust and specific fuel consumption can be determined from direct measurements or backcalculated from the component performance measurements.

STATUS SUMMARY

The current status and plans may be summarized as follows:

(1) The aerodynamic development program is completed. Confidence in the feasibility of developing, between Mach 4 and 8, high levels of thrust and efficiency has continued to increase.

(2) The flight-system development program is completed. Flight system feasibility may be considered to be assured.

(3) The structural development program is completed. The SAM tests have proved the overall successful design of a hydrogen-cooled flightweight engine structure for hypersonic flight to Mach 8, and, more specifically, have demonstrated:

(a) Succesful and stable operation of independently controlled parallel cooling loops

(b) Adequacy of design approach coping with localized stresses induced by nonuniformities of heating associated with the aerodynamic realities of a complete engine

(4) The aerothermodynamic integration model (AIM) is ready and awaits test. Tests this year at the Lewis Plum Brook Facility should:

(a) Illuminate the critical unknowns of aerodynamic integration between scramjet components

(b) Provide interim solutions for the problems of aerodynamic interference pending better solutions from the basic research inspired by the AIM findings

(c) Provide solid performance data on a realistic hypersonic scramjet operating at Mach 5, 6, and 7.

REFERENCES

1. Engineering Staff: Hypersonic Research Engine Project. Phase IIA – Fuel System Development. Terminal Summary Report. AP-68-4611 (Contract NAS 1-6666), AiResearch Manufacturing Co., The Garrett Corp., Dec. 17, 1968. (Available as NASA CR-111902.)

2. Engineering Staff: Hypersonic Research Engine Project. Phase IIA – Control System Development. Terminal Summary Report. AP-68-4540 (Contract NAS 1-6666), AiResearch Manufacturing Co., The Garrett Corp., Apr. 16, 1969. (Available as NASA CR-111903.)

3. Buchmann, O. A.: Hypersonic Research Engine Project. Phase IIA – Structures and Cooling Development. First Interim Technical Data Report. AP-67-2161 (Contract No. NAS 1-6666), AiResearch Manufacturing Co., The Garrett Corp., May 12, 1967. (Available as NASA CR-66997.)

4. Engineering Staff: Hypersonic Research Engine Project. Phase IIA – Structures and Cooling Development. Third Interim Technical Data Report. AP-67-2833 (Contract No. NAS 1-6666), AiResearch Manufacturing Co., The Garrett Corp., Dec. 4, 1967. (Available as NASA CR-66996.)

5. Engineering Staff: Hypersonic Research Engine Project. Phase II – Structures and Cooling Development. Twelfth Interim Technical Data Report. AP-70-6116 (Contract No. NAS 1-6666), AiResearch Manufacturing Co., The Garrett Corp., Mar. 11, 1970. (Available as NASA CR-66983.)

6. Hube, Frederick K.; and Bontrager, Paul J.: Wind Tunnel Tests of a Two-Thirds Scale NASA HRE Inlet at Mach Numbers 4, 5, 6, and 8. AEDC-TR-69-9, U.S. Air Force, Feb. 1969.

7. Pearson, L. W.: Hypersonic Research Engine Project. Phase IIA – Inlet Program. Final Technical Data Report. AP-69-4883 (Contract No. NAS 1-6666), AiResearch Manufacturing Co., The Garrett Corp., Mar. 27, 1969. (Available as NASA CR-66797.)

8. Pearson, L. W.; Gaede, A. E.; Thornberg, G. H.; and Nelson, G. H.: Hypersonic Research Engine Project: Exhaust Nozzle Development Program. Paper presented at AIAA Fifth Propulsion Joint Specialist Conference (Colorado Springs, Colo.), June 1969.

9. Engineering Staff: Hypersonic Research Engine Project. Phase IIA – Nozzle Program. Terminal Summary Report. AP-68-4451 (Contract No. NAS 1-6666), AiResearch Manufacturing Co., The Garrett Corp., Dec. 17, 1968. (Available as NASA CR-101532.)

10. Engineering Staff: Hypersonic Research Engine Project. Phase II – Chemical Kinetics Study for a Supersonic Combustor Model. AP-70-6319 (Contract No. NAS 1-6666), AiResearch Manufacturing Co., The Garrett Corp., May 20, 1970. (Available as NASA CR-66932.)

11. Short, G. R.; Sotter, J. G.; and Sun, Y. H. Hypersonic Research Engine Combustor Development Program. Paper presented at AIAA Fifth Propulsion Joint Specialist Conference (Colorado Springs, Colo.), June 1969.

12. Engineering Staff: Hypersonic Research Engine Project. Phase IIA – Phase II Boilerplate Engine Development. First Interim Technical Data Report. AP-68-3895 (Contract No. NAS 1-6666), AiResearch Manufacturing Co., The Garrett Corp., July 9, 1968. (Available as NASA CR-66988.)

13. Engineering Staff: Hypersonic Research Engine Project. Phase II – Aerothermodynamic Integration Model Development. Eighth Interim Technical Data Report. AP-70-6397 (Contract No. NAS 1-6666), AiResearch Manufacturing Co., The Garrett Corp., Apr. 24, 1970. (Available as NASA CR-66984.)

Figure 1.- X-15 with pylon-mounted HRE.

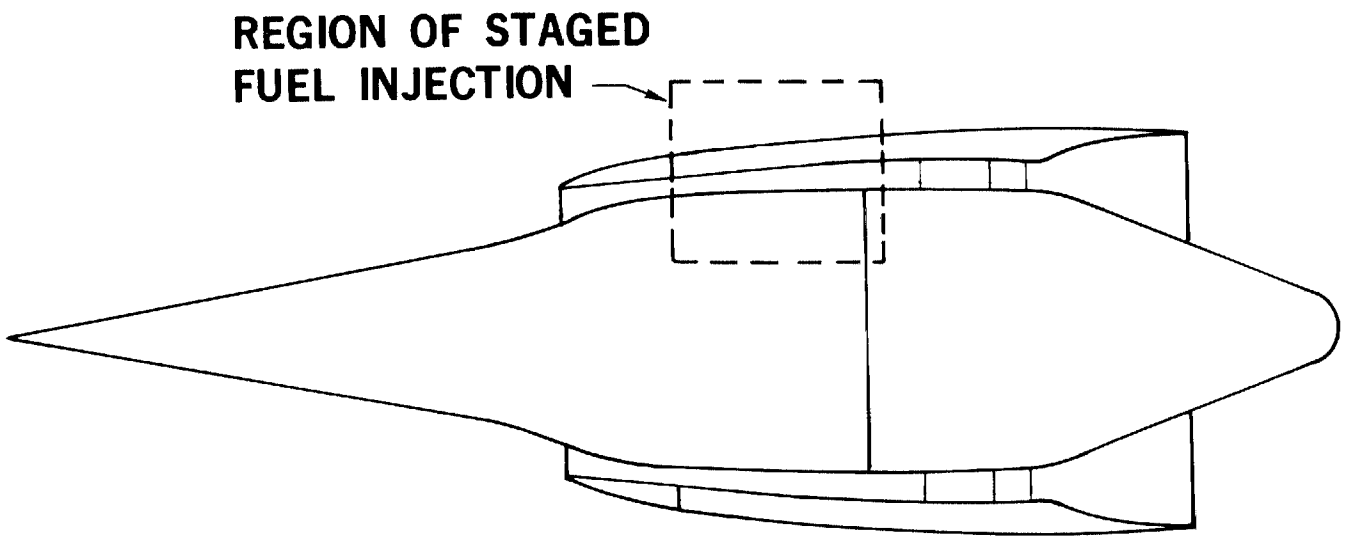

- AXISYMMETRIC
- CONVERTIBLE
- STAGED COMBUSTION
- EXTERNAL-INTERNAL COMPRESSION

Figure 2.- HRE concept.

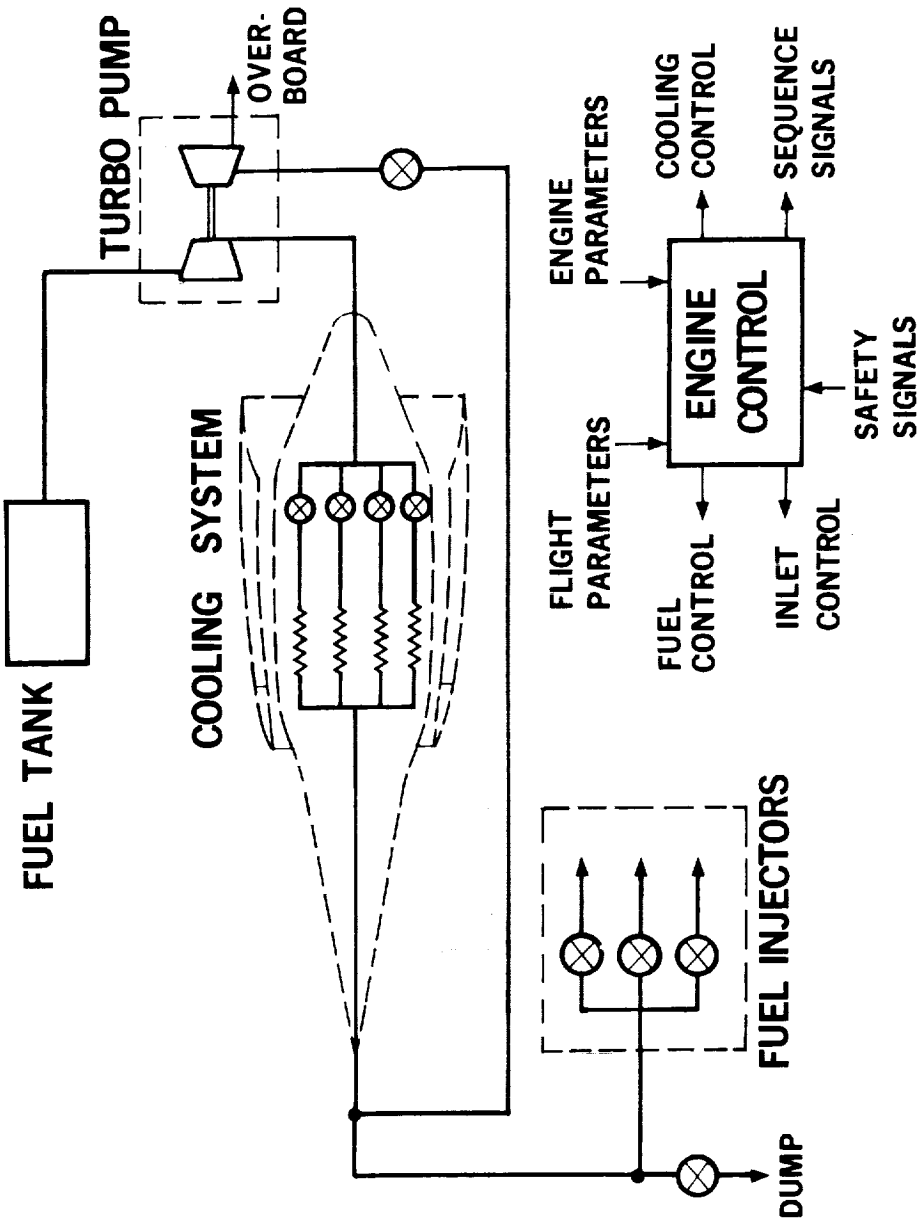

Figure 3.- Fuel and control systems.

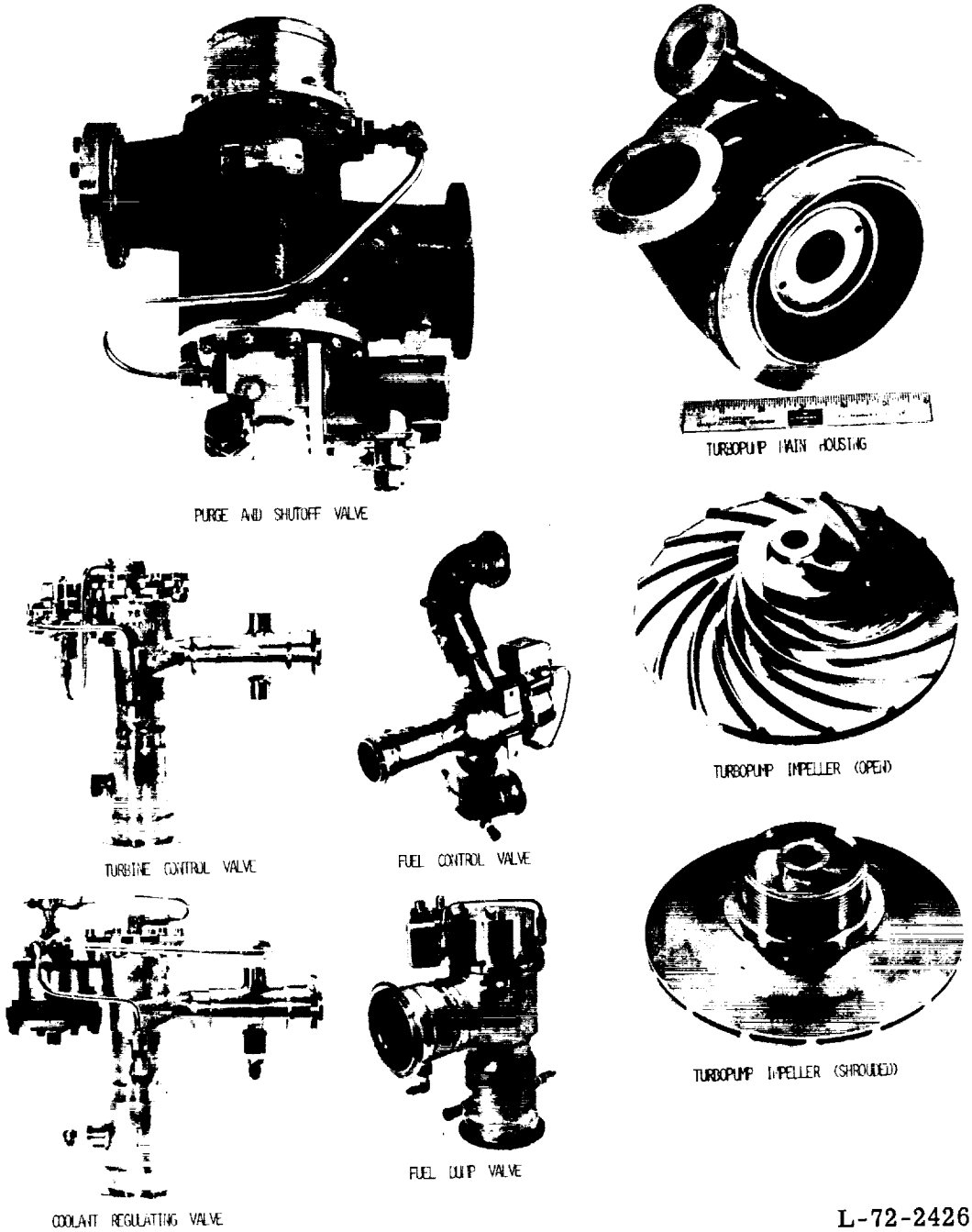

Figure 4.- HRE hydrogen system hardware.

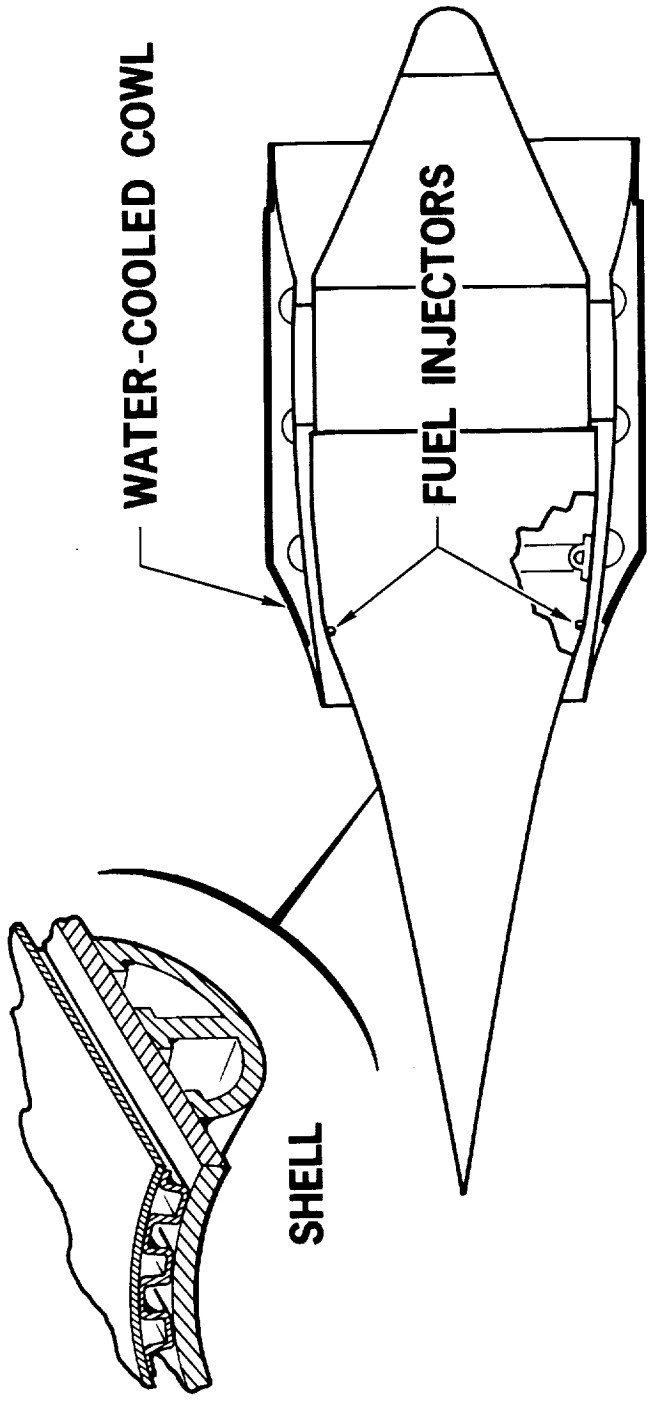

Figure 5.- SAM design features.

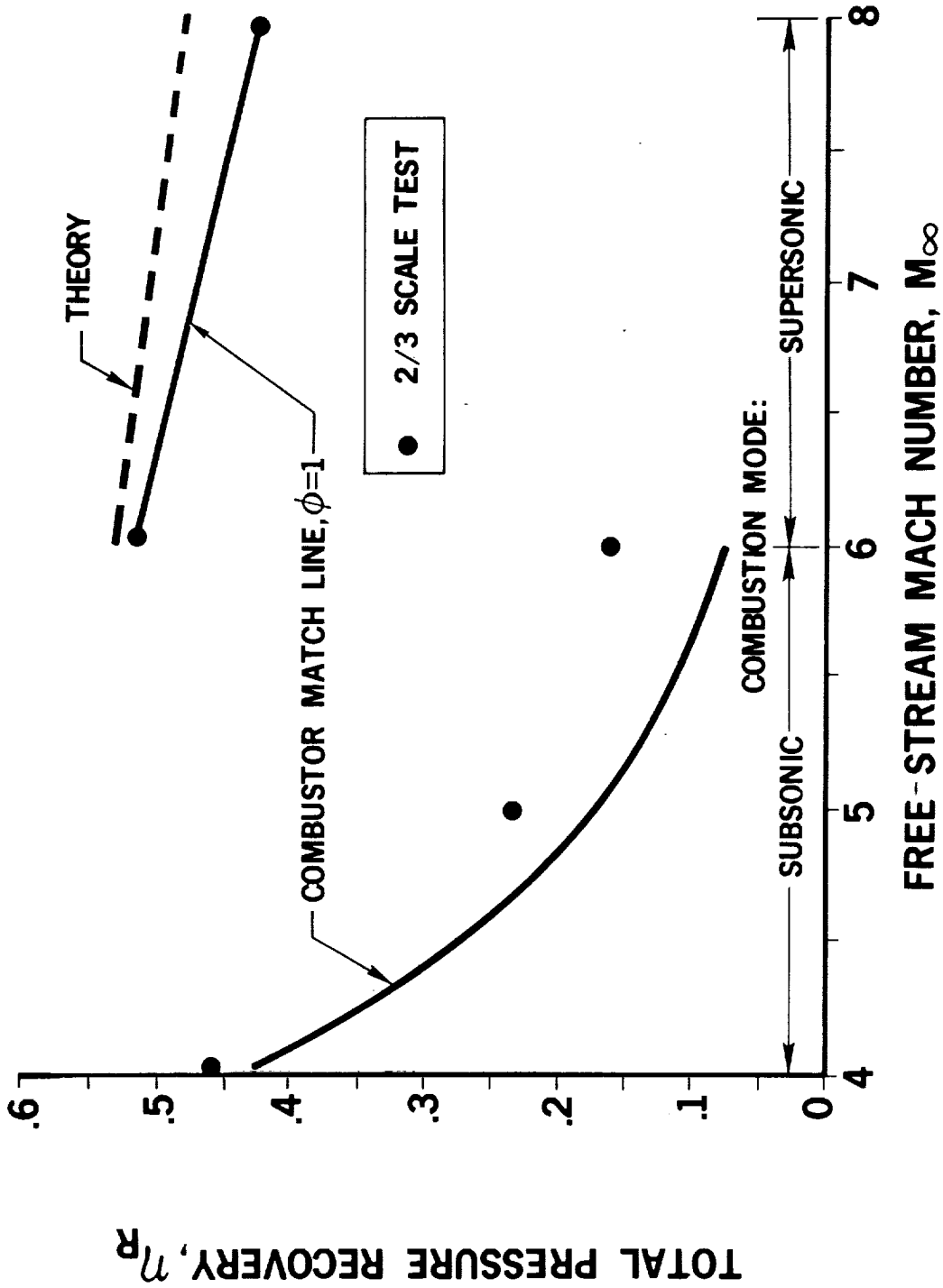

Figure 6.- Inlet performance.

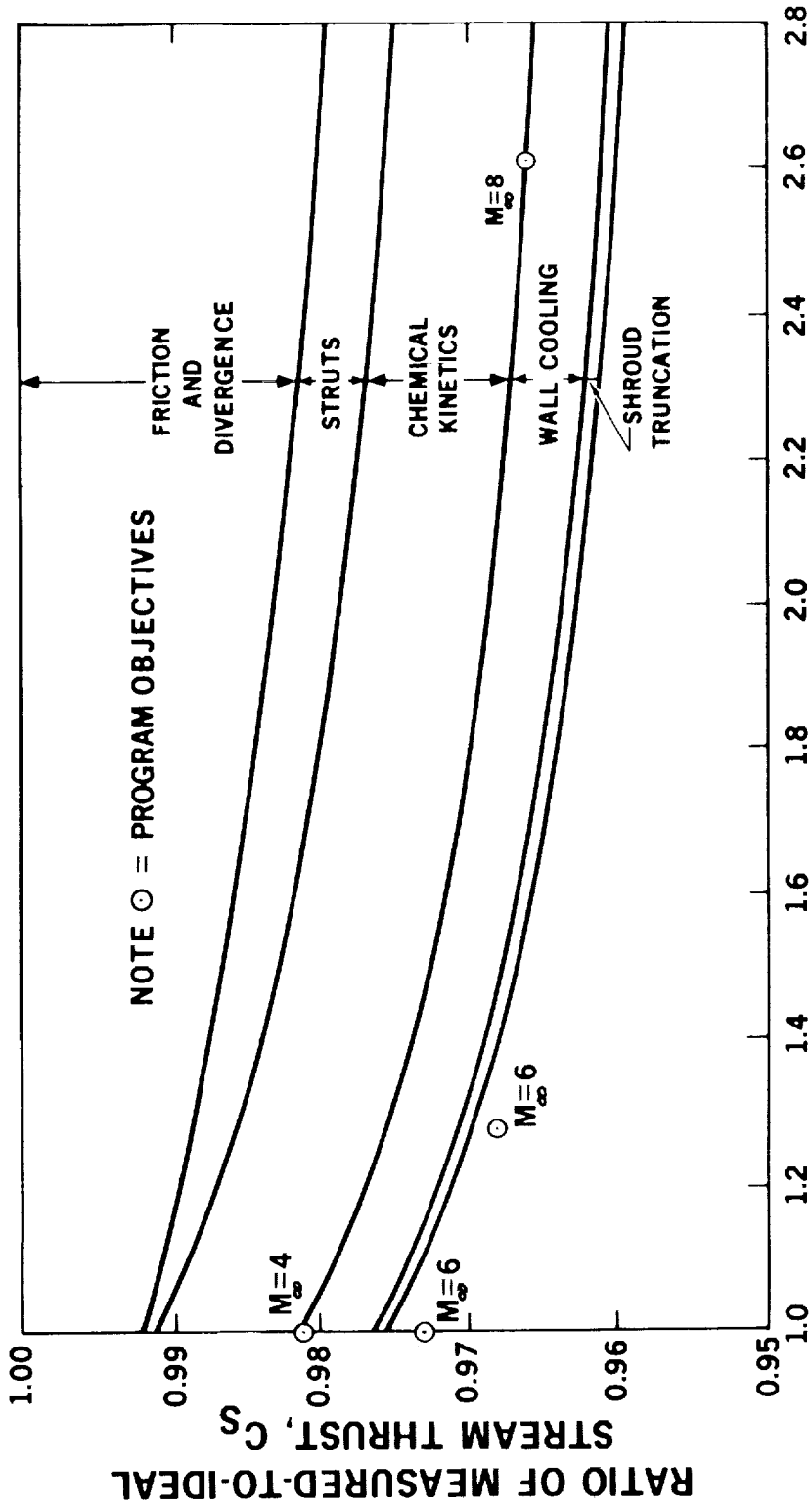

Figure 7.- Nozzle performance.

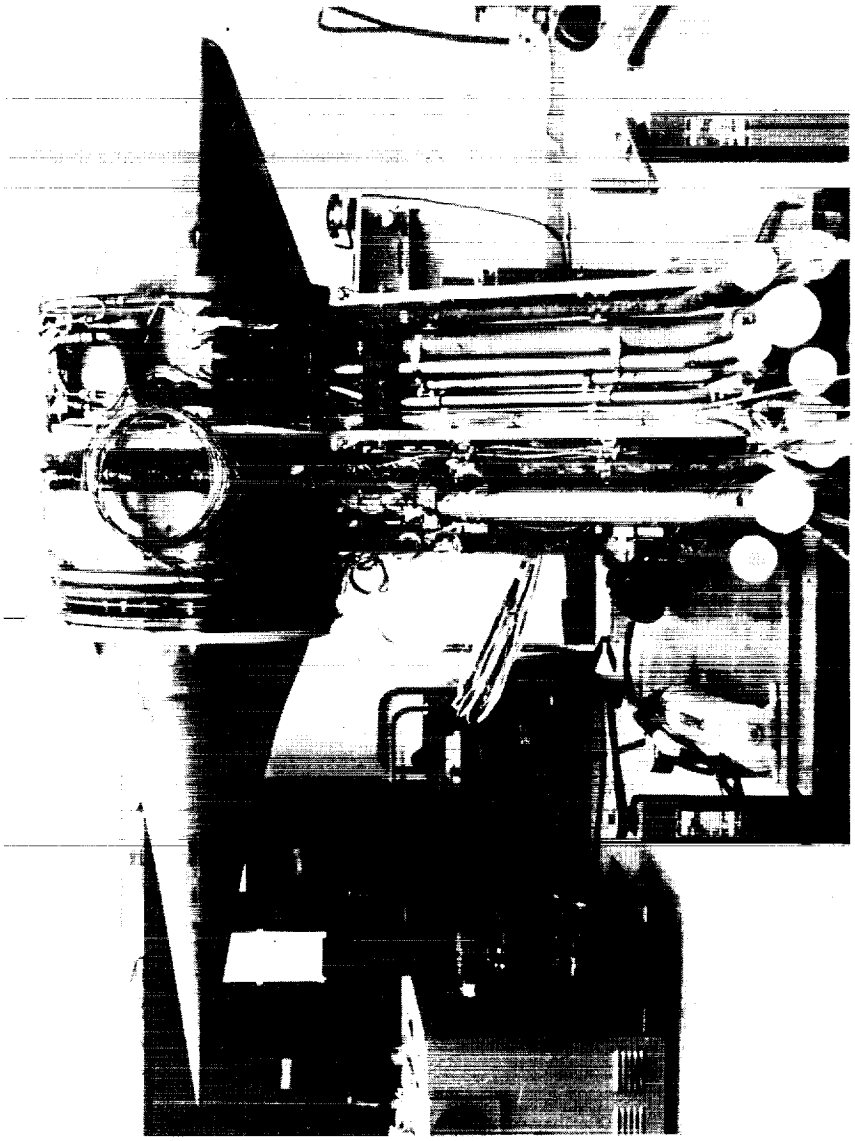

L-72-2427

Figure 8.- HRE/AIM during assembly.

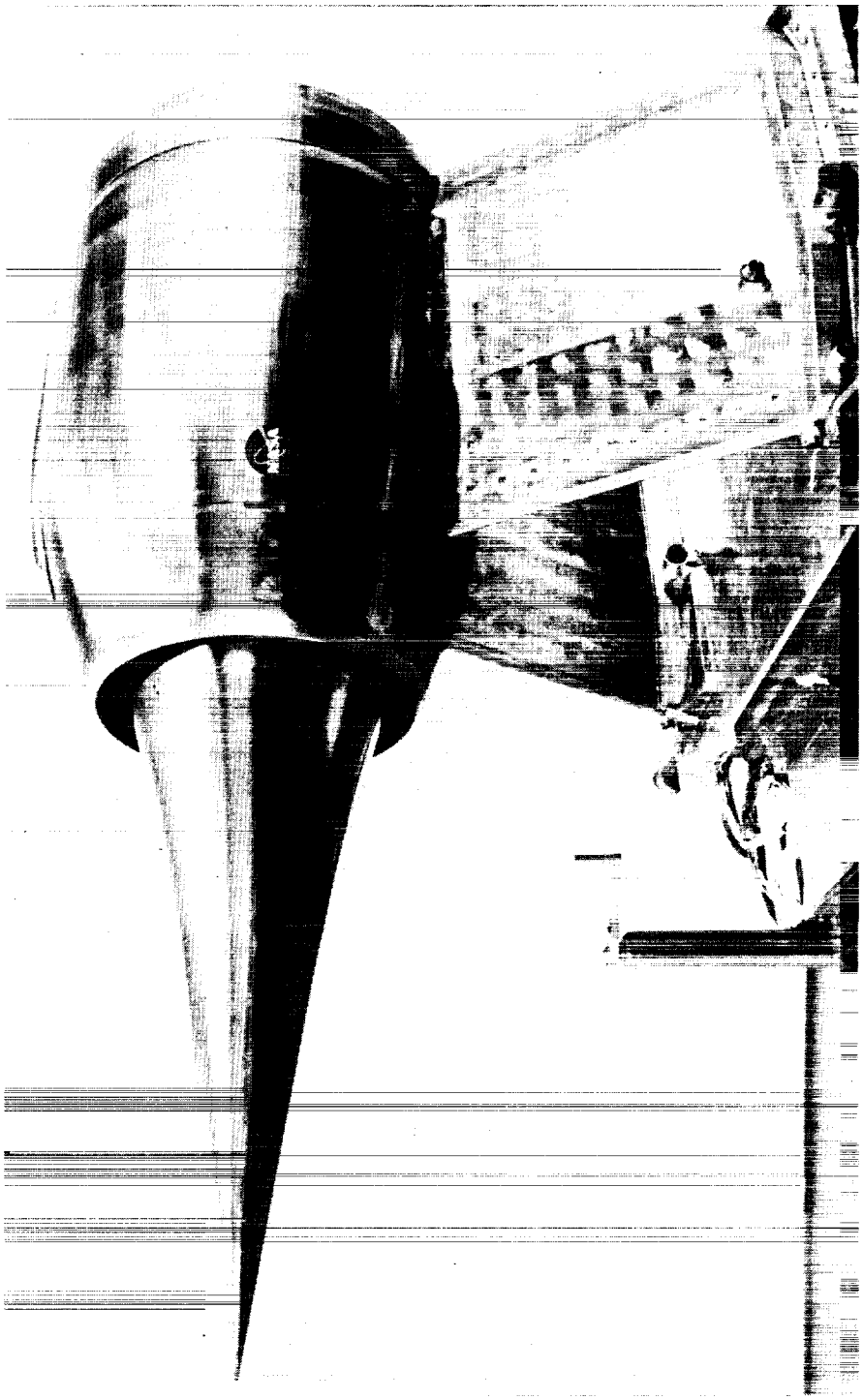

L-72-381

Figure 9.- HRE/AIM final assembly.

EXPERIMENTAL INVESTIGATION OF SUPERSONIC COMBUSTION AND APPLICATION TO COMBUSTOR DESIGN

By Y. H. Sun and W. C. Sanio
AiResearch Manufacturing Co., The Garrett Corp.

INTRODUCTION

Dual-mode combustor development, unlike that of inlets and nozzles, is not yet very amenable to straightforward analytical design supplemented by experimental verification. In developing the combustor for the NASA hypersonic research engine initial investigations, quasi-two-dimensional experiments were conducted prior to laying out the actual engine combustor. Investigations of the subsonic combustion mode and some results in the supersonic combustion mode were reported at the AIAA Fifth Propulsion Joint Specialist Conference. (See ref. 1.) The present paper deals with additional results and the design of the HRE combustor.

Despite the extensive experimental and analytical information available in the literature, much more is needed to optimize supersonic combustor design. Although some excellent basic studies have been carried out, much of the work cannot be applied directly to the problem in hand. The basic problem of developing an efficient combustor for the NASA hypersonic research engine (HRE) is one of applying to the design of a stepless diverging combustor, in which the longitudinal pressure gradient may be favorable or adverse according to the rate of heat release, data which for the most part have been taken under classically simple conditions, such as at constant pressure.

The basic objective of the HRE two-dimensional experimental program was acquisition of an enhanced understanding of the interplay of the various effects in subsonic and in supersonic combustion, and of data on which to base the design of the fuel injectors. The experimental conditions were varied over a range of stream temperatures from 1222 K (2200° R) to 2110 K (3800° R), corresponding to flight speeds from Mach 5 to 7 and hydrogen fuel temperatures up to 832 K (1500° R).

SYMBOLS

A area, cm^2

b lateral distance from injector hole to edge of mixing region (where the hydrogen fuel concentration approaches zero), cm

C_D	discharge coefficient for fuel-injector hole area
D	fuel-injector hole diameter, cm
d_{j_*}	effective fuel-jet diameter; equal to $DC_D^{1/2}$, cm
f, g_1, g_2	functions
h	combustor duct height, cm
M_o	Mach number at entrance to combustor
p	combustor airstream static pressure, atmospheres
p_t	combustor airstream total pressure, atmospheres
$p_{t,j}$	fuel-jet total pressure, atmospheres
s	spacing between injector holes, cm
T	air static temperature, K
T_t	combustor airstream total temperature, K
V	combustor airstream velocity, meters/sec
v_j	velocity of injected fuel at the injector hole (sonic velocity for these data), meters/sec
v_o	velocity of airstream approaching the fuel injector hole, meters/sec
x	axial distance, cm
y	height above injector hole of penetration of edge of mixing region (where the hydrogen fuel concentration approaches zero), cm
Z	penetration parameter, $y/h\phi$
α	combustor wall divergence angle, deg

β angle measured from combustor wall upstream of hole to center line of injector hole; for normal injection $\beta = 90^{o}$

η_c combustor chemical efficiency, percent

ρ_j density of injected fuel at injector hole (sonic flow conditions), kg/m^3

ρ_o density of airstream approaching the fuel injector hole, kg/m^3

τ_{ID} ignition delay time, μsec

ϕ fuel equivalence ratio; ratio of fuel to stoichiometric fuel flow

ϕ_1 fuel equivalence ratio; fuel injected from upstream (first-stage) injectors

ϕ_2 fuel equivalence ratio; fuel injected from downstream (second-stage) injectors

ϕ_t total fuel equivalence ratio, $\phi_1 + \phi_2$

APPARATUS AND TESTS

Test rig.- The test combustor was a variable-geometry two-dimensional duct built in two sections as shown in figure 1. The first section is a constant-area duct 30.48 cm (12 in.) long and 15.24 cm (6 in.) wide. The height could be set at either 1.52 cm (0.6 in.) to approximate the inlet gap height of the HRE or at 5.08 cm (2.0 in.) to provide more room for the insertion of probes. Provision is made for the installation of replaceable fuel injector orifice inserts at three stations, two in the lower wall and one in the upper wall. The second section, 43.18 cm (17 in.) long, is provided with swinging top and bottom panels to permit adjustment of the angle of divergence. One top-wall injector station and one bottom-wall injector station are provided in this divergent section approximately 22.86 cm (9 in.) upstream of the end. Discharge was to the atmosphere.

Instrumentation.- The test combustor was fitted with numerous wall thermocouples and wall static-pressure taps and was mounted on a dynamometer for measuring longitudinal thrust. Fuel and airflows were measured at appropriate orifices. Water flow and temperature rise through sections of the cooling jacket were measured as an aid to studying the distribution of heat release. The fixed instrumentation was supplemented with probes for pressures, temperatures, and gas samples. An online mass spectrometer

was used for analyzing the composition of the samples. Complete descriptions of the apparatus, instrumentation, and tests are given in reference 2.

Scope of tests.- In addition to varying the simulated flight Mach number and the fuel temperature, the ratio of combustor exit area to inlet area was set at values of 2.0 and 3.7 for the "true scale" tests. A wide variety of injector geometry was used. Spacings of the hole diameters were varied. Upstream-angled injection to 45° from normal to the wall was investigated. Experiments were made with two-stage injection as well as with single-stage injection. Equivalence ratio was a prime variable throughout the program, both as to value in the single-stage tests and also as to distribution in the two-stage tests.

COMBUSTOR TESTS

Single-Stage Combustion

Index of mixing effectiveness.- The occurrence of chemical reaction is the best possible proof of effectiveness in mixing; the degree of the required molecular contact of fuel and oxidizer is difficult to measure by other means. Provided that mixture temperatures are high enough and remain high enough to eliminate combustion kinetics as a factor controlling the rate of heat release, the fraction of theoretical heat release, or "chemical efficiency," as deduced from the wall static-pressure development makes a good index of mixing effectiveness and is used in the subsequent discussion of "mixing-controlled" experimental results.

Penetration.- If the stream flow were truly two-dimensional and the combustion mixing-controlled, the penetration of a transverse jet of fuel would be the dominant factor in achieving good combustion efficiency. Combustion efficiency might therefore be expected to correlate well in terms of a parameter indexing fuel/air equivalence ratio and the degree of penetration. Penetration is generally recognized to be functionally related to the momentum flux ratio between the fuel jet and the airstream; further mixing occurs with downstream diffusion. Figure 2 illustrates the formulation of a convenient penetration parameter Z which is used here to examine the effectiveness of mixing as measured by chemical efficiency in a mixing-controlled experiment in relation to penetration as correlated by the parameter Z.

By plotting the maximum observed value of chemical efficiency regardless of streamwise distance x against the penetration parameter Z and coding the symbols for injector geometry, the effects of these variables are exhibited in figure 3. Subject to the limitations of such a representation it appears that

(a) The peak chemical efficiency is a strong function of the penetration parameter and levels off at a value of penetration parameter of about 1.7.

(b) The peak chemical efficiency is a weak function of the hole spacing diameter ratio; s/D values of between 5.5 and 6.0 are associated with good peak combustion efficiencies.

(c) For a given value of penetration parameter, smaller diameter injectors give better peak chemical efficiency.

(d) Further refinement of the mixing parameter to include spreading between jets as well as penetration is needed.

Spreading.- Mixing is, of course, a three-dimensional process, and the correlations obtained by using a simplified two-dimensional approach were inadequate for acceptable evaluations. It becomes necessary, therefore, to sacrifice simplicity for accuracy and to construct a three-dimensional mathematical mixing model. As the jet penetrates into the stream by a distance y it also spreads laterally by a width b as illustrated in figure 4. The area invaded by the fuel is thus measured by both y and b. The minimum area to provide oxygen for complete combustion is the duct height multiplied by the product of hole spacing and equivalence ratio. The ratio of "invaded" area to the theoretically minimum or "target" area can, therefore, define a comprehensive mixing parameter. Since the penetration parameter has been defined as the ratio of penetration to duct height, divided by equivalence ratio, and the spreading parameter has been defined as the ratio of spreading b to spacing s, the area-ratio mixing parameter becomes the algebraic product of the penetration parameter and the spreading parameter.

Just as the penetration parameter was formulated in terms of the generally accepted parameters influencing penetration, so also can the spreading parameter b/s be represented as a function of the parameter which should affect the spreading. To this end, it is postulated that the spreading parameter b/s is a function of the pressure ratio of the jet, the diameter of the injector hole D, and the downstream distance x. It is further assumed that the width b is a linear function of the distance x as appears in a turbulent jet.

Three-dimensional correlation.- The chemical efficiency from a series of tests at a common inlet air temperature is shown in figure 5, with penetration parameter as the abscissa and the data plotted in groups identified by values of the spreading parameter. The correlation of these data from tests using injectors differing in diameter, spacing, and angle of injection is better than might have been anticipated. In this figure the chemical efficiency increases almost linearly with the value of the penetration parameter up to about 85 to 90 percent efficiency, after which the curves level off very rapidly. At a high value of penetration parameter the value of the spreading parameter required for a given efficiency is lower than the value required with lesser values of the penetration parameter, as is consistent with the concept of mixing area.

Figure 5 also suggests that it is easier to achieve high chemical efficiency at high values of the penetration parameter. For example, if one wished to improve the chemical efficiency from 60 to 80 percent at a penetration parameter value of 1.73, it is only necessary to increase the spreading parameter value from 6 to 8. If, however, the penetration has a value of 1.5, the spreading parameter value of 12 must be increased to one of 18.

Not shown on the curve is the effect of lowering the inlet temperature, which shifts the curves toward the right-hand side of the figure; thus, the appearance of effects deriving from the chemical kinetics of the combustion is indicated.

Two-Stage Combustion

Two-stage combustion is used in the HRE concept as a means to effect stoichiometric combustion without choking the combustor in consequence of insufficient cross-sectional area at the point of initial injection; as much fuel as possible is injected and burned at the point of minimum area and the balance of the fuel is injected with the intention of completing the heat addition in a region of greater area. Consequently, second-stage injection is combined with duct divergence, and the problems of the former are intimately associated with the problems of the latter. Before describing and discussing the experiments with two-stage combustion, it may be helpful to review briefly some of the relevant concepts and attributes of mixing and combustion kinetics.

Mixing.- The basic process of mixing in a supersonic combustor may be interpreted in three distinct but frequently concurrent phases: (1) jet penetration in which the primary introduction of the fuel into the airstream is accomplished through the medium of the jet momentum; (2) turbulent mixing, in which the turbulence existing in the airstream or generated by the fuel injection breaks up the fuel stream into many small lumps; and (3) molecular diffusion which disperses the fuel molecules from these small lumps into the intermingled airstream to make contact with oxygen molecules or the dissociation products thereof.

Molecular diffusion is the slowest of these processes. Therefore, in order to hasten the mixing, strong turbulence of a suitable scale is desired in order to reduce the size of the small lumps and to shorten the distance which must be covered by molecular diffusion. Macroscopic stream conditions can have a profound influence on the state of turbulence in the airstream, since adverse pressure gradients produced by separation and heat addition in the supersonic stream favor a buildup of turbulence and favorable pressure gradients in consequence of duct divergence and heat loss act to suppress turbulence. Thus, the very conditions resulting from successful supersonic combustion are favorable to mixing and those attending failure to burn in a diverging supersonic stream are detrimental to mixing.

Combustion kinetics.- Flame propagation by the transmittal of heat from a burning gas to as yet unburned gas, or deflagration, is too slow to permit supersonic combustors of acceptable length, and autoignition is a necessary operating mode. Autoignition can be treated as two successive phases. The first, or delay period, in which dissociation of the molecules and the formation of chain-carrying radicals proceed at a rate which depends upon the temperature and pressure. Heat release during the delay period is insignificant. When a sufficient concentration of chain carriers is achieved, heat release becomes significant and the associated rise in temperature greatly accelerates the process and establishes what is commonly called the "reaction" period.

Where the initial temperature of the combustible mixture is only slightly above that required for autoignition, as is the case for scramjets optimized on the basis of the many other factors which determine the performance, the delay time is the dominant factor in determining combustion kinetic behavior. Once the delay period is followed by the main reaction with its rapid evolution of heat, the consequent rise in temperature tends to overcome lesser factors operating to the detriment of the combustion process.

The length of the initial delay period as affected by the initial values of temperature and pressure is illustrated in figure 6 for flow in a constant-area duct in which, because of the absence of significant heat release, the process is essentially one of constant pressure, temperature, and density. At the higher temperature and lower pressure, the delay period shortens very systematically with increase in either pressure or temperature. At marginal autoignition temperatures, however, excessive pressure rise lengthens the delay period. Kinetic calculations omitting the HO_2 species do not show this effect, which is consequent upon the chain-breaking property of the HO_2. At a "through-flow" velocity of 1000 meters/second, which is quite representative of scramjet combustor velocity, an ignition delay of 100 microseconds corresponds to a distance in the combustor of 10 centimeters; this result points up the critical importance of initial temperature in the design of the combustor.

With a diverging combustor, the expansion induced in the supersonic flow progressively reduces the temperature during the progress of the delay period; and if the expansion is too rapid, the combustion is aborted before reaching the point of significant heat release. The temperature history starting from 1222 K (2200° R) at atmospheric pressure computed for several rates of duct expansion (fig. 7) clearly shows this divergence effect on supersonic combustion.

Experimental results.- A number of tests were made to investigate two-stage combustion at inlet total temperatures corresponding to Mach 5 and 6 flight conditions. Analytical results recently obtained indicate a reversal in trend or shortening of the delay period at even higher pressures. (See ref. 3.) Injector holes at stations 1b and 1c constituted the first stage of injection. The holes at station 1c are interdigitated relative to

those at station 1b. The holes were 0.25 cm (0.1 in.) in diameter and were spaced 1.53 cm (0.6 in.) apart. The same scheme followed at stations 2e and 2f, but using 0.407-cm-diameter (0.16-in.) holes spaced 4.57 cm (1.8 in.) apart, constituted the second stage. The first-stage equivalence ratio was varied between 0.2 and 0.3; that of the second stage, between 0.4 and 1.4.

A longitudinal pressure distribution typical of the results of these tests is shown in figure 8. Pressure rise induced by second-stage injection is significantly lower than that induced by the first-stage injection and unlike the first stage, the pressure-rise effect is limited to the region downstream of the injector except at very high values of equivalence ratio.

The calculated chemical efficiency with two-stage injection was substantially less than that desired and a number of tests were made to improve the second-stage combustion efficiency. Variation of the second-stage hole size and spacing, relocation further upstream, and the use of supersonic injection nozzles were all of little or no benefit. Tests at a considerable elevation of inlet temperature which would have shortened ignition delay were of no advantage, but they showed that the inadequacy of second-stage mixing was the dominant problem. Increasing the oxygen content of the stream by 50 percent likewise had no significant effect on the pressure rise.

Results of these tests are summarized in figure 9 which shows bands of efficiencies for the overall and second-stage combustors with the various injectors used. Because of the low efficiency of the 22.9-cm-long (9-in.) second-stage combustor, the overall efficiency never exceeded 66 percent. It is not certain whether the low chemical efficiency should be attributed to insufficient residence time or poor mixing, or both. Even with the higher inlet total temperature and the oxygen-rich stream, which should have rendered the oxygen more accessible to the hydrogen and shortened the reaction time, no benefit accrued. Flame at the combustor exit was observed during all second-stage combustor experiments, contrary to the observations of first-stage combustion, where no flame was observed during complete combustion.

Analysis of an experiment.- An analysis (ref. 4) was made for comparison with the second-stage performance by using a finite-rate chemistry combustion computer program. The basis of the analysis was a comparison of the longitudinal development of geometry combustor cross-sectional area, shown by the solid line of figure 10, with the development of a theoretical area which would be required to exhibit the wall static pressure as actually observed, with the heat release calculated from kinetic combustion chemistry. Inherent in making this calculation is postulation of a mixing rate, by means of which the rate at which the fuel enters the calculation is determined. If then, in fact, a correct postulate as to mixing rate is made, the theoretical area development should match the geometric development. If too rapid mixing is postulated, the theoretical area requirement will

exceed that of the geometric; if too slow a mixing is postulated, the theoretical points will lie below the geometric.

With the assumption of complete mixing in the first stage, the calculated area points show a plausible blockage of the constant-area part of the duct, indicative of a separation bubble caused by the injection, followed by reattachment of the flow near the entrance to the divergent part of the first-stage combustor. The first-stage results demonstrated efficiencies of 95 percent at station 33 and nearly 100 percent beyond.

On the assumption of 100-percent mixing at the second stage, the calculated areas suggest a plausible 15-percent blockage at the second-stage injector station but the flow requires areas in excess of the geometric further downstream; since this condition is impossible, the assumption of 100-percent mixing at the injector is untenable. On the assumption of 60-percent mixing of the second-stage fuel, a good match at the exit is obtained with departure at the upstream stations.

This method of analysis appears to have considerable possibilities for analyzing the experimental results; however, time did not permit futher exploration of postulated mixing assumptions. The combustion efficiencies were generally high in the two cases calculated and suggested strongly that in this test the deficiency in performance stemmed from inadequacies of mixing rather than from tardy reaction.

AEROTHERMODYNAMIC INTEGRATION MODEL (AIM)

COMBUSTOR DESIGN

On the basis of the experimental results previously discussed, the HRE combustor was designed to provide not only efficient combustion but also flexibility in the aerothermodynamic evaluation of a research engine. The selected combustor configuration is explained with reference to figure 11. From the inlet throat at the front to the thermal throat at the rear, the combustor comprises three combustion sections. The first 17.8 cm (7 in.) are at an area increase approximately equivalent to a 1.5° included angle, two-dimensional passage. This section, with its slow rate of area increase which avoids the detrimental effects of rapid expansion, is the primary zone for supersonic combustion and the only one at maximum flight speed. It serves as the initial section of a subsonic diffuser for operation at low flight speed in the subsonic combustion mode. After the first section, the rate of area increase is increased to that of a 6.8° included angle two-dimensional passage. In this section at less than maximum flight speeds, high rates of heat release can be accommodated with thermal choking of the upstream sections. The rearward part of the combustor just ahead of the thermal throat is the subsonic combustion zone used at lowest flight speeds. The step at the start of this zone created by the

inlet spike telescoping over the inner body serves as the subsonic combustion flame holder in the annular HRE combustor. This final design evolved through modification of early designs in the light of the results of the two-dimensional experiments.

Initial design.- As originally designed, three sets of fuel injectors were provided, each set connected to its own fuel manifold and fuel control valve. The first set of injectors (1a and 1b) is placed almost at the inlet throat. At Mach 6 the inner row is 1.9 cm (0.75 in.) upstream of the outer row; forward translation of the spike with rising Mach number increases this distance 7.62 cm (3 in.) at Mach 8. This set of injectors is used whenever operating in the supersonic combustion mode, but at Mach 6 is limited to an equivalence ratio of 0.2 or less to avoid choking. At Mach 8 the full equivalence ratio of unity is to be handled by these injectors.

The second two rows of injectors (2a and 2b) spaced about 6.35 cm (2.5 in.) apart are both placed on the outer surface because of the interference between translating spike and innerbody. These injectors are primarily intended for second-stage injection in the supersonic combustion mode when operating at less than the full Mach 8 flight speed.

The third set of injectors is used primarily for subsonic combustion, but can also provide for fuel-rich operation with supersonic combustion. The injectors on the outer shell are located approximately 5.08 cm (2 in.) upstream of the spike skirt in its fully retracted Mach 6 flight position, and the holes on the inner shell are located just downstream of the step. At Mach 4 the terminal shock is to be located in the diverging passage upstream of both inner and outer injectors. At Mach 6 the shock is to be established between the inner and outer rows of injectors.

Modification.- Inert-gas-injection tests which were part of the 2/3-scale inlet component development (ref. 5) confirmed the view that substantial injection could be accomplished without unstarting the inlet; nevertheless, they promoted a degree of caution with respect to excessive boundary-layer separation resulting from the fuel injection. To permit investigating this effect in the integration experiments, the aerothermodynamic integration model (AIM) was fitted with another row of injectors (1c) on the centerbody about 10 cm (4 in.) downstream of injector (1a) by means of which the fuel may be introduced in a region of slightly greater area somewhat farther from the inlet throat.

The tardy mixing and consequent poor chemical efficiencies of second-stage injection revealed by the two-dimensional investigation prompted shifting second-stage injection farther upstream. The initial injector (2b) in the outer shell was replaced with injector (4) about 9 cm (3.5 in.) downstream of injector (1b) and another injector (2c) was added to the inner shell about 5 cm (2 in.) downstream of injector (1c). This array of injectors equips the AIM for maximum flexibility in investigating engine performance in relation to longitudinal distribution of fuel injection. It is not expected that as many

injectors will be required once the optimum injection guidelines are established in the AIM experimental program.

All injectors had sonic nozzles normal to the stream with the exception of a few rows which were angled slightly upstream to increase penetration.[1] Ratios of spacing to diameter of the individual orifices were kept between 6 and 7 and the penetration parameter equal to or greater than 1.7. Adjacent rows of holes were interdigitized.

UARL EXPERIMENTS

Recently, additional two-dimensional experiments have been conducted by the United Aircraft Research Laboratories (ref. 6) by use of diverging ducts which in some configurations closely approximate the area development which has been built into the AIM. Typical longitudinal pressure profiles are shown in figure 12 for divergence half-angles of 2.5°, 4.5°, and 6.8°. The much higher pressure rise at the 2.5° setting is notable. The exact mechanism of mixing and kinetics is still, as with the earlier HRE experiments, far from clear, but the finding of extreme sensitivity of supersonic combustion to wall divergence is strongly corroborated.

The effect on upstream pressure development of varying the amount of first-stage injection is shown in figure 13. The arrows denoting fuel injectors are identified in keeping with the AIM injector longitudinal arrangement shown in figure 11. The height, slope, and location of the pressure profile is seen to change substantially with an almost trivial change in the amount of first-stage fuel flow.

The implication of this effect as to anticipated AIM operating characteristics is developed in figure 14, in which the ratio of static pressure with fuel injection to the undisturbed pressure at the combustor entrance is plotted against total equivalence ratio for varying amounts of first-stage injection. Superimposed on this curve is the inlet unstart limit obtained in the 2/3-scale inlet tests by use of inert gas injection to produce mass-addition induced unstart. The dotted lines and shaded areas show derived estimates of AIM characteristics with first-stage fuel flow at an equivalence ratio of 0.18, slightly less than the originally intended value of 0.20. It can be concluded from this figure that at this slightly reduced first-stage injection overall stoichiometric supersonic combustion at Mach 6 flight can be maintained without unstarting the inlet flow.

CONCLUSIONS

Consideration of the hypersonic research engine (HRE) test combustor data, the aerothermodynamic integration model (AIM) design, and the United Aircraft Research

[1] Recent cold-flow data indicate an opposite trend. (See ref. 7.)

Laboratory combustor data leads to the following conclusions:

1. Normal injection from flush-wall sonic injectors into supersonic flow in a constant-area combustor creates a flow separation upstream of the injector. This phenomenon appears to be important in achieving good autoignition and combustion. The amount of fuel which can be so injected is limited by inlet unstart and thermal choking.

2. Two-dimensional experiments indicate that chemical efficiency increases with the value of the penetration parameter up to a penetration parameter value of about 1.7. High chemical efficiency was achieved at ratios of orifice spacing to diameter from 5.5 to 6.0. For given values of penetration parameter and ratio of space to diameter, smaller orifices gave better chemical efficiency.

3. Supersonic combustion in a diverging duct is extremely sensitive to the rate of duct divergence. It appears that the strong interaction between stages may be used to advantage in supersonic combustor design.

4. Obtaining adequate jet penetration does not appear to be a problem for the hypersonic research engine (HRE). Much remains to be learned relative to lateral spreading and mixing at a scale close to molecular diffusion.

5. As presently equipped for investigation of the effect on supersonic combustion efficiency of tailoring longitudinal fuel injection distribution to the needs of a combustor of practical length, the HRE aerothermodynamic integration model (AIM) in its experiments this year is expected to answer many of the questions which have been raised by the small-scale experiments to date.

REFERENCES

1. Short, G. R.; Sotter, J. G.; and Sun, Y. H.: Hypersonic Research Engine Combustor Development Program. Paper presented at AIAA Fifth Propulsion Joint Specialist Conference (Colorado Springs, Colo.), June 1969.

2. Engineering Staff: Hypersonic Research Engine Project. Phase II – Combustor Program. Final Technical Data Report. AP-70-6054 (Contract No. NAS 1-6666), AiResearch Manufacturing Co., The Garrett Corp., Mar. 23, 1970. (Available as NASA CR-66932.)

3. Bahn, Gilbert S.: Calculations on the Autoignition of Mixtures of Hydrogen and Air. NASA CR-112067, 1972.

4. Engineering Staff: Hypersonic Research Engine Project. Phase II – Chemical Kinetics Study for a Supersonic Combustor Model. AP-70-6319 (Contract No. NAS 1-6666), AiResearch Manufacturing Co., The Garrett Corp., May 20, 1970. (Available as NASA CR-66952.)

5. Pearson, L. W.: Hypersonic Research Engine Project. Phase IIA – Inlet Program. Final Technical Data Report. AP-69-4883 (Contract No. NAS 1-6666), AiResearch Manufacturing Co., The Garrett Corp., Mar. 27, 1969. (Available as NASA CR-66797.)

6. Kay, Ira W.; and McVey, John B.: Hydrocarbon-Fueled Scramjet. Vol. X – Wall Divergence Investigation. AFAPL-TR-68-146, Vol. X, U.S. Air Force, Dec. 1971.

7. McClinton, Charles R.: The Effect of Injection Angle on the Interaction Between Sonic Secondary Jets and a Supersonic Free Stream. NASA TN D-6669, 1972.

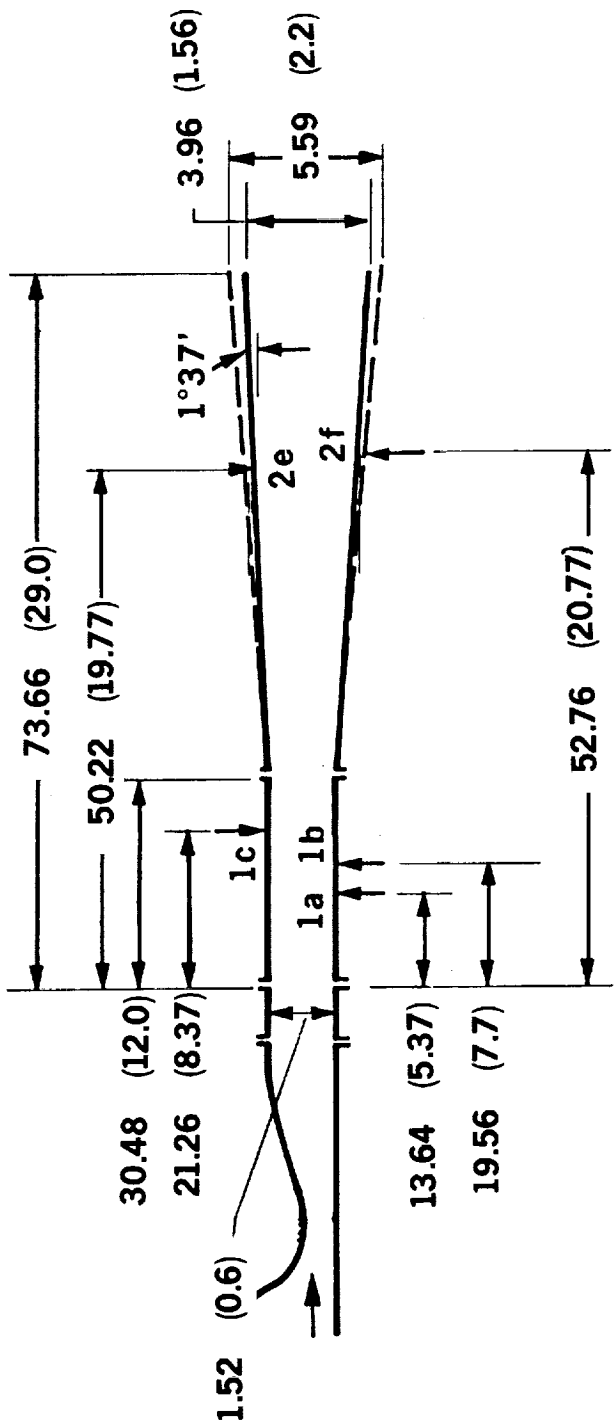

Figure 1.- Combustor configuration schematic. Dimensions in centimeters (inches).

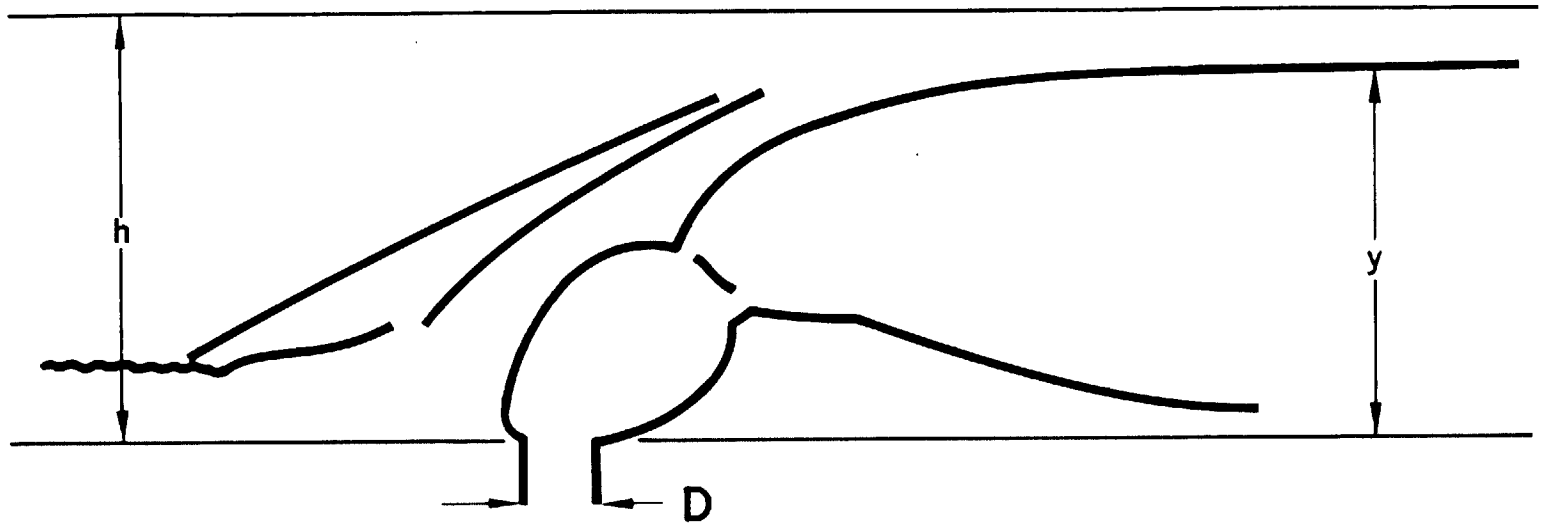

$$Z = \text{PENETRATION PARAMETER} = \frac{y}{h\phi}$$

$$y = 2.91 \left(\frac{\rho_j \, v_j^2}{\rho_o \, v_o^2}\right)^{.5} \left(\frac{x}{d_{j_*}}\right)^{.0866} d_{j_*} \qquad \left(d_{j_*} = D\sqrt{C_D}\right)$$

Figure 2.- Concept of penetration parameter Z.

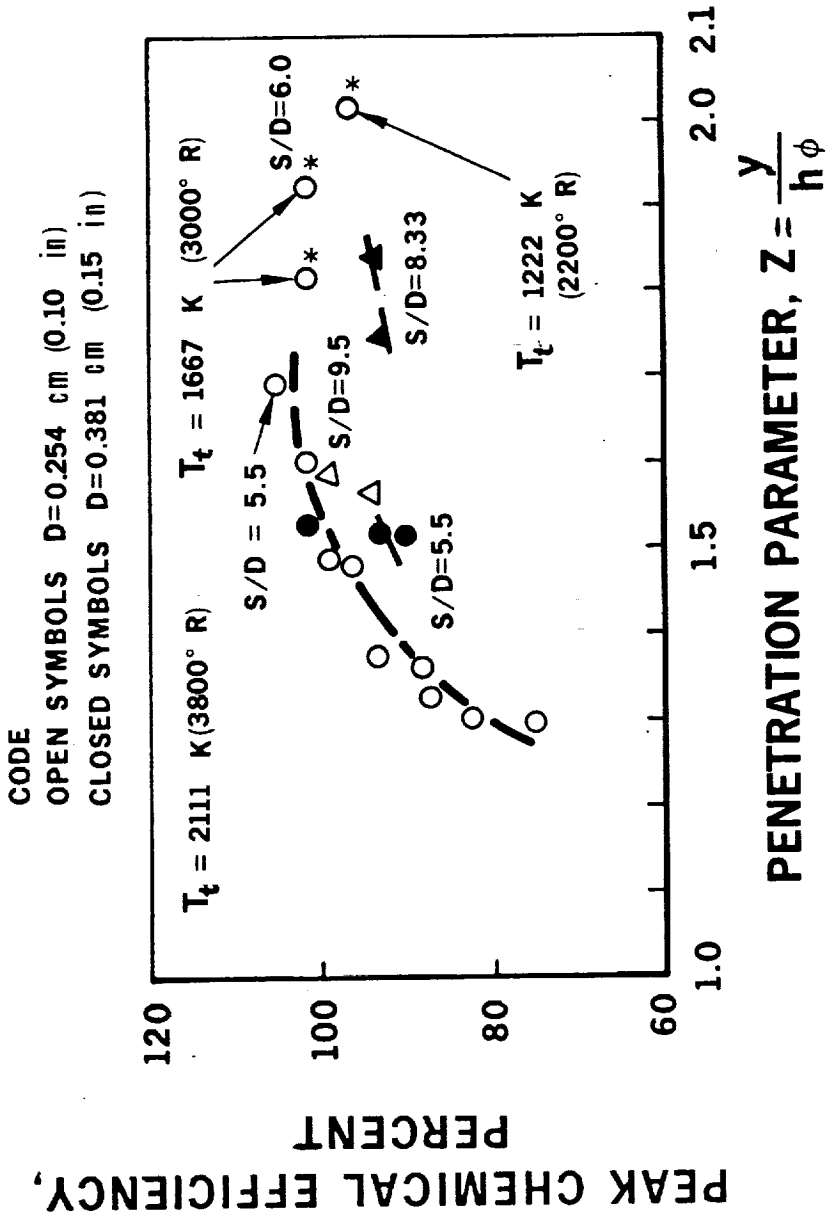

Figure 3.- Variation of peak chemical efficiency with Z.

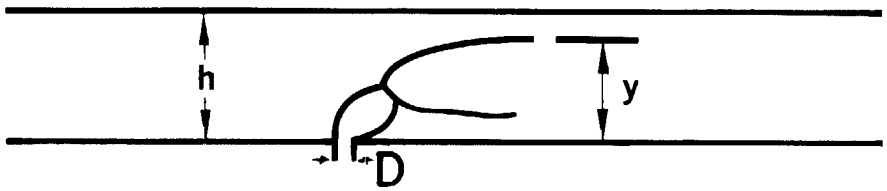

MINIMUM MIXING AREA REQUIRED FOR 100% COMBUSTION = $h \cdot s \cdot \phi$

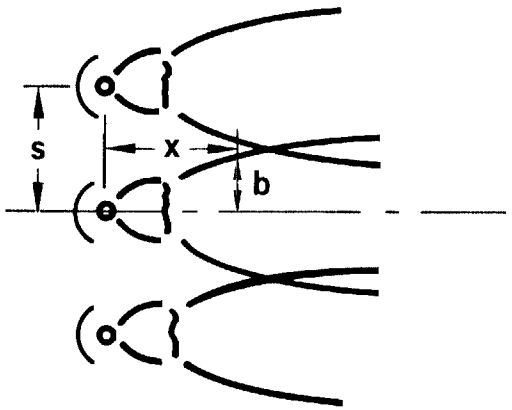

ACTUAL MIXING AREA = $g_1(y)\, g_2(b)$

$$\text{MIXING PARAMETER} = \frac{g_1(y)\, g_2(b)}{h\ s\ \phi}$$

Figure 4.- Concept of mixing parameter.

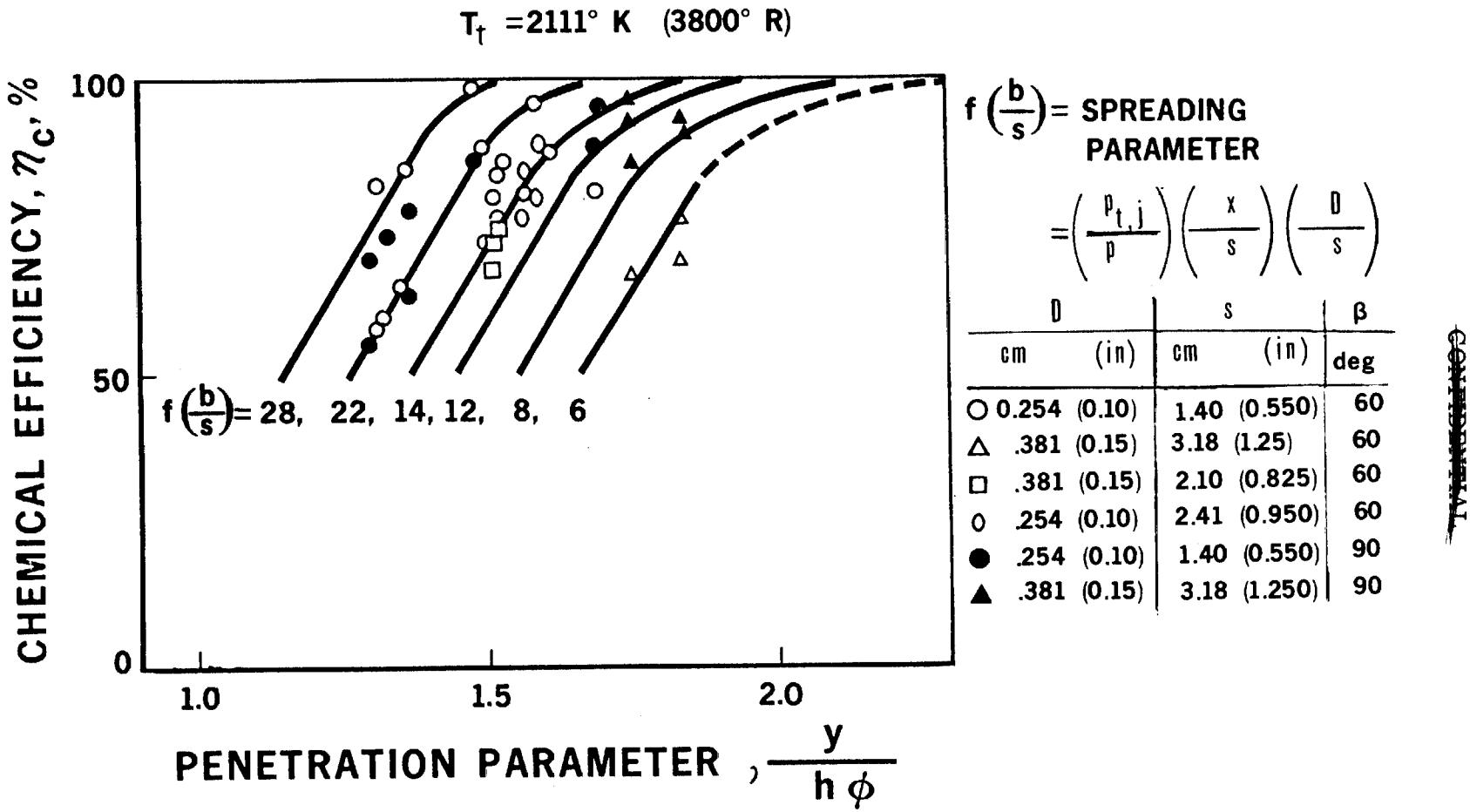

	D		s		β
	cm	(in)	cm	(in)	deg
○	0.254	(0.10)	1.40	(0.550)	60
△	.381	(0.15)	3.18	(1.25)	60
□	.381	(0.15)	2.10	(0.825)	60
◊	.254	(0.10)	2.41	(0.950)	60
●	.254	(0.10)	1.40	(0.550)	90
▲	.381	(0.15)	3.18	(1.250)	90

Figure 5.- Correlation of chemical efficiencies.

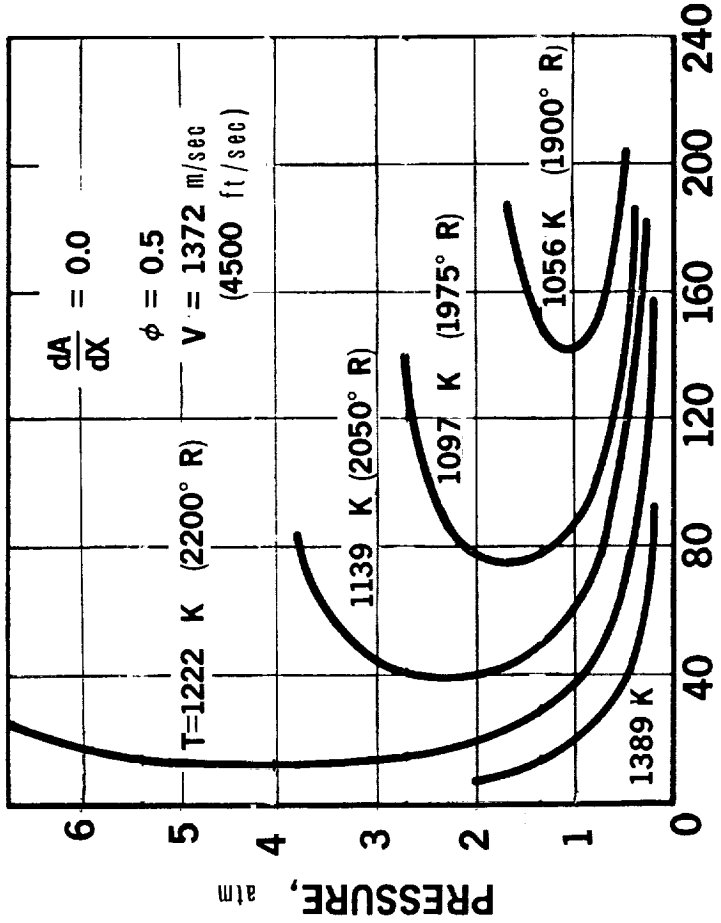

Figure 6.- Effect of initial static pressure and temperature on ignition delay time for unvitiated air-hydrogen mixture.

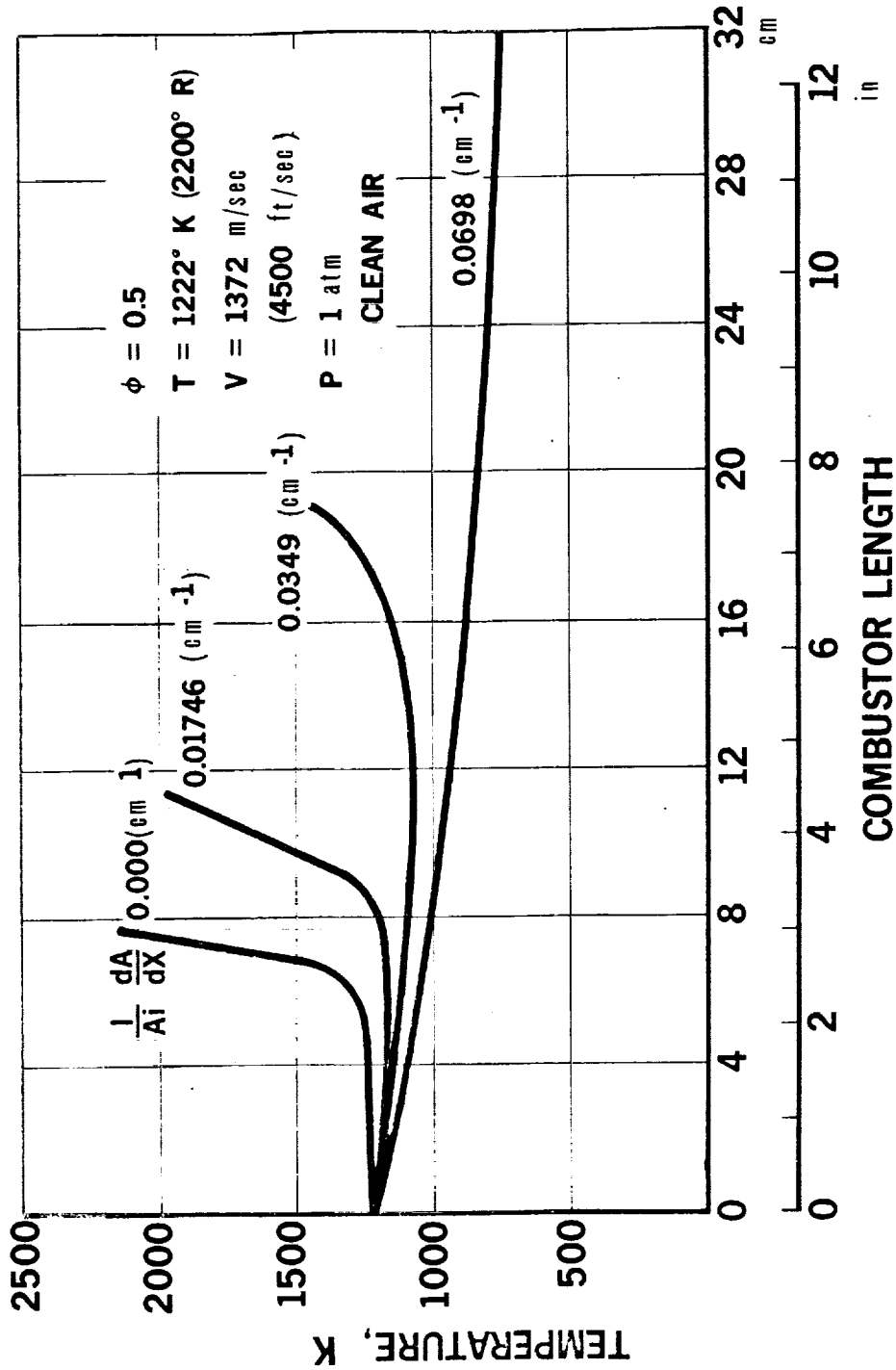

Figure 7.- Effects of combustor divergence.

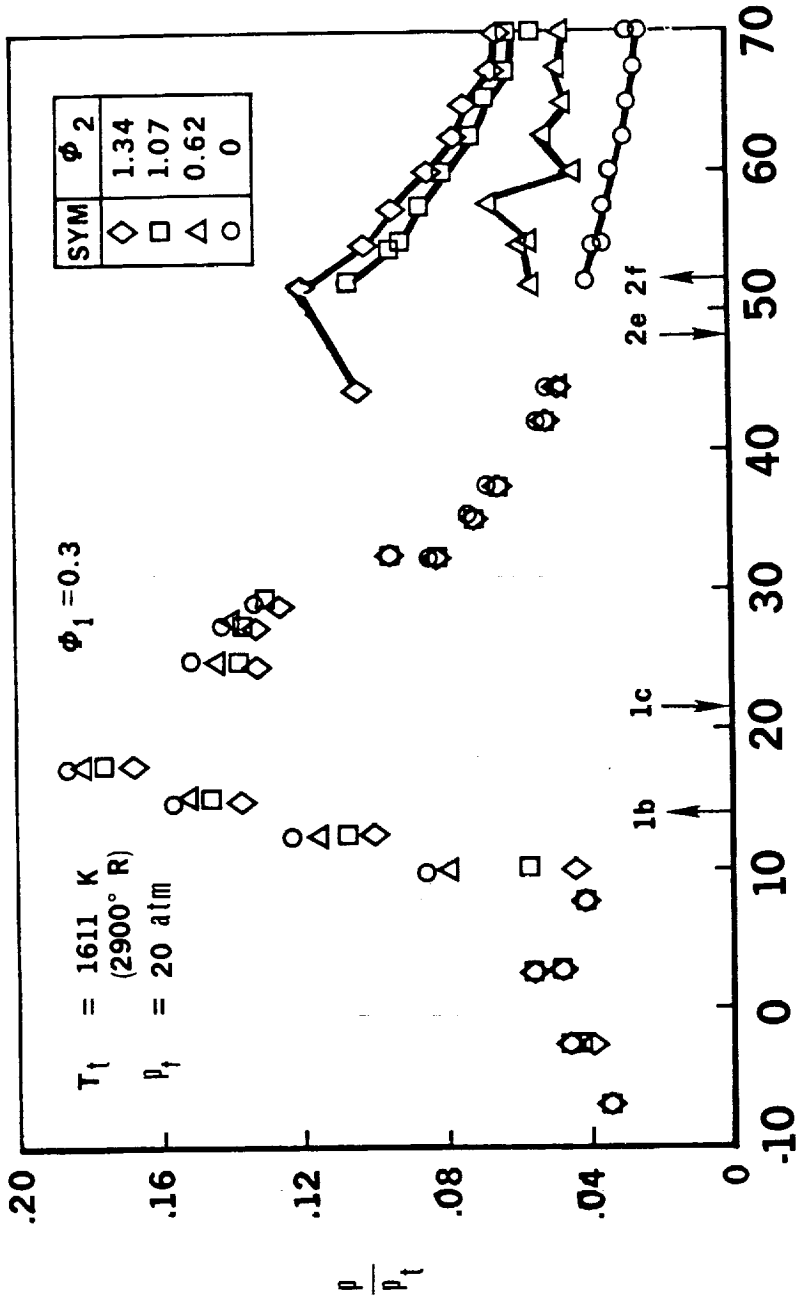

Figure 8.- Pressure distribution for staged combustion.

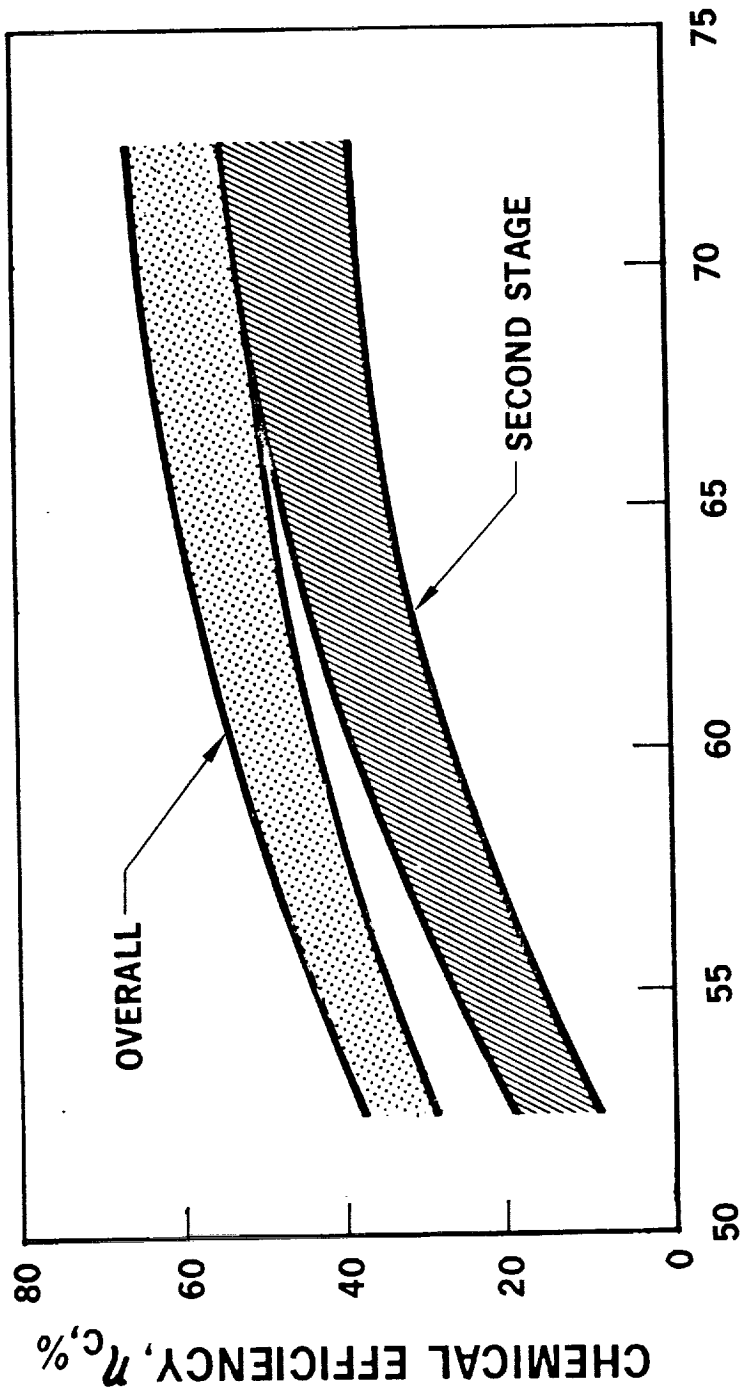

Figure 9.- Overall and second-stage chemical efficiencies.

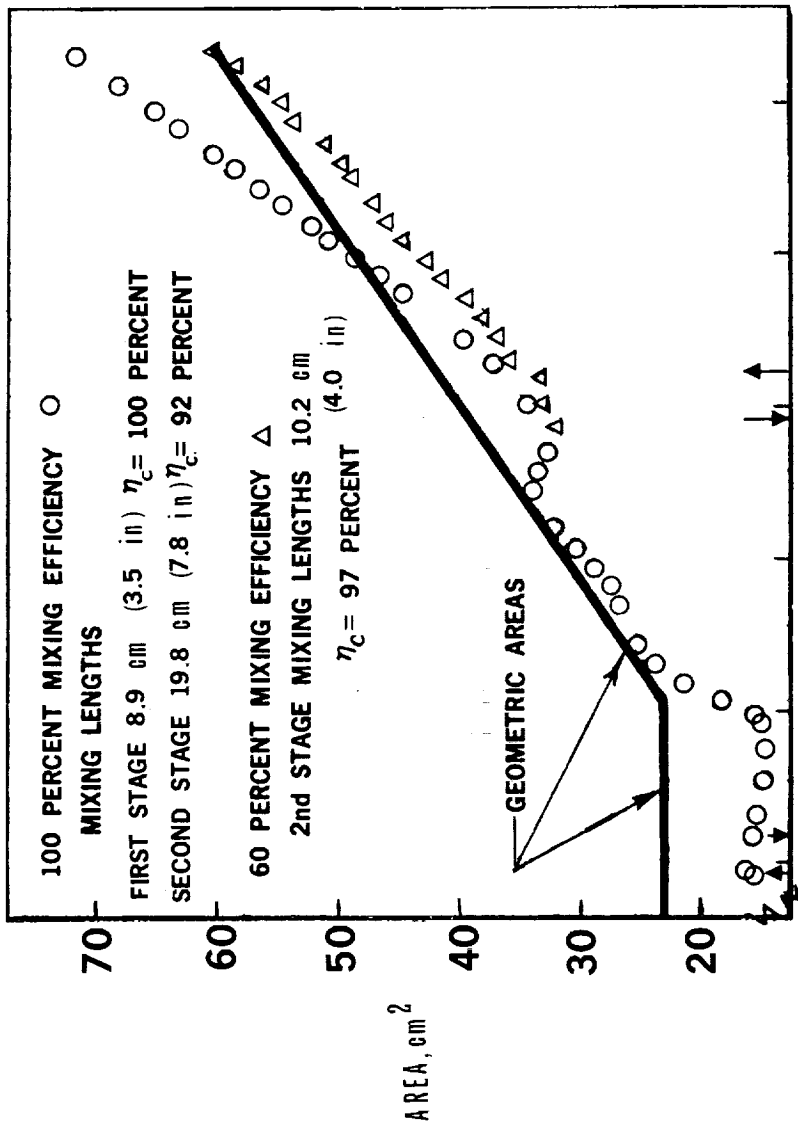

Figure 10.- Matching of theoretical and geometric combustor areas.

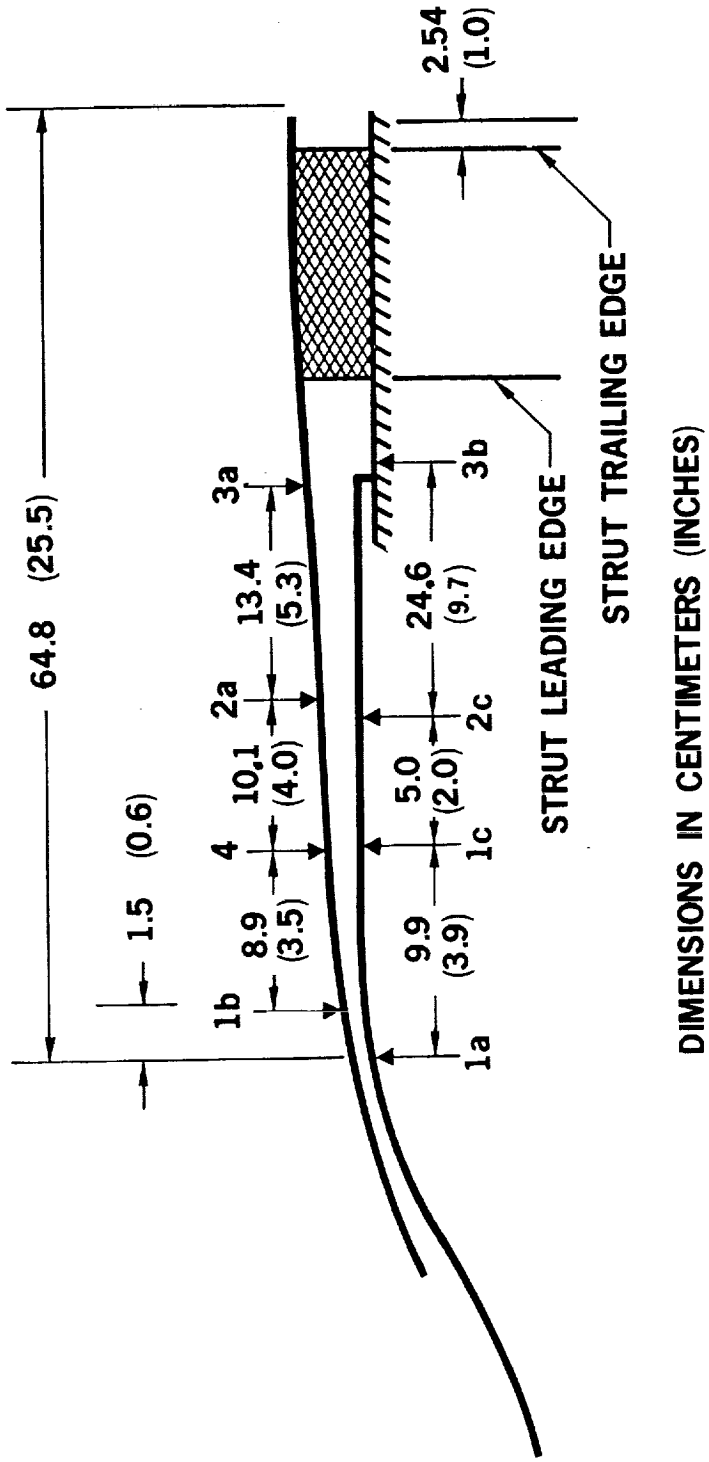

Figure 11.- AIM combustor configuration.

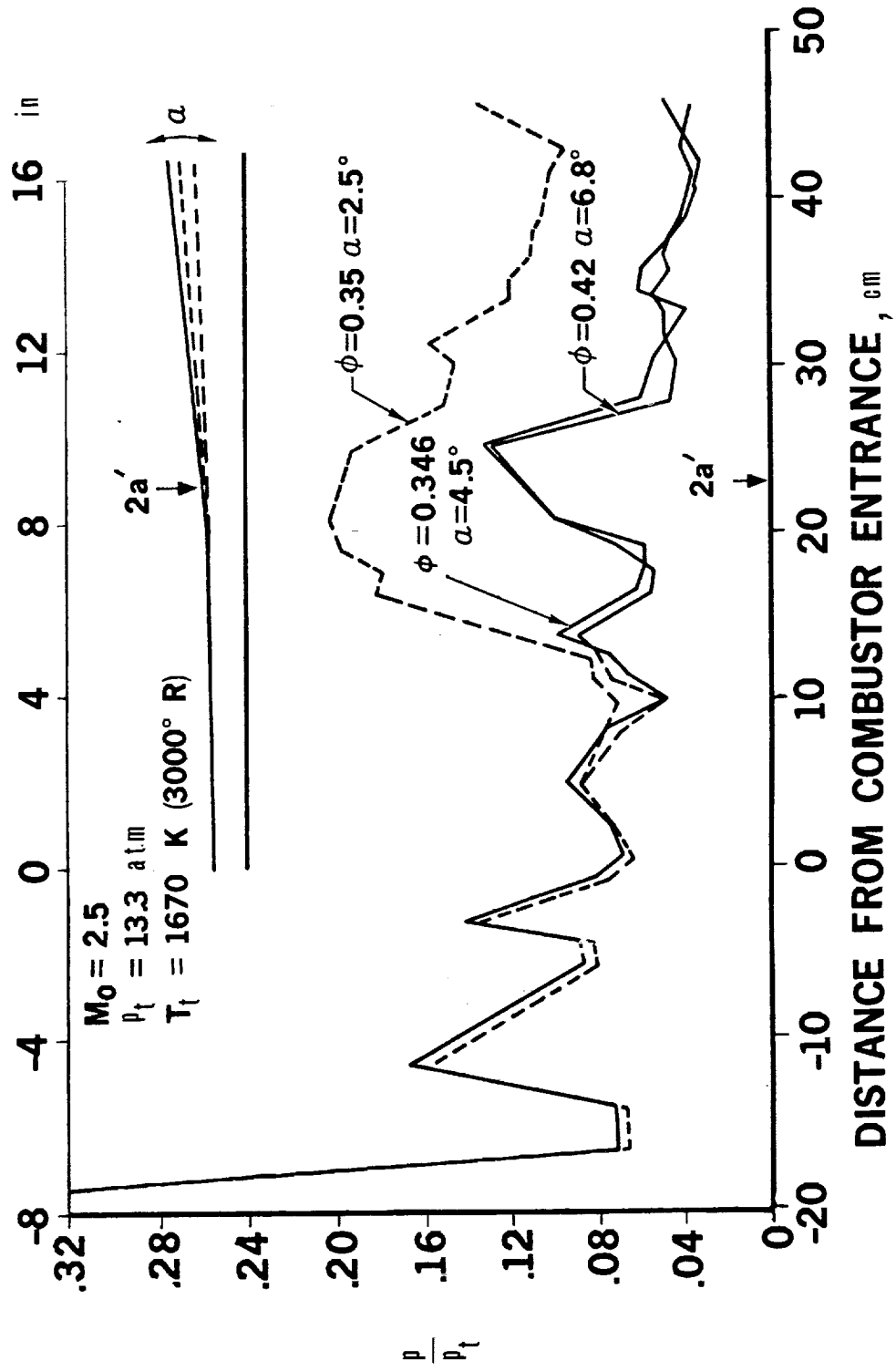

Figure 12.- Combustor divergence tests.

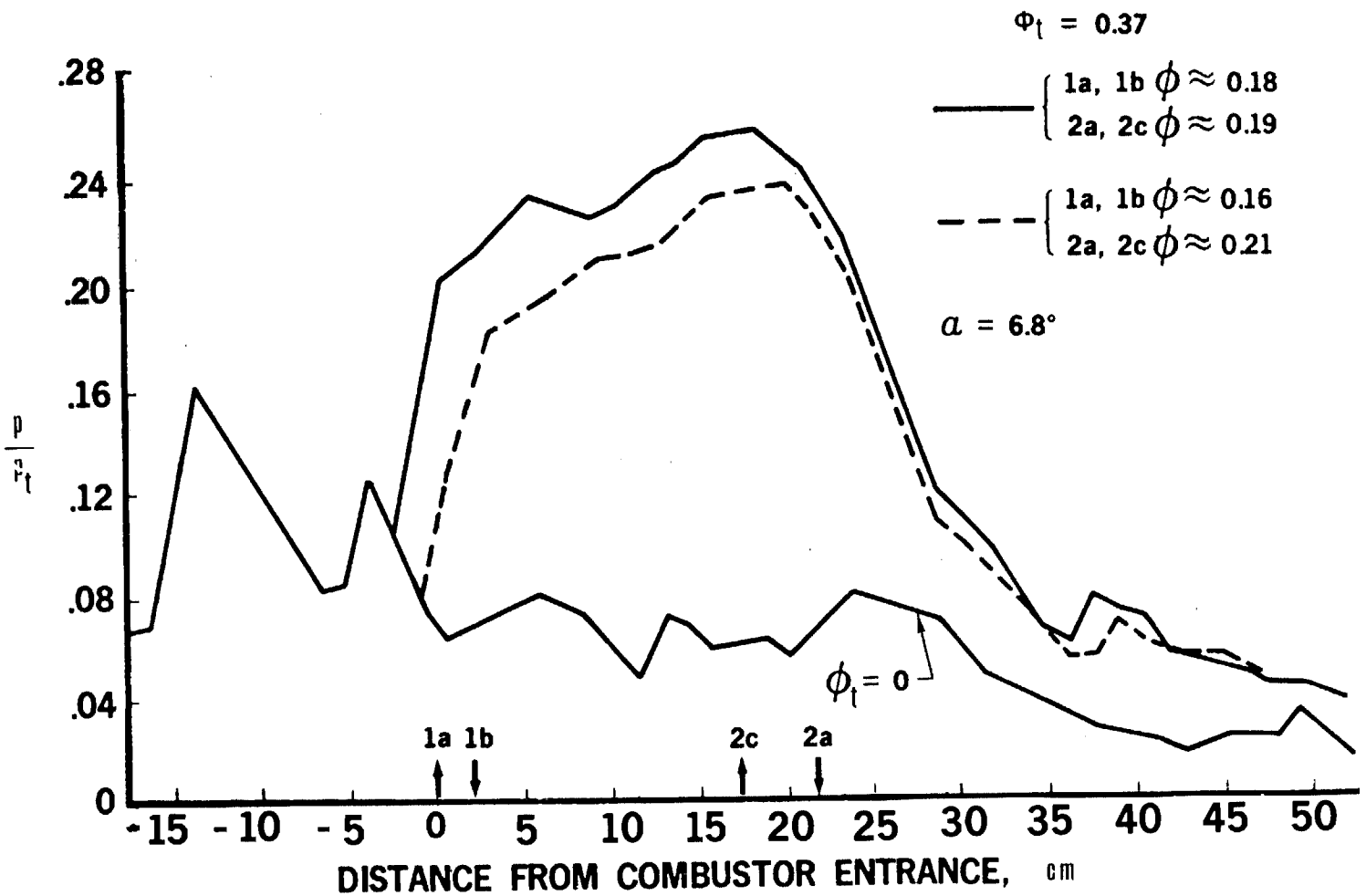

Figure 13.- Sensitivity of first-stage injection.

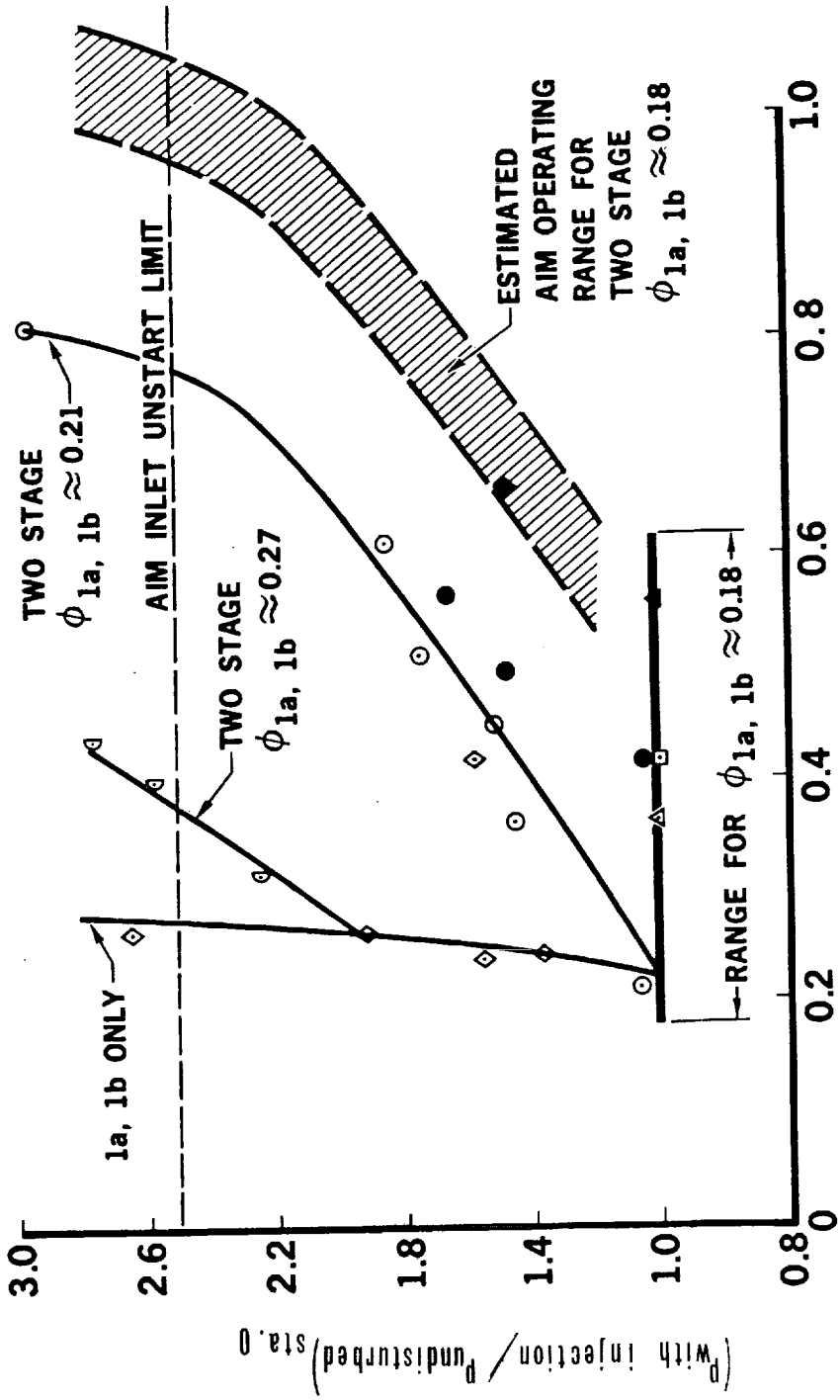

Figure 14.- AIM inlet unstart characteristics. Mach 6.

DESIGN OF ACTIVELY COOLED HYPERSONIC ENGINE STRUCTURES

By O. A. Buchmann and W. G. Flieder
AiResearch Manufacturing Co., The Garrett Corp.

INTRODUCTION

The design and fabrication of lightweight, reusable, airbreathing propulsion system structures suitable for manned hypersonic vehicles is one of todays most challenging problems. Although scaled "boilerplate" (heavier than acceptable for flight use) ramjet engines have been designed and flown on unmanned carriers and limited flightweight engine components have been designed, fabricated, and tested (refs. 1 and 2), the demonstration of a full-scale integrated hydrogen-cooled propulsion system suitable for this purpose and meeting all requirements remains to be accomplished.

This paper deals with the design and fabrication of a research-scale complete regeneratively cooled engine structural system that was undertaken to satisfy the requirements set forth earlier in this compilation. While providing the geometric surfaces and controls required for the aerothermochemical processes involved in supersonic combustion, the structure had to withstand the environment of Mach 8 flight for 100 missions. The reliability required for flight on a manned carrier aircraft, the environmental conditions, weight limitations, and cycle life needed combined to make the structural and thermal control design of this engine a very challenging task and required extensions in technology in the areas of materials application, structural design, and fabrication. Where these special extensions arose, tests were conducted to provide the needed data. Techniques were then developed to satisfy design requirements and to improve design capability. This paper presents these experiences in a summary fashion although specific design problems are discussed in some detail.

SYMBOLS

M_∞	free-stream Mach number
M_l	local Mach number in front of HRE when in flow field of X-15 airplane
q_∞	free-stream dynamic pressure, atm
q_l	local dynamic pressure, atm
T	temperature, K

ΔT temperature difference, K (^{o}R)

σ structural fatigue cycles

Abbreviations:

CRV coolant regulating valve with subscripts which denote different circuits

FDV fuel dump valve

PCV pressure control valve

ENGINE DESIGN REQUIREMENTS

The program objectives as well as design flight requirements have been specified earlier in this compilation. These specifications establish the basis for determining the maximum heating and loading to the structure, limit the maximum allowable weight of the engine, instrumentation, and associated systems, and specify reuse requirements. In addition, a number of general guidelines for design were imposed. These guidelines included:

(1) No ablation materials were to be used where they might modify the combustion processes of the engine.

(2) A smooth aerodynamic surface was desirable.

(3) The structure must withstand the heating and loads associated with an inlet unstart at the severest flight condition.

(4) Design factor of safety was 1.5 with the maximum allowable stress being that required for buckling or 0.85 of yield (0.2-percent offset).

STRUCTURE DESIGN CONDITIONS

With the aerodynamic shape (fig. 1) and the design requirements defined, the detailed local design heating and loading were established. The heating and loading distributions developed for design purposes were computed as outlined in reference 3 and substantiated to a limited extent by 2/3-scale inlet tests of reference 4. The design ground rules used are summarized in table I.

Pressure Loads

The governing design pressure distribution was based on calculations for engine operation in the X-15 shock field and 2/3-scale inlet test data taken at Arnold Engineering Development Center which produced the pressure profile in figure 2. The pressure

TABLE I.- DESIGN GROUND RULES

Material	Hastelloy X
Temperature:	
Maximum hot surface	1144 K (2060° R)
Maximum cold structure	889 K (1600° R)
Flow routing	Match surface temperatures Conserve coolant
Structure	Satisfy $\sigma \leqq \sigma_{Fail}/1.5$ Satisfy $\sigma \leqq 0.85\sigma_{0.2\ Yield}$
Coolant pressure:	
Inlet	47.7 atm
Outlet	34 atm
Design goal life	≧100 cycles

profiles for inlet started and unstarted are illustrated. The unstart pressures are significantly higher, and a greater length of the engine is subjected to high pressures due to the unstart condition. Engine operation at an angle of attack can also lead to an asymmetrical engine unstart. With the engine unstarted at angle of attack, the inlet-started pressure levels might be expected on one side of the engine and inlet-unstart pressure levels on the opposite side. This condition resulted in a calculated side load of about 133.5 kN (30 000 lb). This load became a design requirement.

Heating Loads

Initial wall (T = 555 K (1000° R)) heat-flux distributions through the engine for the design conditions (ref. 3) are presented as figure 3. These heat-flux values are based on the computed inlet characteristics, on one-dimensional flow calculations from the inlet throat to the engine exit, on the reference enthalpy method of heat-transfer calculation, and the assumption of constant surface temperature. Of course, the heat-flux distribution with a real structural wall will differ from these initial input data.

STRUCTURAL DESIGN DEVELOPMENT

The structural design of the engine was developed from the design objectives and criteria outlined. Important detail design problems are encountered in the integration of load-carrying and thermal requirements. The following discussion is concerned with some of the considerations used in developing the solution to the more critical problems.

Preliminary Design

Figure 1 shows a schematic of the engine. The significant dimensions are indicated. The inlet spike was required to modulate over a 7.5-cm (3-in.) stroke to provide variable-geometry inlet performance. Struts provide the structural carrythrough from the inner shell to the outer body and are connected to the stiffening rings fore and aft. The engine mount attaches to the aft stiffening ring on the outlet manifold of the outer body. Access to the engine cavity is provided by a nozzle plug bolted to the inner shell; the nozzle plug may be removed as required. The leading edge is bolted to the front of the outer shell.

The preliminary design indicated that the success of the engine strongly hinged upon an effective integration of the thermal and structural aspects of the design. Figure 4 highlights the specific design problem areas.

The plate-fin sandwich concept was selected for all shells. The sandwich provided the coolant flow passages as well as the strength to contain the high-pressure hydrogen. The thickness of the structural shells varied depending upon the loading from minimum gage (0.038 cm (0.015 in.)) in areas such as the fore spike and aft nozzle to about 0.159 cm thick (0.0625 in.) in the centerbody. The resulting structure was adequate for shock, inertia, and vibratory loads anticipated.

The coolant inlet, outlet, and crossover manifolds, as well as fuel injector rings, also served multiple functions. They reinforced the structural shells by providing the strength for asymmetric static-pressure distributions, for shell-buckling stability against external pressure loads, and shell-bending loads. Manifold rings also provided for structural attachment of the struts and a load path from the engine to the mounts.

Thermal control of the structure was effected by the selection of coolant flow route directions and the control of coolant flow rates. A major design objective was to protect the primary structure from abrupt local temperature discontinuities due to transient or steady-state operating conditions. This thermal control was essential to prevent distortions of the primary structure that would cause departure from the required aerodynamic shape as well as excessive thermal stress. Surface temperature control was necessary to prevent excessive metal temperatures or excessive local temperature differences between the heated surfaces and the colder structural shells. This control was accomplished by selection of different fin height and spacing configurations for different parts of the engine.

Final Design

The preliminary design effort provided the basic design concept, design ground rules, and thermal analysis needed for material selection. After considerable screening activity, Hastelloy-X material was selected for the structure. This material selection

was made because of the large experience base for its fabrication and because of its excellent ductility which is required to resist thermal fatigue. The maximum working temperature for Hastelloy-X was set at 1140 K (2060° R). This temperature was allowed only in the hot regeneratively cooled surfaces of the engine which were not considered primary structures and, hence, were not subject to the safety factor specified in the design requirements. The load-carrying structure temperature was limited to 889 K (1600° R).

Figure 5 shows the basic sandwich panel and two important design areas associated with the fabrication of the cooled shells. Except in selected areas, the offset fins shown in the sketch were used for all surfaces. Assembly of the plate-fin sandwich and the face sheets is accomplished by brazing. The brazing alloys selected were of the gold-palladium-nickel series which were well suited for multiple-step brazing and which experience had shown minimized the loss of parent metal ductility. The features obtained from the sandwich panel were as follows:

(1) Smooth aerodynamic surfaces

(2) Acceptability of some blockage of fin flow area, either due to braze filler alloy or foreign object damage, without loss of the part. The offset fin permits some crossflow and thus avoids complete starvation of the flow passages in line with the blocked area. The amount of blockage that can be tolerated is a function of the local heat flux. (See ref. 5.)

(3) Ease of interruption of flow passages for installation of inserts or structural members. Insert installation is a major consideration since the HRE used a total of 400 fuel injection nozzles and approximately 100 instrumentation inserts which penetrate the shells. Figure 5(b) shows a typical installation. The fins are cut away to give an annular space surrounding the insert. The size of the annular space is selected to insure uniform flow up to the insert and resumption of uniform flow downstream from the insert. The parameters required to prevent hot spots were verified in flat-plate flow tests with the aid of temperature-indicating paints.

(4) Joining of shells to produce smooth aerodynamic surface using the technique shown in figure 5(c). By the same method, the fin height can be varied in adjacent panel sections to assure the best heat transfer and pressure drop performance. The fins are removed between face sheets to permit installation of doublers on the back side of the aerodynamic surface. For different fin heights, a stepped doubler is used on the cold surface. A smooth aerodynamic surface was an important design requirement for the inlet spike, where wind-tunnel tests showed low Mach number starting problems with external doublers.

(5) Capability of incorporation of coolant and fuel manifolding into the sandwich shells.

Thermal fatigue of the heated surface is a major design consideration for cooled structures in this application. Analytical work was carried out to assess the tolerable limits in surface temperature and local ΔT.

Figure 6 shows an elemental structural section and the time-temperature history that would occur in an engine application. The heated skin responds more rapidly to the heating than the cold structural shell and causes a transient amplification of the steady-state differential temperatures (ΔT). The figure shows the curve of structural cycle life as a function of engine ΔT. To assure the design goal for 100 cycles for the HRE at maximum metal temperature, a maximum design ΔT of approximately 444 K (800° R) was selected. It may be noted that a design goal of several hundred cycles would mean a lower ΔT; for example, 400 cycles would require a ΔT limit of 319 K (575° R). This limit would, in turn, have an effect on flow-passage design, flow-rate control, and coolant pressures.

Shell Assemblies

Incorporation of the basic panel concept in axisymmetric cooled shells involves a number of problems. The shells must be, first of all, accurately sized for control of aerodynamic contours and assembly fit. In addition, inserts, structural attachments, manifolds, and stiffeners must be incorporated in the basic shell in a way that is compatible with the thermal structural requirements. Provision must also be made in the design to allow for inspections at intervals in the manufacturing process, particularly of braze joints. To establish the basic manufacturing parameters and to provide design information, various experimental evaluations of the sandwich structure were performed.

Shell sandwich tests.- Two major problem areas that required experimental evaluation for the shell structures were the fin strength for pressure containment and the plate-fin fatigue life characteristics. The structural response of the shell structures to system static aerodynamic pressure loads and the design vibratory environment was considered to be fully predictable with available analytical procedures. The only degree of uncertainty would be the actual magnitudes of these loads compared with those developed and defined during the design phase.

Accordingly, specimen testing was limited to small rectangular test pieces shown in figure 7. Several different offset fins were utilized in these specimens, and these fins were tested for burst at room temperature and 1145 K (2060° R). (See ref. 6.) Creep rupture tests were also performed at 1145 K (2060° R). (See refs. 3 and 7.) The test results provided data relative to the strength of the fins, and these data were instrumental in determining the different fins that were used in the engine.

The thermal-fatigue evaluation of the sandwich shells was achieved by employing the specimen configurations shown in figure 7. These specimens were thermally cycled with applied ΔT values from 361 K (650° R) to 528 K (950° R). (See refs. 2, 6, and 7.)

The test results were used to establish the fatigue design curve presented in figure 6. These test results verified the capability to meet the design goal of 100 cycles at an engine ΔT of 444 K (800° R). More importantly, this information demonstrated that the fin configuration and the design flow rates to achieve the ΔT and maximum temperature limits were acceptable for this specific application. In the more general application, tests results like these would be used to define coolant passage design and coolant flow rate.

Assembly fabrication.- As a required development and demonstration of fabrication techniques, a compound curved section of the inlet spike was constructed at 1/2 scale. This development (refs. 6 and 7) was made with full-scale fin heights and skin thickness which made the fabrication in the area of compound curvature even more difficult than for the corresponding full-scale part. The techniques developed in this part of the program were then used in the fabrication of the full-scale shells. Manufacture of the shell assembly required three separate brazing cycles. After brazing of the basic shell sandwich, the shell was machined to accept the various inserts required. These inserts were installed and brazed in a separate cycle. This procedure allowed testing and repair of the inserts at this stage of assembly without jeopardizing the sandwich shell. Provision for a repair operation was necessary at this point because some of these inserts become inaccessible in subsequent operations. Finally, various manifolds and structural attachments are installed and brazed on to the sandwich shells, as shown in figure 8.

The manifold at the right (fig. 8) serves as a ring stiffener and also as a bolting flange for attachment of the nozzle. The fuel manifold at the left of the shell is a primary structural member that provides support for the strut sockets. The fuel manifold in the center stiffens the shell against buckling loads; however, it does not serve as a primary load-carrying structural member as do the other two manifolds mentioned. The tubular manifold itself is of minimum section to minimize thermal stresses in the shells resulting from temperature differentials.

The joint between the coolant inlet manifold (fig. 8) and the hot sheet is representative of the type of design that was used with relatively high heat fluxes. The joint cross section is minimized. This minimization limits the temperature rise in the face sheet as a result of the increased conduction path associated with the bigger sections. Also, the coolant is forced to sweep the joint area to increase the available cooling.

On the left-hand manifold (fig. 8), the cross-sectional wall thickness and the overall dimension size were dictated by structural load. The I-beam section was needed to provide a direct tension tie between the manifold semicylindrical wall and the structural shell to satisfy pressure containment stresses. Credit was taken for the I-beam section modulus in determining the manifold load capability.

The gold-palladium-nickel filler alloys were used (ref. 8) for brazing because they provide relatively strong and ductile braze joints and because they could be prepared in compositions that permit step brazing over reasonable temperature intervals (42 K to 56 K (75° R to 100° R)). Since all shells were brazed with the center line vertical, there was a tendency of the filler alloy to flow downward and plug fin passages near the bottom of the structural part. Where this condition became a problem, the basic shell was designed with excess length. This extra length collected the filler alloy and was subsequently cut off. Other problem areas were handled by recycling the braze and using blotters to absorb excess braze material.

Acceptance testing.- After each of the three brazing cycles described, the shell subassemblies were inspected with regard to filler-alloy plugging and braze-joint integrity. Radiographic inspection covering 100 percent of the surfaces was used to inspect for plugging and braze-joint uniformity. In the manifold joints, in particular, the radiographic inspections were able to detect braze voids.

Inspection of the fin-to-shell braze joints could not be successfully accomplished radiographically. Instead, a technique that utilized a brittle lacquer coating ("Stresscoat" manufactured by the Magnaflux Corp.) on the shell face sheets was evolved. The coated shells were pressurized with water to levels approaching the yield strength of either the face sheet or the fins, whichever was controlling, and inspected for cracks in the coating. The results obtained were consistent and reliable in terms of both braze-void detection and visualization.

To establish a basis for use of this technique, a number of flat panels were fabricated and provided with intentional voids. These panels were then pressurized and the cracking of the coating observed. Figure 9 shows the results of the tests with various void sizes. The line for burst pressure represents the actual pressure at which the various panels burst. The lines for fin and face-sheet yield pressures are estimated from parent metal properties. The range of pressures at which the Stresscoat showed cracks is shown to be below any of the other strength limits for the panels. The vertical line on the left shows the equivalent void size for perfect panels with 20 fins per inch.

SPECIAL DESIGN PROBLEMS

In several instances detailed design problems arose which required the development of specific technology to achieve a working solution. Two such cases are the inlet leading-edge design and the centerbody strut design. The following discussions delineate these two design problems and outline the steps to their solution.

Cowl Leading Edge

The cowl leading edge represents a critical interface with the aerodynamic design of the engine. Design considerations included the following:

(1) Inlet performance requires a minimum possible radius at the leading-edge tip.

(2) The external wedge angle behind the tip is aerodynamically limited by shock detachment even though external drag was not a critical design consideration.

(3) Heat fluxes on the leading edge are very high, up to 19.26 MW/m^2 (1700 Btu/ft^2-sec) for the design operation with spike shock on the cowl lip, at total temperatures up to 2670 K (4800° R).

(4) Ablative cooling of the leading edge was not permitted by the specifications because of contamination of the propulsive stream.

These considerations led to the selection of a regeneratively cooled leading-edge design.

Design problem.- Selection of the leading-edge radius was based on practical manufacturing limits and what were anticipated to be practical cooling limits. This radius was 0.076 cm (0.03 in.). The resulting inside radius is 0.038 cm (0.015 in.). Use of smaller passage sizes was also objectionable because of the possibility of plugging with braze filler alloy.

Two leading-edge tip configurations were considered for the application and are shown in figure 10. The design on the left uses flow that is perpendicular to the leading edge. The coolant geometry upstream and downstream of the leading edge includes fins 0.051 cm (0.020 in.) high. With this design, the coolant flow through the leading edge is controlled by the heat load on the internal leading edge and forward outer shell surfaces. Even though the leading-edge heat flux will not always vary in direct proportion to the heat load on the internal surfaces, analysis showed that sufficient cooling would be available at all anticipated conditions.

The second design configuration has the same external geometry but uses flow which is parallel to the leading edge. This flow can be separately ducted and controlled or can be in parallel with an existing flow route. Shown above the leading-edge design is a typical manifolding configuration using three inlets and three outlets. With fewer inlets and outlets, the pressure drop became too high for the required flow rate. At the same time, the size and area of the tip passage are limited by the requirements of internal pressure containment. The configuration aft of the tip itself is the same as that for the other design.

Performance tests.- Tests were carried out (ref. 9) to evaluate thermal performance of the two candidate coolant configurations, and low cycle fatigue performance and creep-rupture containment strength of the two configurations. Specimens with Hastelloy-X and nickel 200 leading edges were tested. A straight-section test specimen, 20.32 cm (8 in.) long, that incorporated all the internal design details of a full-scale curved section, was considered to be adequate for these evaluations. The tests consisted of exposing the leading edge to the heating of quartz lamps focused by a reflector to give a realistic heating level and distribution (ref. 9).

A nickel 200 leading-edge tip with coolant flow perpendicular to the leading-edge stagnation line was selected for the engine design. The test results indicated that nickel 200 provided a greater low-cycle fatigue life than Hastelloy-X at the design flow rates. The perpendicular flow direction provided fabrication advantages due to the simpler flow routing and manifolding and the coolant pressures to achieve the same metal temperatures were lower. Another decisive advantage for this flow routing is its much lower susceptibility to local blockage.

Centerbody Support Struts

The centerbody strut design requirements include the following:

(1) The struts must provide the structural connection between the centerbody and the outerbody and, as such, must carry the large loads associated with inlet unstarts. These loads essentially sized the struts, the strut sockets, and the large manifold rings on the basis of applied stresses and structural rigidity.

(2) The struts must have sufficient internal openings to accommodate all hydrogen, electrical, and instrumentation lines.

(3) The struts must be cooled to withstand the hostile environment of the combustor with total temperatures to 3220 K (5800° R).

(4) The adjacent shell areas must retain structural integrity and be adequately cooled in the face of the shock—boundary-layer interactions resulting from the presence of the struts.

The last requirement is a shell design problem and was resolved by providing the desired flow distribution around the cutouts by using gaps around the cutouts, as illustrated for the insert design in figure 5. The cooling design of the strut itself involves the leading edge and the side walls as distinct problems. Figure 11 shows the strut configuration as finally adopted.

Design problem.- The leading-edge design was constrained by the need to minimize the radius for best internal engine performance. Since a separate flow route for the leading edge was undesirable, use of flow from an existing route was required. This requirement was achieved by routing all the inner body (inner shell and nozzle) flow through the leading edge. Overall pressure-drop limitations and the high heat fluxes resulted in selection of an 0.203-cm (0.080-in.) leading-edge radius. The leading edge itself was made integral with the basic strut body. To enhance heat transfer from the stagnation line of the strut and to maintain acceptable temperatures, a fin was brazed into the leading-edge passage.

The design of the strut sides was governed by the cooling requirements. Specifically, the coolant flow required to accommodate the heat load was relatively small. At

the same time, however, the coolant had to be routed from the aft end to the front to match the temperature gradient in the adjacent shells and to avoid large thermal stresses. Temperature differences of less than 111 K (200° R) were desired between the shells and struts at any station. Thus, it was necessary to flow coolant along each side of the struts, rather than to circulate coolant around the entire strut. This procedure, in turn, resulted in a need for parallel flow paths along the strut sides and the need to insure adequate flow distribution in these parallel paths. To maintain the high heat-transfer coefficients required with the low flow rates, low fins were selected (0.051 cm (0.020 in.)). The single difficulty encountered with the design was the tendency toward filler-alloy plugging of the unusually small fin passages. This condition was overcome by careful placement and control of the quantity of alloy applied for each of the two required braze cycles.

Strut tests.- The strut test specimen (ref. 10) and part of the test unit are shown in figure 12. Because of the intensive stagnation-line heating of the strut leading edge, large temperature differentials would exist at the stagnation-line outer surface relative to the strut body. Thermal-cycle fatigue data as well as creep-rupture data were required to provide assurance of adequate engine life. In order to duplicate engine installation and to simulate the local problems at the strut-to-shell connections, top and bottom support panels were used to represent the shell segments in the vicinity of the shells. Supersonic flow at Mach 1.9 and at up to 2500 K (4500° R) total temperature was used to simulate the operating environment. Thermal evaluations were made to assess leading-edge cooling and heating around the entire strut socket area and in the gap between the strut and the socket.

Initial test results (ref. 10) demonstrated the need for a fin in the leading-edge passage. Tests using the finned leading edge showed that it would be satisfactory for at least 163 thermal fatigue cycles and, hence, a satisfactory design. The test data also indicated that the gap between the strut and the socket would have to be carefully controlled, and that a gap size of 0.013 cm (0.005 in.) would limit local metal temperature to an acceptable 889 K (1600° R).

Successful flow distribution was effected in the support panels (representing the shells) by the use of varying coolant orifices at the inlet and outlet manifolds in addition to an unfinned channel around the strut socket. To solve the problem of flow distribution in the strut sides, struts were evaluated by using separate inlets to each of the parallel paths. Based on the test results, each of the paths was provided with orifice holes to give the correct pressure differential. The heat-transfer test results confirmed the adequacy of the coolant split between the two sides of the strut.

STRUCTURE ASSEMBLY MODEL

As the project progressed and the project scope was altered, a revised structural ground test program was developed which included tests of a full-scale hydrogen-cooled flight-type engine in the Langley 8-foot high-temperature structures tunnel. This engine was assembled from components already developed and fabricated in the HRE structures program and was called the structural assembly model (SAM). (See fig. 13.) The results of these tests are discussed in this compilation.

The SAM engine assembly is mounted to a suspension frame that was directly carried over from the flight-design configuration. The forward mount is a block designed to carry loads in all axes and to measure thrust by deflection; axially flexible aft mounts are used to minimize axial restraint as a result of differential thermal expansion.

Insofar as the structure is concerned, the SAM was designed and fabricated to retain all essential features of the HRE flight engines. Structural differences were only in the number of fuel injectors and their arrangement and in the external cowl (not shown) which was water cooled for the ground test whereas it was covered with ablation material for flight tests. The coolant flow control system was redesigned for the ground tests to allow greater flexibility.

The hydrogen flow system for the SAM is shown in figure 14. The flow routes were selected on the basis of temperature-matching requirements, pressure drop limitations, and the need to minimize coolant consumption. To insure the desired coolant distribution during the wind-tunnel tests, each of the flow routes has a valve which is preset for a test. In a flight system, the flow in each route would be separately controlled by the temperatures of the route. The temperature control system for the SAM modulates the fuel dump valve (FDV) only. System pressure is automatically controlled by means of a valve (PCV) at the inlet to the model. A separate injection control valve is used to route hydrogen from the outlet of the model to the fuel injectors to permit thermal cycling of the associated structures.

CONCLUDING REMARKS

The design and fabrication of a complete regeneratively cooled hypersonic engine has been accomplished. Although the scale of the engine is less than that required to propel a manned aircraft, most of the problems of the full-scale propulsion system design were present and were solved in a satisfactory manner. Specific achievements that are believed to be significant are:

(a) A working design for a cooled leading-edge radius of 0.076 cm (0.03 in.) capable of withstanding heat fluxes to 20.4 MW/m^2 (1800 Btu/ft^2-sec)

(b) A working design for joining shells that avoids discontinuities in the aerodynamic surface

(c) A working design for a cooled panel which can handle nonuniform heating, accidental obstructions, and stable operation of parallel heating circuits

(d) The ability to introduce inserts into the coolant flow passages without degradation of the cooling

(e) The design of struts and strut installation that avoids large thermal gradients which could lead to unacceptable structural deformation

(f) Integral designs of manifolds and stiffeners which reduce thermal stress and weight

The manufacture of the cooled structure was characterized by the need for maintenance of close tolerances in relatively compliant sheet metal shapes. Step brazing, using four steps at progressively lower temperatures, was required for the shell assemblies and proved to be an acceptable procedure. However, assurance of the integrity of braze joints and the absence of plugged coolant passages is necessary. Procedures were developed to screen out brazing defects and to permit correction during the fabrication sequence.

REFERENCES

1. Schuh, J. R.; and Ranslem, G. R.: Tests of Regeneratively Cooled Components for Hypersonic Ramjet Propulsion Systems. Vol. II: Demonstration of Performance and Structural Capabilities. AFAPL-TR-68-125, Vol. II, U.S. Air Force, Apr. 1969. (Available from DDC as AD 504 116.)

2. Elkins, P. E.; and Rouse, R. W.: 1966 Advanced Ramjet Concepts. Vol. V – Advanced Nozzles and Ramjet Structures. AFAPL-TR-67-118, Vol. V, U.S. Air Force, Mar. 1968.

3. Engineering Staff: Hypersonic Research Engine Project. Phase IIA – Structures and Cooling Development. Third Interim Technical Data Report. AP-67-2833 (Contract No. NAS 1-6666), AiResearch Manufacturing Co., The Garrett Corp., Dec. 4, 1967. (Available as NASA CR-66996.)

4. Pearson, L. W.: Hypersonic Research Engine Project. Phase IIA – Inlet Program. Final Technical Data Report. AP-69-4883 (Contract No. NAS 1-6666), AiResearch Manufacturing Co., The Garrett Corp., Mar. 27, 1969. (Available as NASA CR-66797.)

5. Walters, F. M.: Hypersonic Research Engine Project. Phase IIA – Category I Test Report on Fin Heat Transfer and Pressure Drop Testing Data. AP-69-5348 (Contract No. NAS 1-6666), AiResearch Manufacturing Co., The Garrett Corp., Aug. 7, 1969. (Available as NASA CR-66844.)

6. Buchmann, O. A.: Hypersonic Research Engine Project. Phase IIA – Structures and Cooling Development. First Interim Technical Data Report. AP-67-2161 (Contract No. NAS 1-6666), AiResearch Manufacturing Co., The Garrett Corp., May 12, 1967. (Available as NASA CR-66997.)

7. Engineering Staff: Hypersonic Research Engine Project. Phase IIA – Structures and Cooling Development. [Second] Interim Technical Data Report. AP-67-2537 (Contract No. NAS 1-6666), AiResearch Manufacturing Co., The Garrett Corp., Aug. 23, 1967. (Available as NASA CR-111770.)

8. Engineering Staff: Hypersonic Research Engine Project. Phase IIA – Category I Test Report on Braze Alloy Investigation and Flat Panel Testing. AP-68-3813 (Contract No. NAS 1-6666), AiResearch Manufacturing Co., The Garrett Corp., May 27, 1968. (Available as NASA CR-66845.)

9. Engineering Staff: Hypersonic Research Engine Project. Phase IIA – Category I Test Report on Cowl Leading Edge Straight Section Thermal Performance and Thermal Cycle Testing. AP-69-5347 (Contract No. NAS 1-6666), AiResearch Manufacturing Co., The Garrett Corp., July 30, 1969. (Available as NASA CR-66843.)

10. Engineering Staff: Hypersonic Research Engine Project. Phase II – Category I Test Report on Strut Thermal Performance and Thermal Cycle Testing. AP-69-5547 (Contract No. NAS 1-6666), AiResearch Manufacturing Co., The Garrett Corp., Oct. 3, 1969. (Available as NASA CR-111812.)

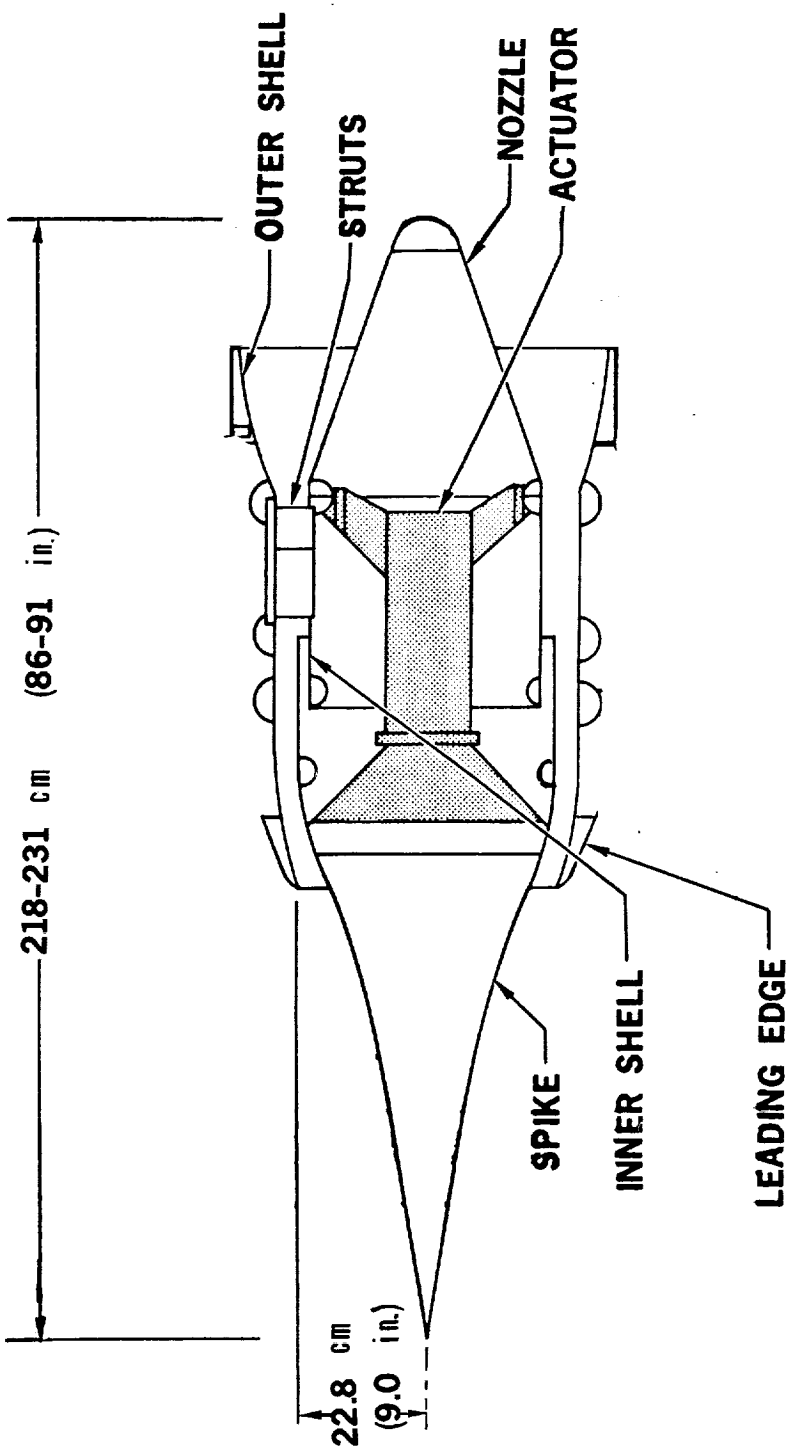

Figure 1.- Schematic of general aerodynamic shape and structural components.

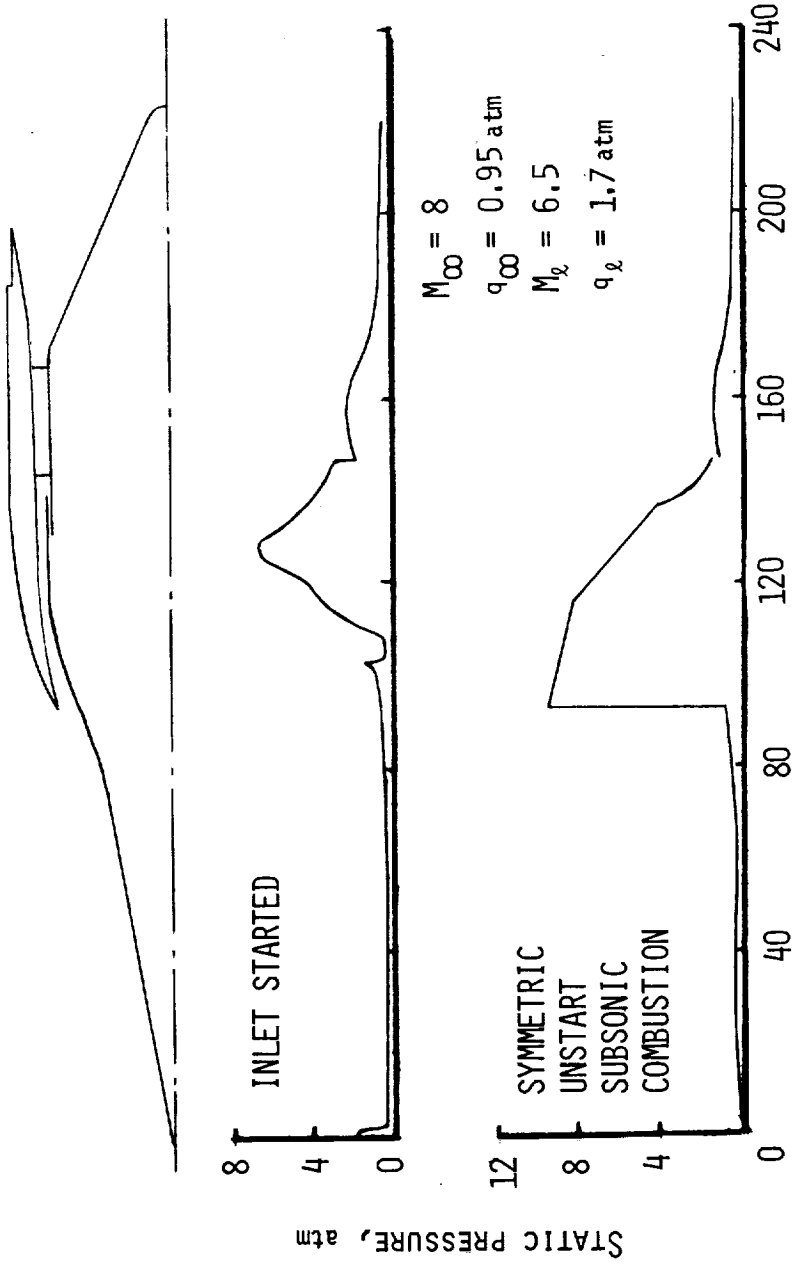

Figure 2.- HRE pressure distribution.

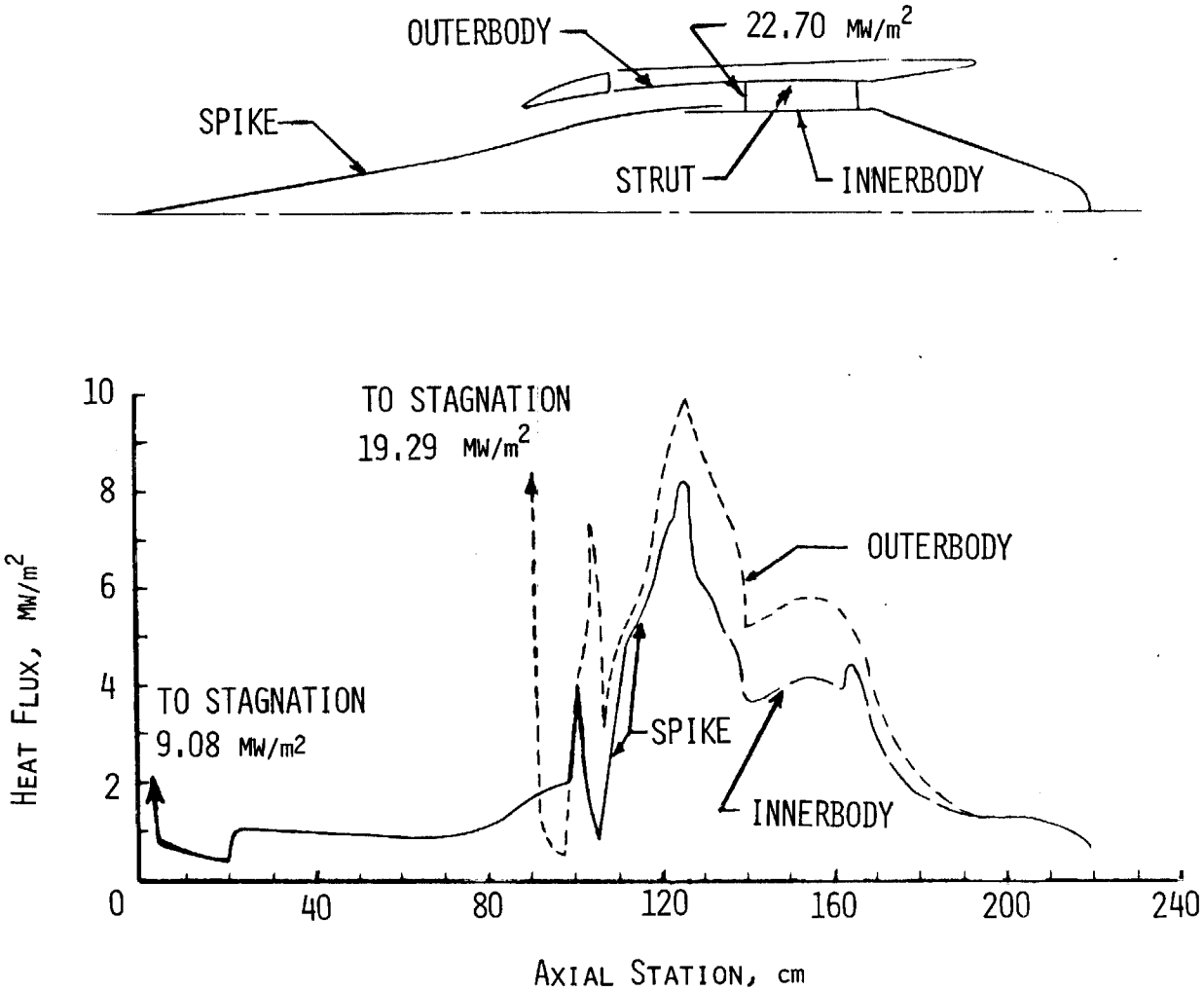

Figure 3.- HRE heat-flux distribution. $M_\infty = 8$.

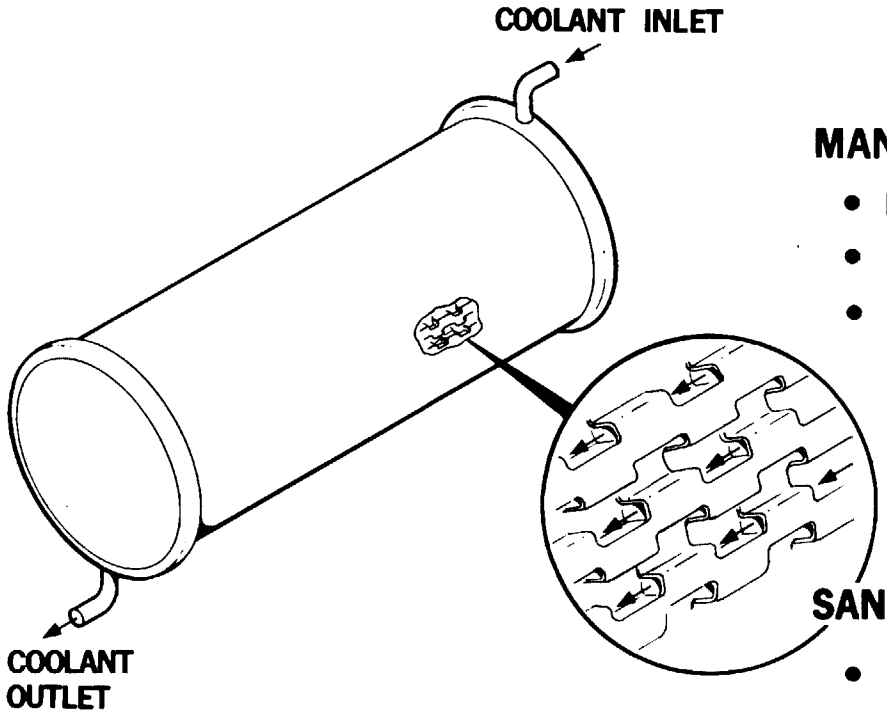

MANIFOLDS

- FLOW INLET/OUTLET
- RING REINFORCEMENT
- SUPPORT STRUCTURE

SANDWICH SHELLS

- AERODYNAMIC CONTOURS
- COOLANT FLOW PASSAGES
- AERODYNAMIC PRESSURES
- SHOCK, INERTIA, VIBRATION

THERMAL CONTROL

- AERODYNAMIC SHAPE
- DISTORTION OF PRIMARY STRUCTURE
- LOCAL ΔT
- TRANSIENT T AND ΔT

Figure 4.- Thermal-structural integration.

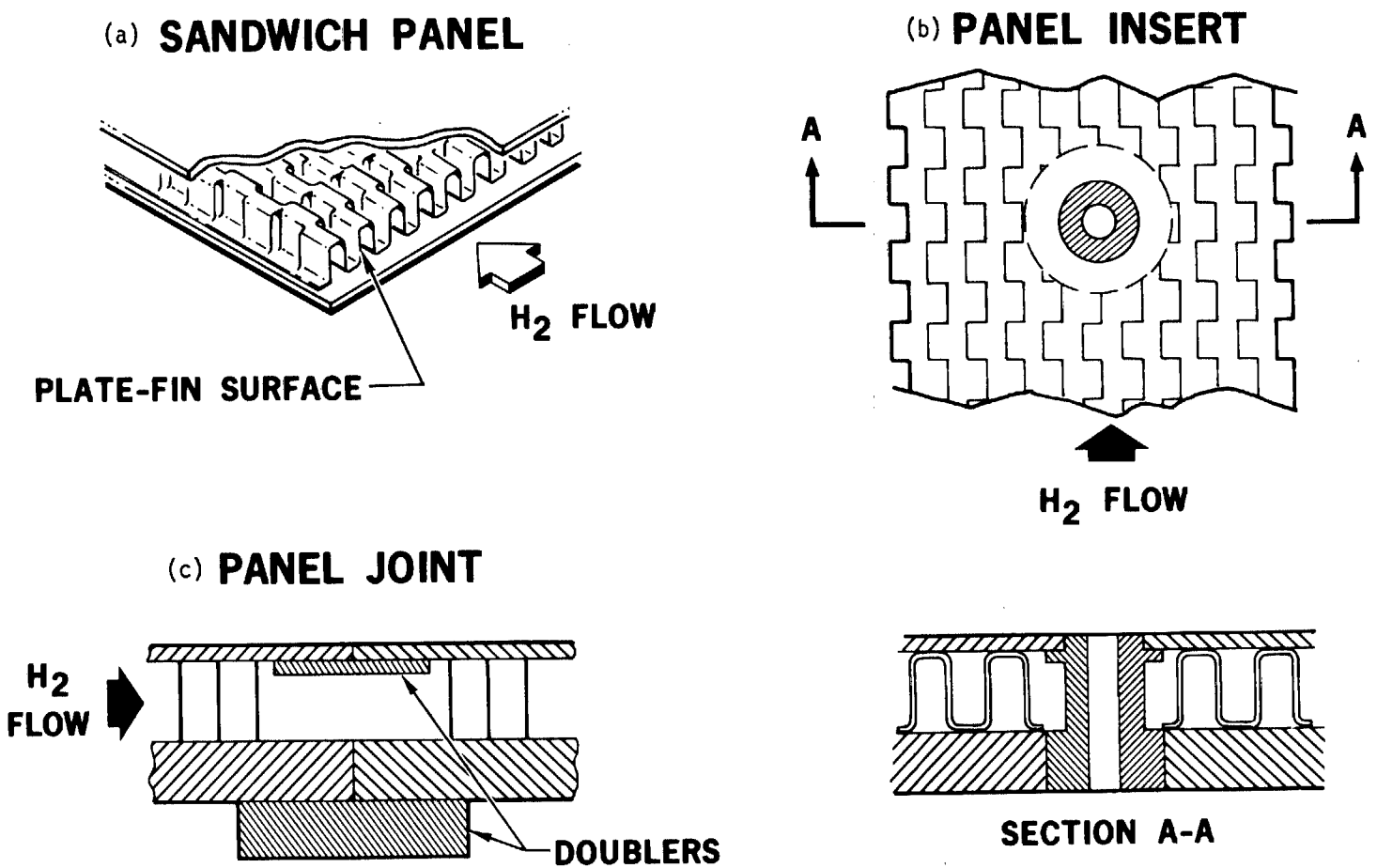

Figure 5.- Sandwich panel features.

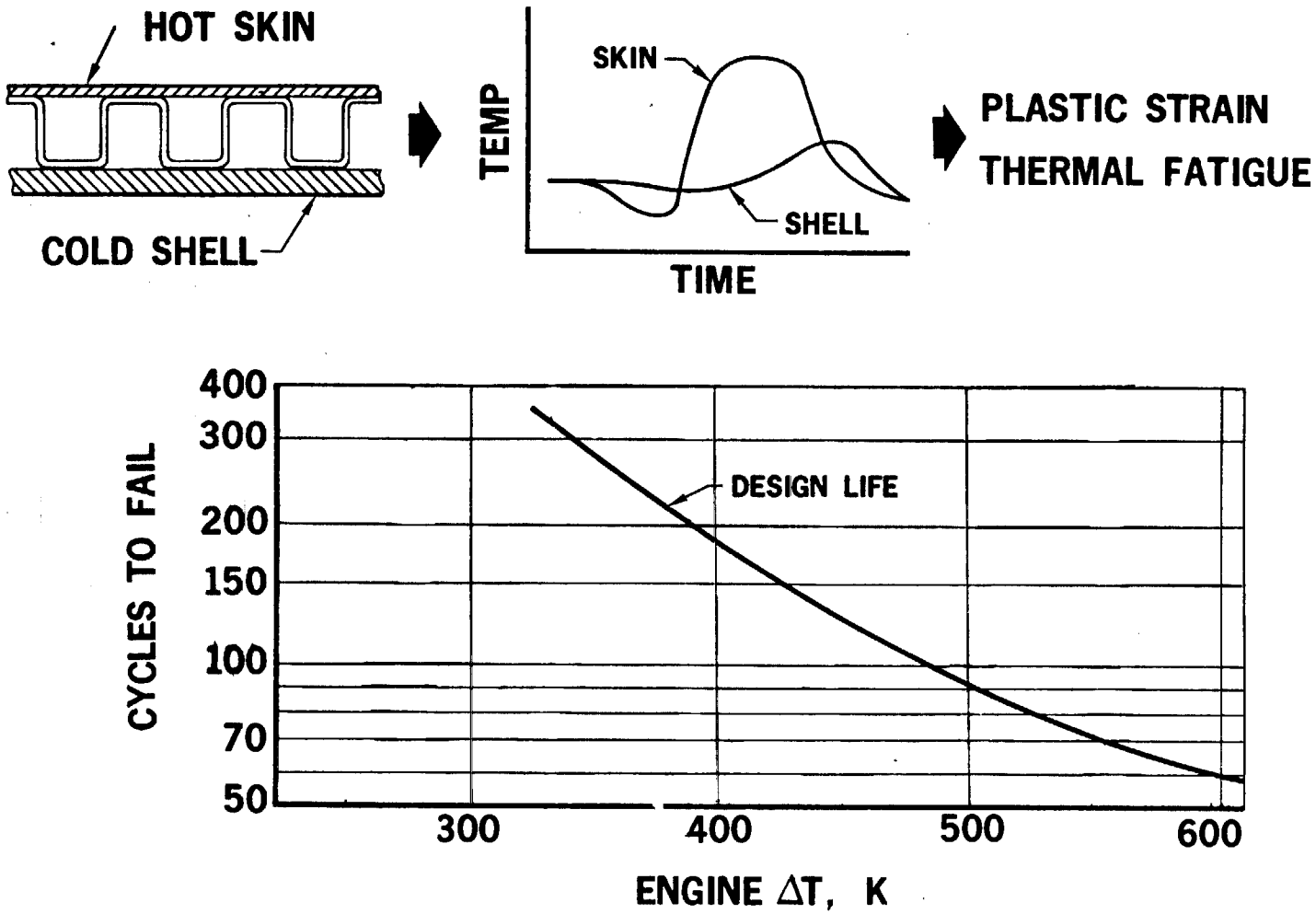

Figure 6.- Thermal fatigue.

PRESSURE CONTAINMENT

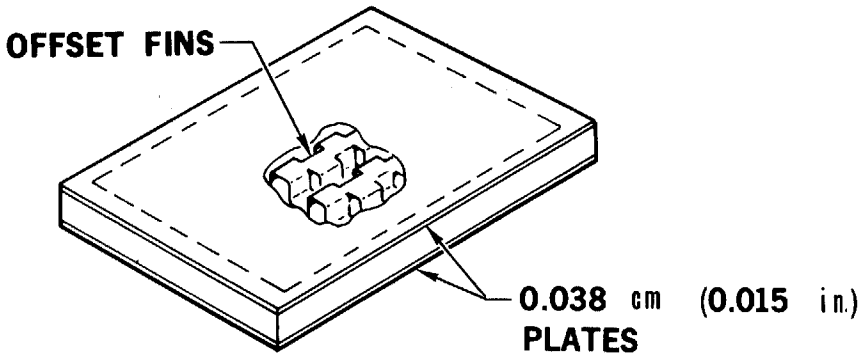

- BURST
  - ROOM TEMPERATURE
  - 1145 K (2060° R)
- CREEP-RUPTURE
  - 1145 K (2060° R)

THERMAL FATIGUE

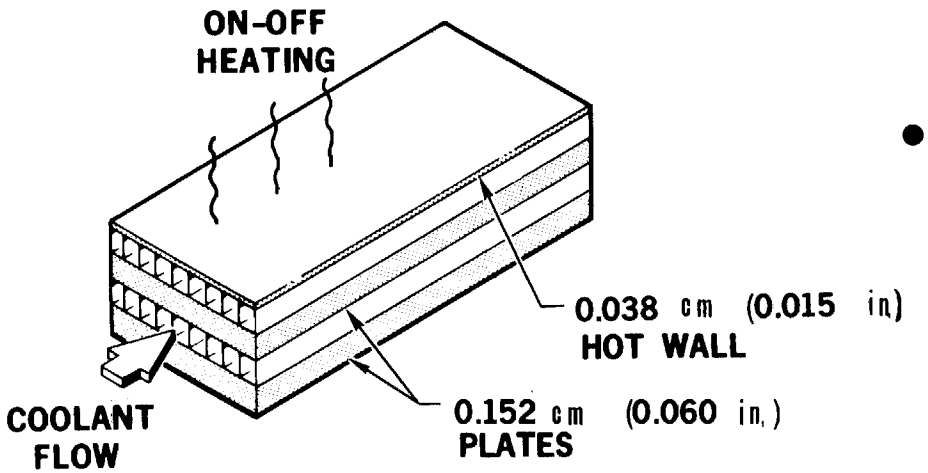

- THERMAL CYCLING
  - ΔT = 361-528 K (650-950° R)
  - T = 1083 K (1960° R)

Figure 7.- Structural sandwich tests.

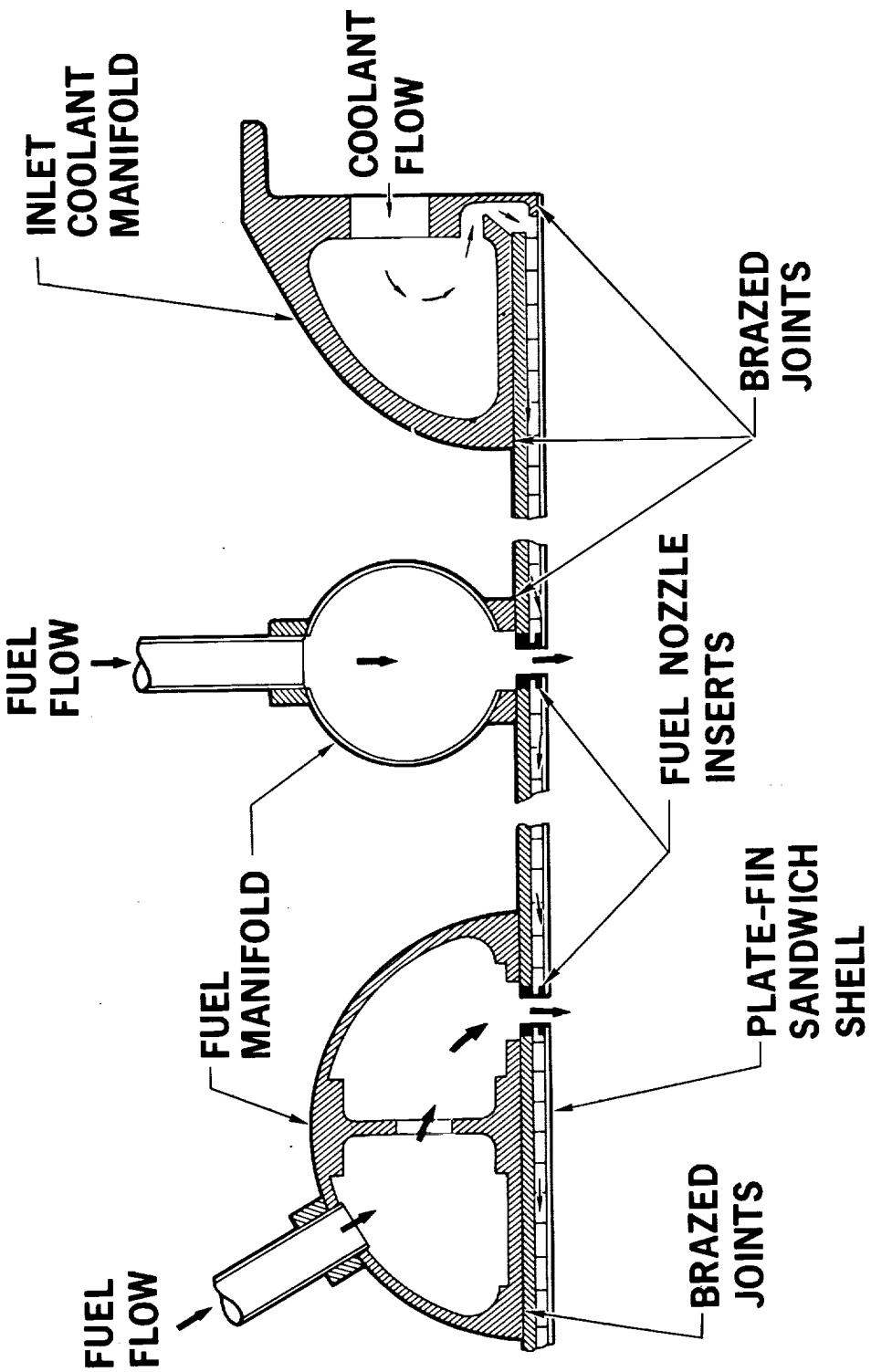

Figure 8.- Shell assembly.

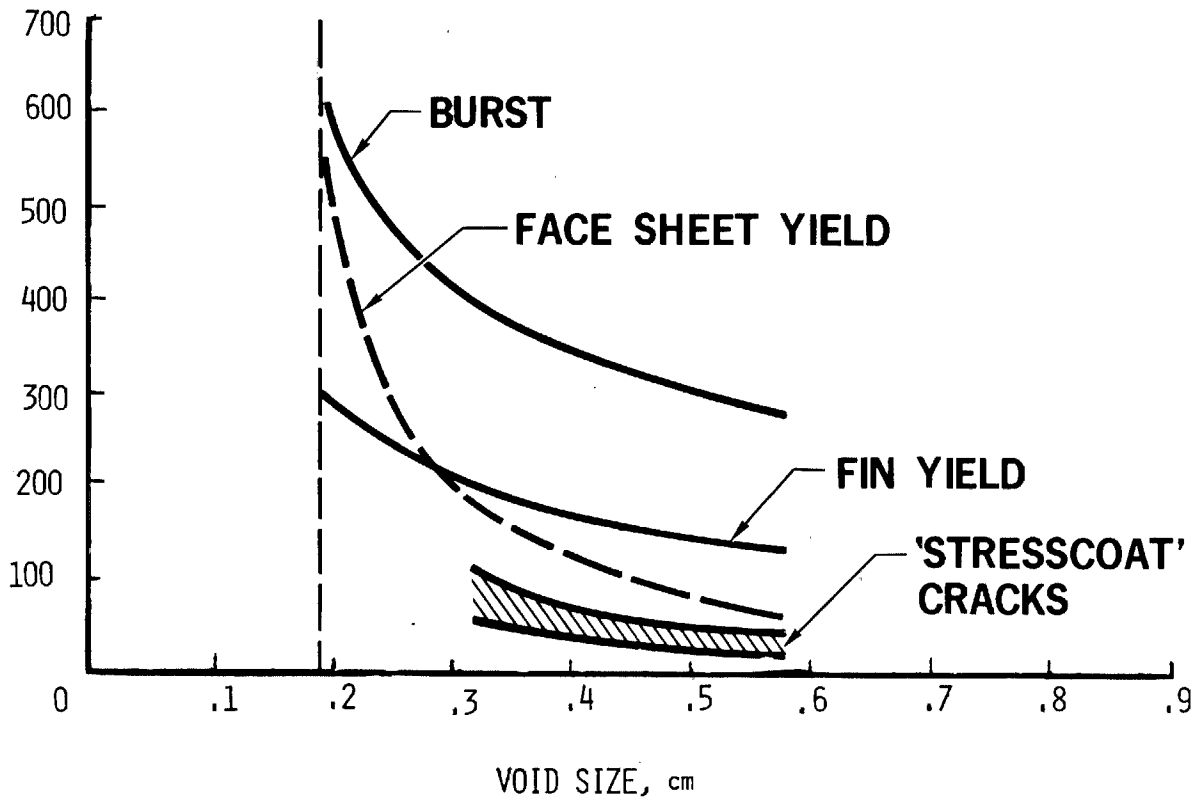

Figure 9.- Nondestructive testing results for cooled structure.

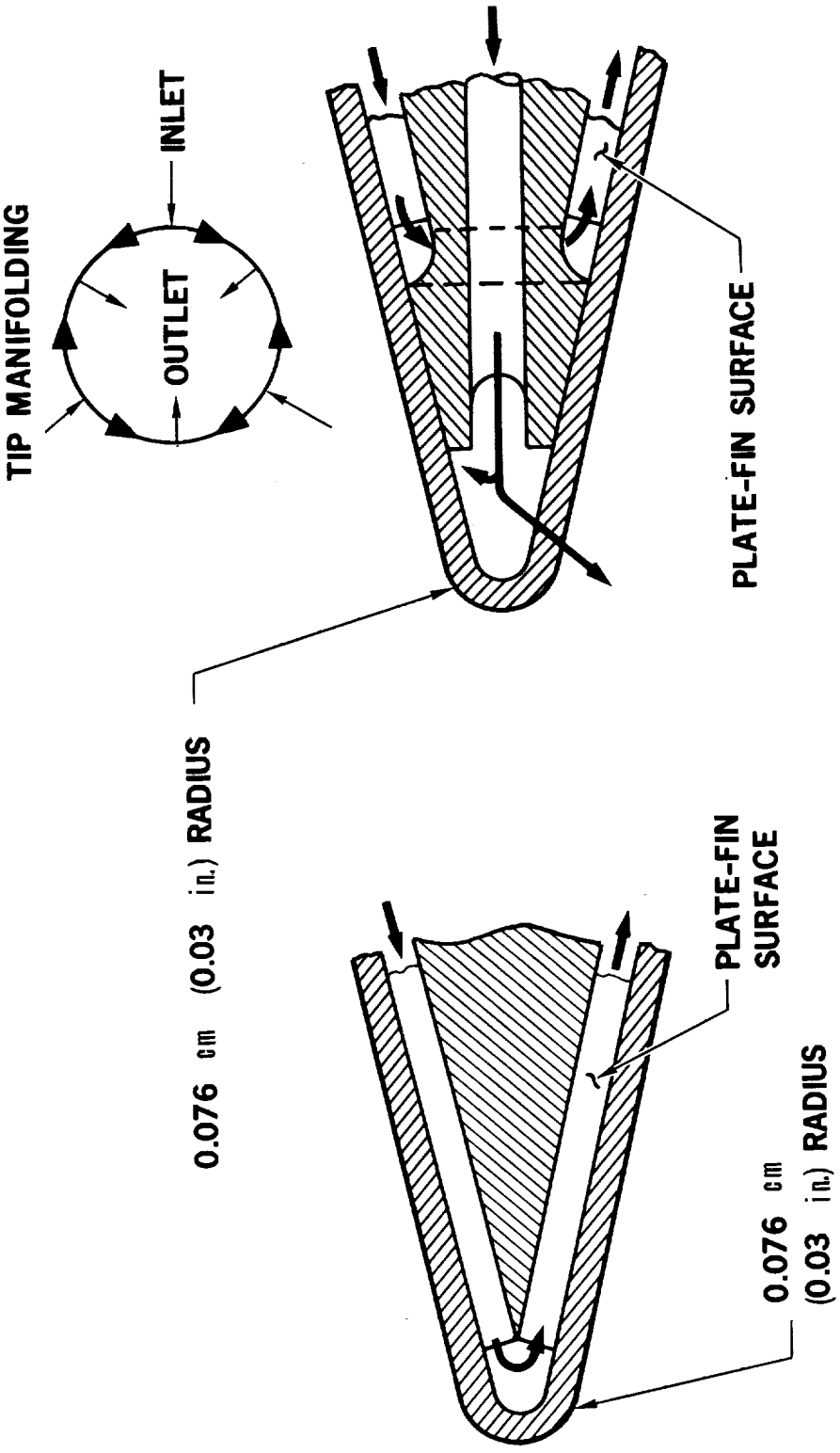

Figure 10.- Leading-edge configurations.

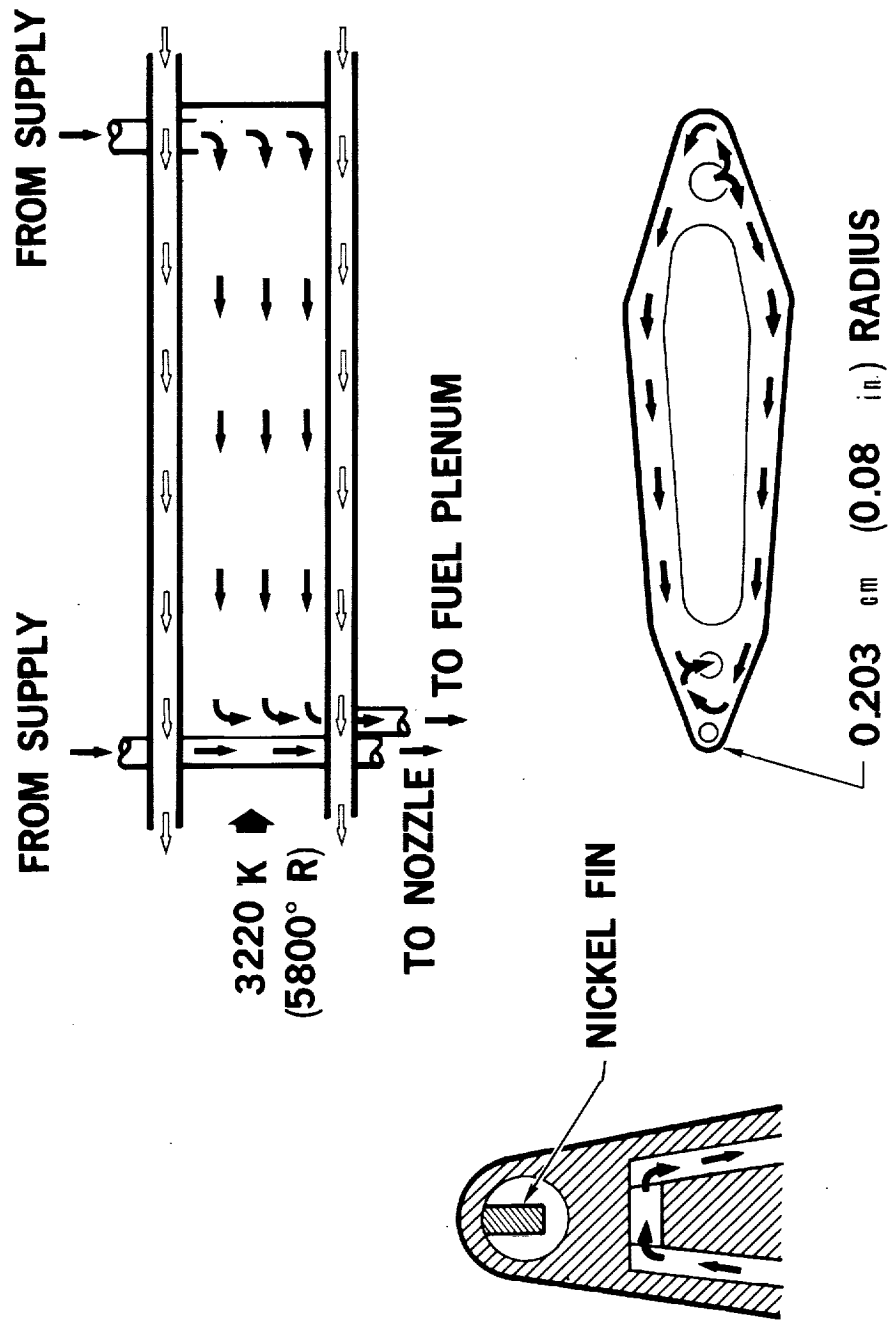

Figure 11.- Strut design.

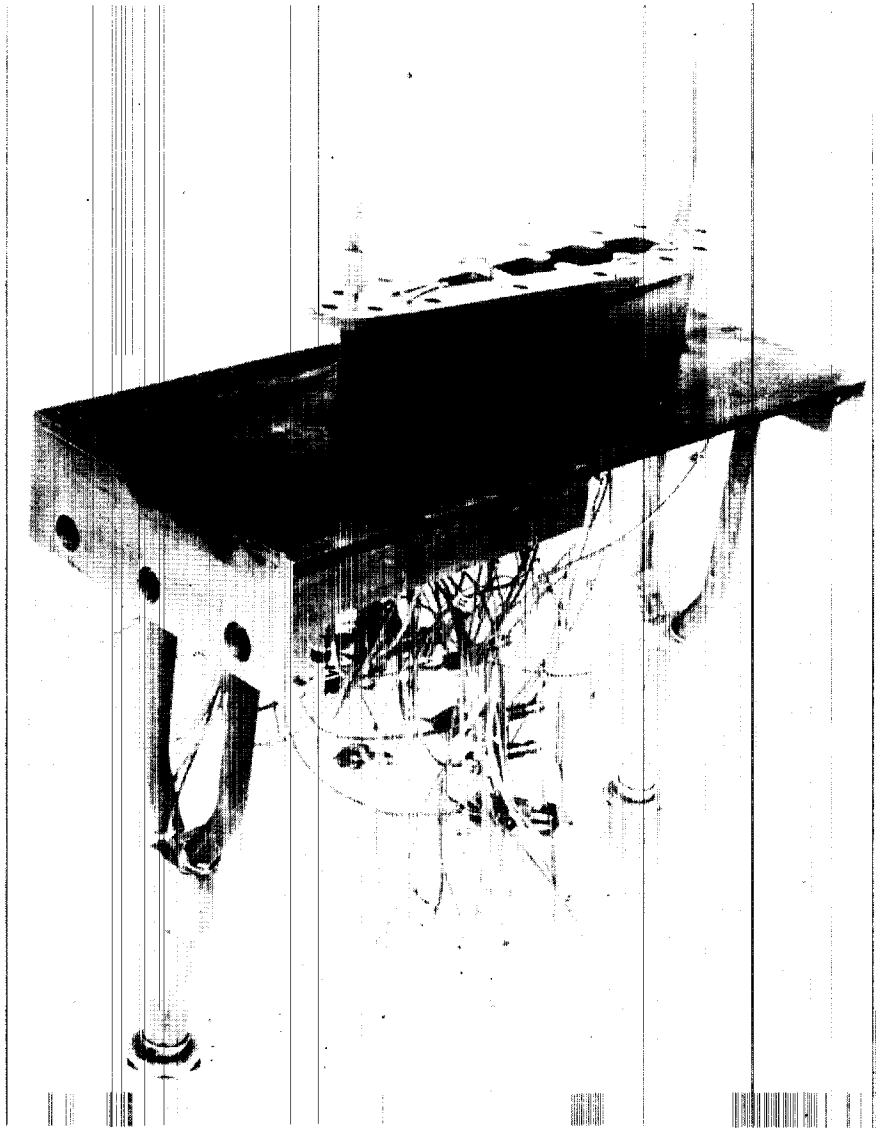

- STRUT L.E. DESIGN
  - 0.203 cm RADIUS
  - FIN
- STRUT-TO-SHELL JOINT DESIGN
- THERMAL FATIGUE
- FLOW DISTRIBUTION
- FABRICATION

L-72-2428

Figure 12.- Strut tests.

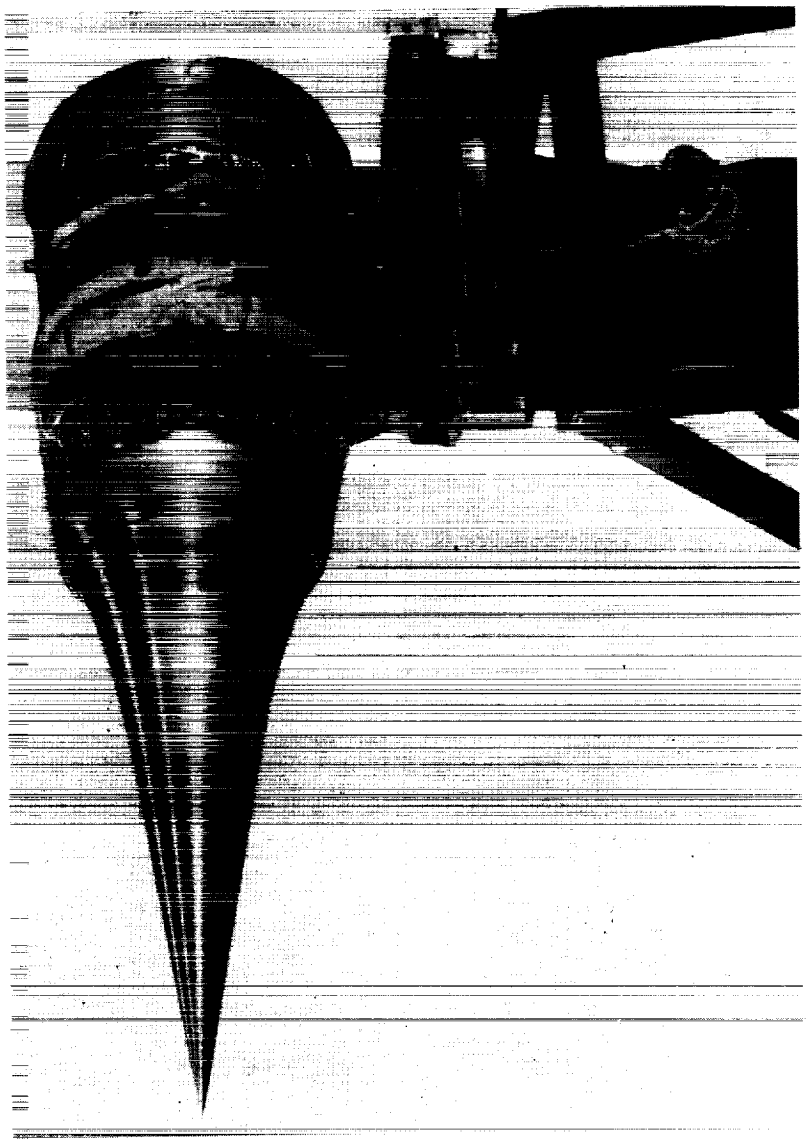

L-72-2429

Figure 13.- HRE SAM engine assembly.

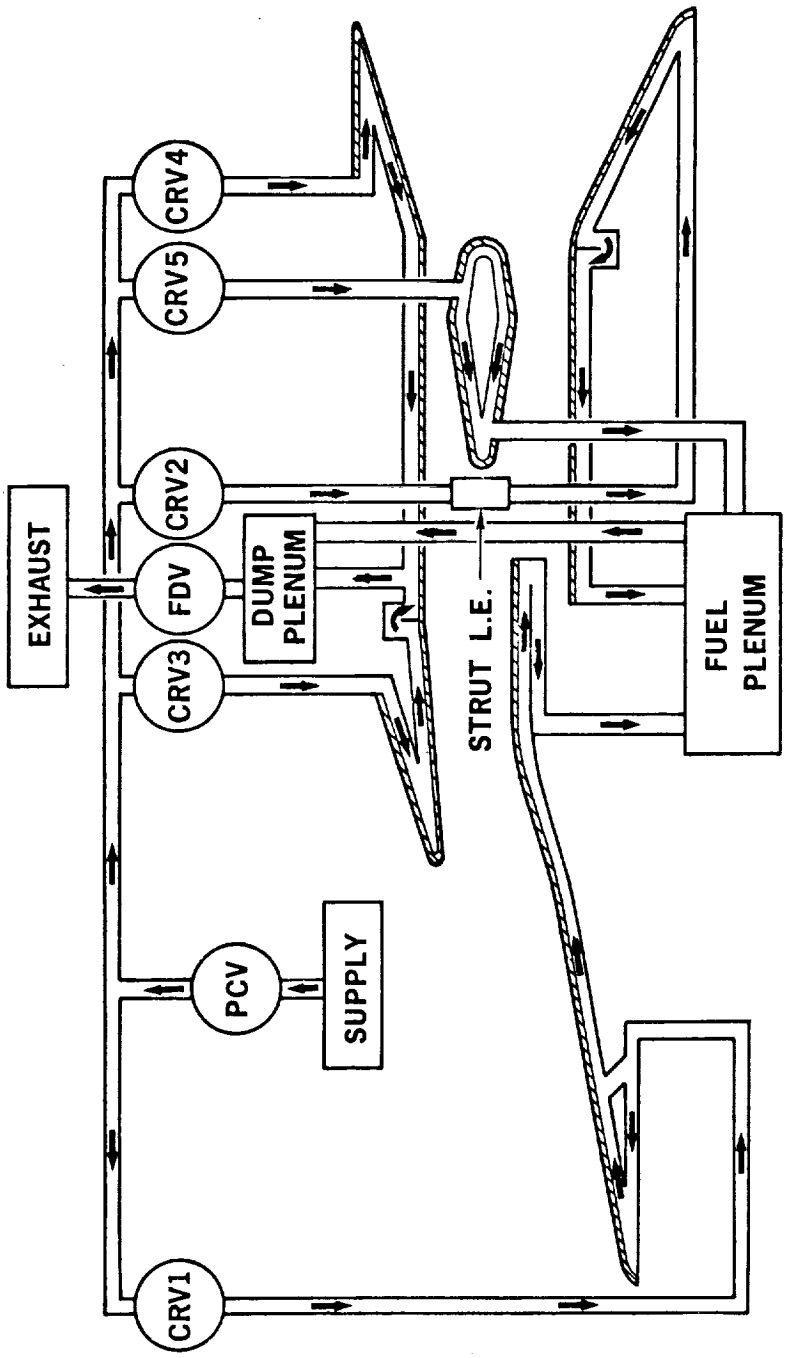

Figure 14.- Schematic of HRE/SAM hydrogen coolant flow routing.

TESTS OF THE HYPERSONIC RESEARCH ENGINE HYDROGEN-COOLED STRUCTURE AT MACH 7

H. N. Kelly
Langley Research Center

and

A. A. Vuigner
AiResearch Manufacturing Co., The Garrett Corp.

INTRODUCTION

Testing of a hydrogen-cooled hypersonic propulsion system in a high-energy level-ground test facility requires the safe and practical integration of the tunnel control, engine, and supporting systems in a rather sophisticated fashion. For not only is it imperative that the testing be accomplished safely and accurately but that neither the expensive engine nor its test facility receive significant damage in the process.

At the time the hypersonic research engine structural assembly model (described in the preceding section of this compilation) was tested in the Langley 8-foot high-temperature structures tunnel, there was no previous experience in ground testing of complete hypersonic flight engines. Prior experience with hydrogen-cooled propulsion structures was largely with tests of single-propulsion system components in a direct-connect type of test. (See ref. 1, for example.) These prior tests, therefore, were not as complex a system nor did they produce the same level of structural and functional interactions as the SAM tests.

The basic objective of these elaborate experiments was to establish the integrity and thermal performance of an aerodynamically and structurally complete, flightweight engine and its cooling system during exposures to simulated hypersonic flight. Through a general analysis of the engine internal flow, data obtained from the tests could be compared with the analytically predicted values and a verification of analytical design techniques could be established. In addition, testing of a complete engine system would provide information on difficult-to-analyze effects such as component interaction effects on localized heating and the resulting impact on the various cooling circuits.

The present paper will review the experimental procedures and some of the experimental results from the recently completed tests. The tests were conducted at a nominal Mach number of 7 over a range of stream total temperature and dynamic pressure.

SYMBOLS

M_∞	Mach number
p	pressure
p_t	facility combustor total pressure
Q/A	heat flux per unit area
q	dynamic pressure
T	temperature
ΔT	temperature difference between hot wall and structure
$\dot{w}_{H_2}$	hydrogen mass flow rate
$(\dot{w}_{H_2})_{889\ K}$	hydrogen mass flow rate for 889 K (1600° R) outlet temperature

Subscripts:

s	static pressure with p or cold structure with T
t	total conditions
w	hot-wall side of structure

Abbreviations:

CH_4	methane
H_2	hydrogen
LN_2	liquid nitrogen
CRV	coolant regulating valve
FDV	fuel dump valve

ICV injection control valve

PCV pressure control valve

APPARATUS AND TESTS

Facility

The tests were performed in the Langley 8-foot high-temperature structures tunnel shown schematically in figure 1. This facility is a hypersonic blowdown tunnel in which the high-energy level for simulating hypersonic flight is attained by burning methane and air in a high-pressure combustor. The resulting combustion gases are expanded through a conical, contoured, 2.44-meter (8-ft) exit diameter nozzle to obtain a nominal Mach 7 flow in an enclosed 4.27-meter-long (14-ft) open jet test section. Downstream of the test region, flow enters a straight tube diffuser and is pumped to atmospheric pressure by a single-stage annular air ejector. The facility is capable of simulating flight conditions for altitudes from 25 900 to 41 150 meters (85 000 to 135 000 ft) for test times from 30 to 200 seconds, depending upon the stagnation pressure. The tunnel stagnation temperature is controlled by regulating the tunnel methane-air ratio; consequently, the degree of vitiation is dependent upon the temperature. For the present tests the stream oxygen content varied from approximately 10 percent at the lowest test temperature to less than 4 percent at the maximum temperature; consequently, normal combustion could not occur in the SAM engine.

The facility is equipped with a hydraulically operated elevator to which the model to be tested is mounted. The elevator can raise the model into the hot test stream or lower the model from the stream in approximately 1 second. During tunnel startup and shutdown, the model is held in the pod below the test section to avoid severe loads associated with the transient flow conditions.

A cryogenic hydrogen handling system was provided for the SAM tests. This system consisted of a gaseous hydrogen supply, a liquid nitrogen bath heat exchanger, flexible lines for conducting cold hydrogen to and hot hydrogen from SAM, and vent stacks for dispersing the hydrogen. In the design of the hydrogen supply, control, and venting system, safety was a major criterion. To avoid possible dangerous accumulation of hydrogen within the tunnel test region, the hydrogen supply system was interlocked with tunnel operation so that hydrogen flow into the test cell and SAM was allowed only if the pressure in the test call region was below 0.07 atm. This test-region pressure level was controlled by the large air ejector normally used for the tunnel operation at reduced pressures. In addition, hydrogen sensors were employed in the tunnel test section to detect leaks and a nitrogen gas inerting system was used to minimize the possibility of damaging deflagration.

Structural Assembly Model (SAM)

The complete SAM engine is shown installed in the open jet test section of the Langley 8-foot high-temperature structures tunnel in figure 2. (The exit of the wind-tunnel nozzle is visible at the right-hand side of the figure.) A water-cooled adapter is used to protect the exterior of the engine and to mount it to that part of the floor of the tunnel which is part of the elevator assembly. (The exposed tubing is part of the water-cooling system.) During an actual test the inlet spike is hydraulically retracted from fully extended position shown to provide the desired inlet opening and to position the spike shock relative to the cowl lip.

Instrumentation.- The fully assembled SAM outside the tunnel (fig. 3) shows some of the complexity of the model installation not apparent in the preceding figure. In the background are manifolds for controlling the hydrogen and valving; in the foreground some of the instrumentation can be seen. The model is equipped with over 300 channels of instrumentation, primarily thermocouples and pressure gages, but including flowmeters, strain gages, and accelerometers.

Approximate axial locations of the pressure and temperature measurements are indicated in figure 4. Four surface pressure orifices were generally installed at each station (four grouped symbols): one at the top, bottom, and each side of the engine. Metal temperature thermocouples were generally installed in pairs (two symbols), one embedded in the hot skin, the other attached to the cooler structural skin. Bulk hydrogen pressures and temperatures were measured in the manifolds and supply lines; in addition, near the outlets of each coolant circuit, numerous thermocouples (distributed around the circumference of the engine) were installed directly in the coolant passages to measure the local hydrogen temperatures. In addition to providing research data on local conditions, these temperatures were used in the coolant flow control system.

Coolant flow control.- Hydrogen flow rates in the model were controlled by the system shown schematically in figure 5. Prior to a test the relative flow rates in the five parallel cooling flow circuits were established by adjusting the coolant regulating valves (CRV). During the test the total flow rate was controlled automatically by the fuel dump valve (FDV) operating in conjunction with the pressure control valve (PCV). The control system for the FDV sensed local coolant outlet temperatures in each of the circuits and compared the temperature with a preset reference temperature range for the particular circuit. If all outlet temperatures were below their respective reference temperature range, the FDV remained at the minimum opening which was preset manually. If any temperature exceeded its reference range, the system actuated the elevator which retracted the model from the stream and aborted the test. Within the reference temperature range, the control system modulated the FDV opening so that the most critical circuit (as determined by the hydrogen outlet temperatures) would be adequately cooled. The control

system for the PCV, in turn, sensed the pressure in the coolant outlet manifold and modulated the valve opening to maintain a preset pressure, usually 37.4 atmospheres, in the exit manifold. The injection control valve (ICV) which controlled the hydrogen flow to the fuel injectors was electronically tied to the FDV so that as the ICV opened in response to a manual command, the FDV closed so as to maintain the total flow rate demanded by the FDV control system.

Test Program and Procedure

The test program consisted of a series of steady-state performance tests and a series of thermal cycle tests. The steady-state tests, in addition to verifying the structural integrity of the engine, provided information on the steady-state performance of the cooling system that could be correlated with design calculations. The thermal-cycle tests were performed for the purpose of accruing a history of cyclic thermal stress on the engine structure. Because of the extensive time required and the backlog of other work to be performed in the facility, it was impractical to test the structure to its design life; however, the test program was sufficiently long to ensure that there were no gross discrepancies in the design of the cooled structure.

Steady-state tests.- The steady-state performance tests were conducted so that a sequence of environments of increasing severity were imposed on the engine. The initial conditions were set by a stream total temperature of 1444 K (2600° R) and a dynamic pressure of 0.212 atm (p_t = 64.5 atm). The maximum conditions were set by a total temperature of 1888 K (3400° R) and a dynamic pressure of 0.944 atm (p_t = 224 atm). At the lower stream total temperature the hydrogen coolant was introduced at ambient temperature; at temperatures of 1666 K (3000° R) and above, cryogenic hydrogen with an inlet temperature of approximately 83 K (150° R) was used. For most of the tests (both steady state and thermal cycle), the inlet spike was positioned so that the shock from the spike tip would lie slightly outside the cowl lip; during the latter runs at the most severe tunnel conditions, however, the spike was positioned so that the shock (as determined from schlieren photographs) impinged directly on the cowl lip. The model was tested at an angle of attack of 0° except for the last three tests where the model was pitched at an angle of attack of 3°.

For each of the performance tests, the procedure was the same; hydrogen coolant flow was established; the model was inserted into the tunnel test stream; the spike was retracted to a predetermined position; hydrogen injection was initiated (if applicable); and the engine was allowed to reach steady-state conditions or as near steady state as tunnel test time would permit.

Steady-state aerodynamic conditions, as determined by model surface static-pressure measurements, were achieved in less than 5 seconds of run time for most

static-pressure orifice locations. The attainment of steady-state thermal conditions was dependent upon the thermal capacity of the flowing coolant relative to the thermal mass of the structure. Steady-state thermal conditions, as determined by hydrogen outlet temperature histories, were achieved in 10 to 30 seconds on the spike and leading-edge flow routes. On the aft routes (innerbody, outerbody, trailing edge, and struts) at total temperatures of 1666 K (3000° R) and above, steady-state conditions were achieved in approximately 40 seconds. At lower test conditions where coolant flow rates were reduced, steady-state conditions were not attained on the aft routes.

Thermal cycle tests.- The thermal cycle tests were performed at a tunnel stagnation temperature and pressure of 1500 K (2700° R) and 92.8 atm (dynamic pressure of 0.331 atm) with ambient-temperature hydrogen as a coolant and with hydrogen injection. The test procedure was similar to that for the steady-state tests; however, no attempt was made to attain steady-state thermal conditions; instead the coolant flow rates and the time in the test stream were adjusted to provide transient temperatures and temperature differentials that were representative of the engine design conditions (flights at $M_\infty = 8$ with combustion). To accelerate the accumulation of thermal-fatigue degradation, the model was cycled in and out of the tunnel stream two or more times during each test.

Hydrogen flow rates.- The range of hydrogen flow rates used for the steady-state performance tests for stagnation temperature above 1666 K (3000° R) and for the thermal cycle tests is indicated in figure 6. These results are presented as the ratio of the actual coolant flow rate in the circuit to the design flow rate (flow rate required for a steady-state coolant outlet temperature of 889 K (1600° R). Thus a flow ratio greater than unity indicates overcooling relative to the design flow rate; a flow ratio less than unity indicates undercooling. During the steady-state tests the initial test at a given tunnel condition was generally significantly overcooled as indicated by the flow ratios; for subsequent tests at that condition the preset reference temperatures were increased (coolant flow rates were reduced) to achieve flow ratios close to 1.0 so that steady-state heat loads could be obtained and correlated. For the thermal cycle tests, the coolant flow rates were reduced so that hot wall surface temperatures and structural temperature differentials were representative of those expected at Mach 8 with combustion. As indicated, the leading-edge route was undercooled only moderately so that foreign-object damage to the cowl lip (to be discussed subsequently) sustained during some of the early tests would not be aggravated.

RESULTS AND DISCUSSION

Steady-State Data

Steady-state results provide a direct evaluation of the thermal performance of the hydrogen cooling system and a basis for an assessment of the adequacy of analytical design methods. In the present section steady-state results obtained at the most severe

test conditions (T_t = 1888 K (3400° R); p_t = 224 atm; q = 0.944 atm) are presented and compared with predictions based on the analytical methods employed in the design of the cooling system for the engine.

Static-pressure distributions.- Experimental static-pressure distributions (measured on the surface of the model along the lateral center line) with and without hydrogen injection are presented in figure 7 and compared with the predicted distribution for the engine without hydrogen injection. The results with injection, denoted by the flagged symbols, were obtained at a hydrogen injection rate of 159 g/sec (0.35 lb/sec) which corresponded to a fuel equivalence ratio of 0.41 based on engine mass flow rate. The analytical results for the spike and the forward part of the inlet were based on an axially symmetric inlet program which utilizes a characteristic solution and accounts for the effects of real gas and a viscous boundary layer. The remainder of the engine internal flow conditions were based on a one-dimensional analysis.

Static-pressure measurements without injection are in good agreement with the prediction on the spike and inlet sections. Pressure measurements in the combustor and nozzle are in fair agreement with the prediction. The one-dimensional analysis does not account for local-shock boundary-layer effects such as occur in the regions of the struts. Experimental results indicate that these interaction effects may vary the pressures locally by as much as a factor of 2.0.

Static-pressure measurements with injection are generally higher than without injection particularly near the injector locations (station 109.5 cm (43.0 in.) on the spike and station 117 cm (46.0 in.) on the outerbody). These increases in static pressure are small and are similar to those data obtained with helium-injection tests of a 2/3-scale inlet model. (See ref. 2.) Since the pressure increase was small and there was no significant rise in the heat load to the engine, it was concluded that the pressure rise was a mass-addition effect and not the result of any general combustion in the engine. If combustion occurred, it was apparently limited to the thermal throat or local regions of shock interactions.

Heat-flux distributions.- From measurements of the hydrogen conditions at various stations along the coolant circuits, it was possible to deduce the average heat fluxes to the engine. These local average heat fluxes, the predicted flux distribution for the engine, and the average of the predicted heat fluxes over the same lengths as the experimental data are presented in figure 8. The predicted distributions are for the nonburning engine at the same conditions as the tests and are based on the experimental pressure distributions presented in figure 7.

The predicted distribution of flux was obtained from the same analytical techniques used in the engine design. Eckert's reference enthalpy method was used for all surfaces

which, except for the spike where Mangler's transformation was used to account for conical flow, were treated as flat plates. The virtual origin of the boundary layer was assumed to be the spike tip for the centerbody and the cowl lip for the outerbody. A transition Reynolds number of 2×10^6 was used on the spike and a transition Reynolds number of 6×10^6 was used on the interior surfaces of the outerbody.

Average calculated heat fluxes are in good agreement with average experimental heat fluxes on most of the engine surfaces except for the section between stations 114.3 cm and 142.2 cm (45 in. and 56 in.). In this region the calculated values on both the innerbody and outerbody are higher than the experimental value by 20 to 40 percent. This difference is balanced by a slight underprediction over the remaining surfaces so that the total calculated heat load is only 5 percent higher than the experimental heat load.

The close correspondence in the total heat loads increases confidence in the ability to predict the heat load of the operating engine. Provided the effect of combustion has been adequately represented in the analysis, the predicted total heat load of 11.4 megawatts (10 800 Btu/sec) for the engine operating at Mach 8 appears to be very realistic.

Surface temperature distributions.- Steady-state surface temperature distributions derived from SAM tests at maximum steady-state test conditions are presented in figure 9 and compared with calculated temperature for the Mach 8 flight engine with combustion. Since coolant hydrogen was introduced at the extremities of the engine and flowed toward the center, the highest surface temperatures occurred near the middle of the engine as indicated in figure 9.

These results illustrate the difficulty encountered in trying to simulate the steady-state temperature distribution of a flight engine in a nonburning engine test. Although it is possible to get reasonable agreement in temperature levels over parts of each flow circuit, it is impossible to approximate the distribution over the engine length of the circuit because of the higher heat flux in the burning engine. On the spike, for example, the test temperatures on the forward spike are slightly higher than those for the flight engine because the hydrogen inlet temperature for the test is approximately 30.5 K (55° R) higher than that for the flight engine (86.1 K compared with 55.6 K or 155° R compared with 100° R); the heat flux as indicated in figure 8 is somewhat higher; and the coolant flow rate is lower (127 g/sec compared with 295 g/sec for flight, or 0.28 lb/sec compared with 0.65 lb/sec); however, inside the engine where combustion occurs in the flight engine, gas surface temperatures exceed those for the SAM test and reach the design temperature of 1028 K (1850° R) near the end of the spike compared with 888 K (1600° R) for the nonburning engine with the low coolant flows. Similarly, the temperature at the outerbody outlet manifold is 907 K (1650° R) for SAM compared with 1138 K (2050° R) for the operating engine. Somewhat better agreement could be obtained at the outlets by further reducing the hydrogen coolant flow; however, as will be discussed

subsequently, the presence of local areas of high heat flux compounded by reduced thermal conductance and slower thermal response at the lower flow rates makes the attainment of the design temperature difficult, especially for the aft flow routes.

Flow Conditions and Transient Response

It was recognized in the design of the cooled structure that localized areas of intense heating would exist in the engine duct. (See ref. 3.) The heating would arise from (1) shocks emanating from the spike and cowl lip impinging and reflecting in the duct passage, (2) shock systems formed around the fuel jets, (3) separation and subsequent reattachment of the flow downstream of the step formed by the aft end of the spike, and (4) shocks emanating from the six support struts. The exact location and intensity of the heating would, of course, be a function of the flow conditions existing in the duct and would therefore vary over the operating range of the engine. The expected heating would not significantly increase the total heat load; however, it would induce sharp local variations in structural and coolant temperatures which the structure and cooling system must accommodate.

During the thermal cycle tests in which the engine was significantly undercooled (see fig. 5), the localized heating produced discolorations in the metal skins which provided a basis for an analysis of the flow field within the engine.

Flow and heating patterns.- A model of the internal flow field of the engine (without fuel injection) and sketches of the discoloration patterns from which the flow field was constructed are presented in figure 10. The indicated maximum metal temperatures were obtained by comparing metal discolorations which occurred during the tests with calibrated discolorations of the same material. The temperatures are in excess of the temperatures obtained during the steady-state tests and approach the maximum steady-state values anticipated for the Mach 8 burning engine. (See fig. 9.)

Also presented in figure 10 are the heating intensification factors which were deduced from the flow model. In areas where there was no flow separation, the local heat-transfer increase was obtained by including local pressure gradient terms in the boundary-layer equations; in the area aft of the step where separation occurred, the method of reference 4 was used to calculate the local heating. In most cases, the localized heating was anticipated in the engine design; however, the heated area behind the step was farther aft than that predicted and the heating in the vicinity and aft of the struts was more severe than that anticipated. The localized intensification in heating in the latter area is not expected to be as great for the Mach 8 operating engine since the local Mach number will be lower and the average heat flux much higher due to the presence of combustion. Nevertheless, it is significant that the cooling system and structure were able to tolerate the severe local variations imposed by the SAM test.

Figure 11 is a photograph of the nozzle showing one of the discoloration areas used in establishing the flow model. The particular area (shown in the mirror) is typical of that occurring aft of each pair of support struts (near station 178 cm or 70 in.) and is apparently due to a coalescence of shocks from the struts. Temperature-sensitive paint has been applied to the adjacent areas to enhance the definition of the heating pattern.

Plate-fin transient analysis.- The local areas of high metal temperatures indicated in the preceding figures were products of high local heat fluxes and low coolant flow rates. The effects of coolant flow rate on the transient response of the plate-fin structure in the nozzle area affected by shock interaction (station 178 cm or 70 in.) are illustrated in figure 12. The time histories presented were based on an analysis presented in reference 5 using a hot-gas heat-transfer coefficient which has been increased by a factor of three to account for the effect of shock impingement. (See fig. 10.) The higher coolant flow rate is the required rate for an 888 K (1600° R) innerbody outlet temperature for a steady-state test at 1666 K (3000° R) and 149.6 atmospheres. The lower coolant flow rate represents an undercooled case actually used during one of the tests at that condition.

Maximum wall temperatures and temperature gradients between the hot wall and structural wall are higher for the lower coolant flow rate and the thermal response is much slower. The hot wall temperature of 944 K (1700° R) predicted for the lower flow rate at the end of 35 seconds compares favorably with temperatures inferred from metal discolorations observed subsequent to tests of the same duration.

Thermal Fatigue

Thermal fatigue was recognized as a critical item in the design of the engine structure. As noted in the preceding part of this report, fatigue life is strongly dependent upon the temperature gradients (ΔT) existing in the structure.

Maximum temperature differences.- Maximum temperature differences for the SAM tests are indicated by the symbols in figure 13. Also presented for comparison are the predicted steady-state temperature differences for the Mach 8, 26 820-meter (88 000-ft) altitude design point flight condition. At the four areas indicated, the test ΔT values are locally greater than the Mach 8 steady-state values.

Transient maximum test ΔT values created by undercooling the plate-fin panels occurred at station 106.6 cm (42 in.) on the leading edge (416 K or 750° R) at station 165 cm (65 in.) on the outer shell (455 K or 820° R) and at station 177.8 cm (70 in.) on the nozzle (555 K or 1000° R). All the locations are in localized hot-gas heating areas where adjacent ΔT values are lower. The maximum leading edge ΔT occurs uniformly around the engine circumference whereas the outer shell and nozzle ΔT values occur at localized regions around the circumference.

The maximum ΔT at the outer body outlet manifold (805 K or 1450° R at station 132 cm or 52 in. on the outer shell) occurred during a test at a total temperature of 1666 K (3000° R). The total ΔT was the result of a 572 K (1030° R) positive ΔT (hot surface to manifold structure) during startup and 233 K (420° R) negative ΔT during test shutdown.

Outerbody outlet manifold.- Because of the large differences in the thermal mass of the manifold and the adjacent hot skin, large temperature differences occur in the region of the outerbody outlet manifold during insertion and retraction of the model from the test stream. The time-temperature histories of the outerbody outlet manifold structure and adjacent hot surface temperature are presented in figure 14 for a typical two cycle test run. From room temperature upon model insertion and spike retraction, the hot surface temperature increased rapidly whereas the cold structure temperature responded at a much slower rate. The structure is heated primarily from the near-stagnant outlet hydrogen in the manifold. The maximum ΔT of a hot surface to a cold structure of 522 K (940° R) occurred during both hot surace and initial structural heating; the peak hot surface temperature of 888 K (1599° R) occurred at the onset of spike extension and model withdrawal in the pod. During the dwell time in the pod, hydrogen coolant flow was maintained and the hot surface temperature decreased below the cold structure temperature and resulted in a small ΔT reversal. The fatigue-life degradation accrued during each cycle is dependent upon the maximum temperature at the maximum positive ΔT and the absolute sum of the two ΔT values.

Upon model insertion and spike retraction, the cycle was repeated; for the second cycle the maximum positive ΔT for a hot surface to a structure of 294 K (529° R) was less than the value of 469 K (844° R) experienced during the first cycle because the structure temperature was higher at the start of the second cycle. At the end of the second cycle, however, the higher structure temperature produced a larger negative ΔT (236 K or 426° R) than that experienced during the first cycle. Thus, the total ΔT was 539 K (970° R) for the first cycle and 542 K (975° R) for the second cycle; hence, the fatigue life degradation accrued in each cycle was approximately the same.

Thermal-fatigue summary.- A summary of the calculated fatigue life degradation incurred in the region of the outerbody outlet manifold is presented in table I. The summary includes the degradation accrued during the performance tests as well as the cyclic tests and is grouped according to tunnel test conditions. Although the cyclic tests account for the largest degradation fraction, some of the performance tests in which the high temperatures and large temperature differences were encountered account for a disproportionate share of the calculated degradation. The total degradation fraction accumulated during the slightly over 30 minutes of testing is 45.7 percent. For the somewhat less

severe design conditions for Mach 8 flight, this fraction would correspond to about 60 thermal duty cycles.

Post-Test Model Condition

Perhaps the single most important result of the investigation was that after completion of the intended test program, the hydrogen-cooled structure remained intact and there was no visible evidence of thermal fatigue cracking in the hot skin of the model. This result does not mean, however, that the model did not sustain some minor damage; this damage will be discussed with the aid of the remaining figures.

Nozzle innerbody.- During tests where high nozzle surface temperatures were desired, the nozzle coolant flow rate was much reduced. This reduced coolant flow combined with the localized heating of the nozzle near station 178 cm (70 in.) produced some distortion of the nozzle surface. (See fig. 15.) As shown by the sketch, the distortion which occurred only in the area of local heating was approximately 0.019 cm (0.007 in.) high and was located in an area where the hot skin is not supported by the manifold or heat-transfer fins. The shrinking of this distorted metal upon cooldown forced the relatively thin forward edge of the manifold to distort between attachment bolts. The distortion and the related rolling of the manifold edge allowed some hydrogen leakage around the transfer ports. However, by relieving the lip of the manifold and replacing the "0"-ring seals, this leakage was stopped.

Some slight hydrogen leakage was also detected further forward on the innerbody around the base of the struts. Although unconfirmed without dismantling the engine, it is believed that the leakage occurred in the brazed joints between the hot skin and the headers around the strut cutouts in the innerbody and may have been precipitated by nonuniform heating in the area. In any event, the leakage was not sufficiently severe to curtail testing.

Foreign object damage.- The most significant damage to the hydrogen-cooled structure was that caused by foreign objects impinging on the forward section of the model. Figure 16 is a closeup photograph of some of the damage to the cowl leading edge. As can be seen, there are numerous dents which are sufficiently large to completely block hydrogen flow passages locally and actual holes, which are up to 0.159 cm (0.0625 in.) in diameter, in this area of critical stagnation and shock-impingement heating. Some of this damage occurred early in the test program; however, there is no evidence of thermal distress or coolant starvation. The ability of the cowl leading edge to tolerate this damage tends to confirm the suitability of the selected design which features coolant flow in the streamwise direction normal to the leading edge.

CONCLUDING REMARKS

The HRE-SAM tests have exposed a complete, representative, hydrogen-cooled engine structure to a realistic, hypersonic-flight environment. The model was subjected to stream total temperature up to 1888 K (3400° R) at dynamic pressures up to 0.944 atm (2000 psf) and was in the Mach 7 stream for a total of 55 times to accumulate 30 minutes of test exposure. The structure was exposed to temperatures and temperature differences that met or exceeded the Mach 8 design conditions.

The serviceability of the flightweight SAM plate fin-cooled structure was clearly demonstrated even with foreign object damages to the cowl leading edge. The coolant system was capable of maintaining acceptable temperature levels and was tolerant of large heating nonuniformities. The design methods for predicting aerodynamic and thermal conditions in the engine appear to be adequate.

REFERENCES

1. Elkins, P. E.; and Rouse, R. W.: 1966 Advanced Ramjet Concepts. Vol. V – Advanced Nozzles and Ramjet Structures. AFAPL-TR-67-118, Vol. V, U.S. Air Force, Mar. 1968.

2. Pearson, L. W.: Hypersonic Research Engine Project. Phase IIA – Inlet Program. Final Technical Data Report. AP-69-4883 (Contract No. NAS 1-6666), AiResearch Manufacturing Co., The Garrett Corp., Mar. 27, 1969. (Available as NASA CR-66797.)

3. Engineering Staff: Hypersonic Research Engine Project. Phase IIA – Structures and Cooling Development. Eighth Interim Technical Data Report. AP-69-4759 (Contract No. NAS 1-6666), AiResearch Manufacturing Co., The Garrett Corp., Feb. 27, 1969. (Available as NASA CR-66998.)

4. Engineering Staff: Hypersonic Research Engine Project. Phase II – Structures and Cooling Development. Sixteenth Interim Technical Data Report. AP-71-7185 (Contract No. NAS 1-6666), AiResearch Manufacturing Co., The Garrett Corp., Mar. 18, 1971. (Available as NASA CR-112057.)

5. Engineering Staff: Hypersonic Research Engine Project. Phase II – Structures Assembly Model (SAM) Test Report. AP-71-7702 (Contract No. NAS 1-6666), AiResearch Manufacturing Co., The Garrett Corp., Sept. 22, 1971. (Available as NASA CR-111993.)

TABLE I.- THERMAL-FATIGUE SUMMARY

OUTERBODY OUTLET MANIFOLD

Tunnel conditions		Number of cycles	Time in stream, sec	Average cycle temperatures		Degradation fraction, percent
p_t, atm	T_t, K			T_{max}, K	T, K	
64.5	1440	5	172	754	407	1.30
88.2	1500	3	135	802	527	2.12
93.6	1500	33	851	802	503	20.50
101.7	1500	3	138	872	639	3.77
149.2	1670	5	266	882	714	8.36
190	1830	1	58	796	679	1.19
224	1890	5	163	844	749	8.46
Total		55	1783 sec or 29.7 min			45.70

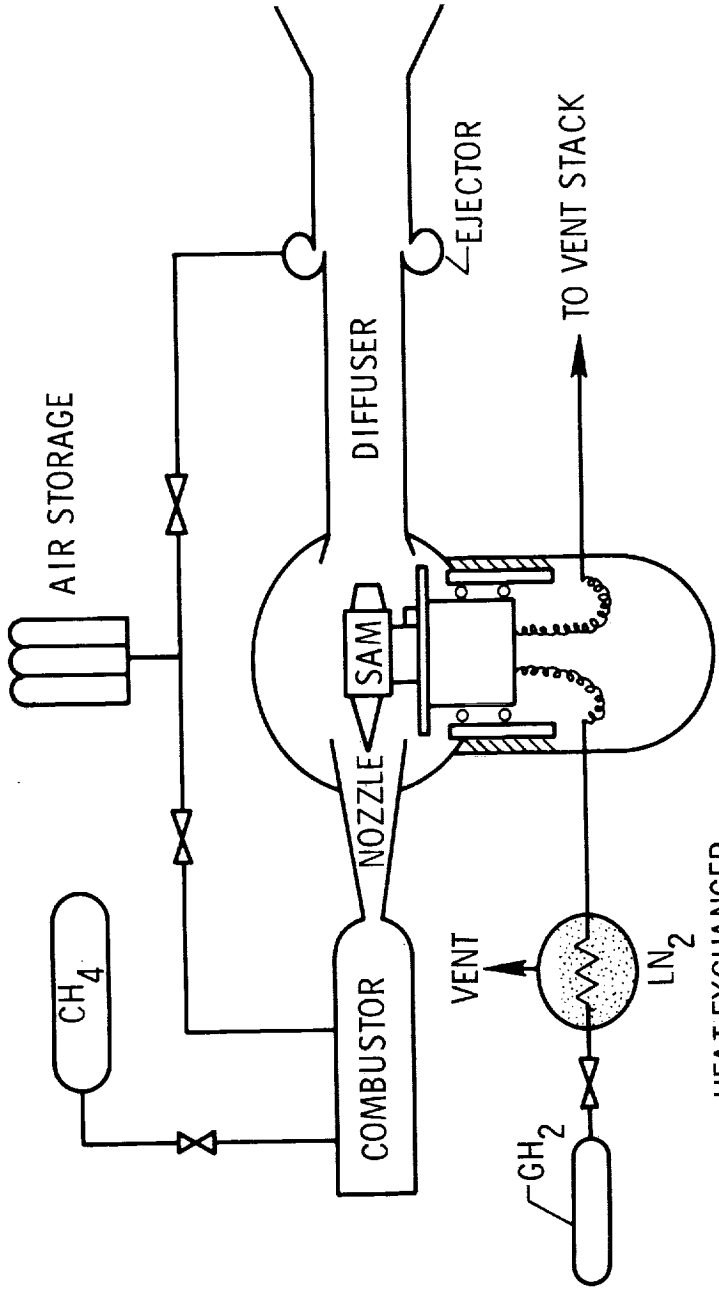

Figure 1.- Langley 8-foot high-temperature structures tunnel. HRE/SAM installation.

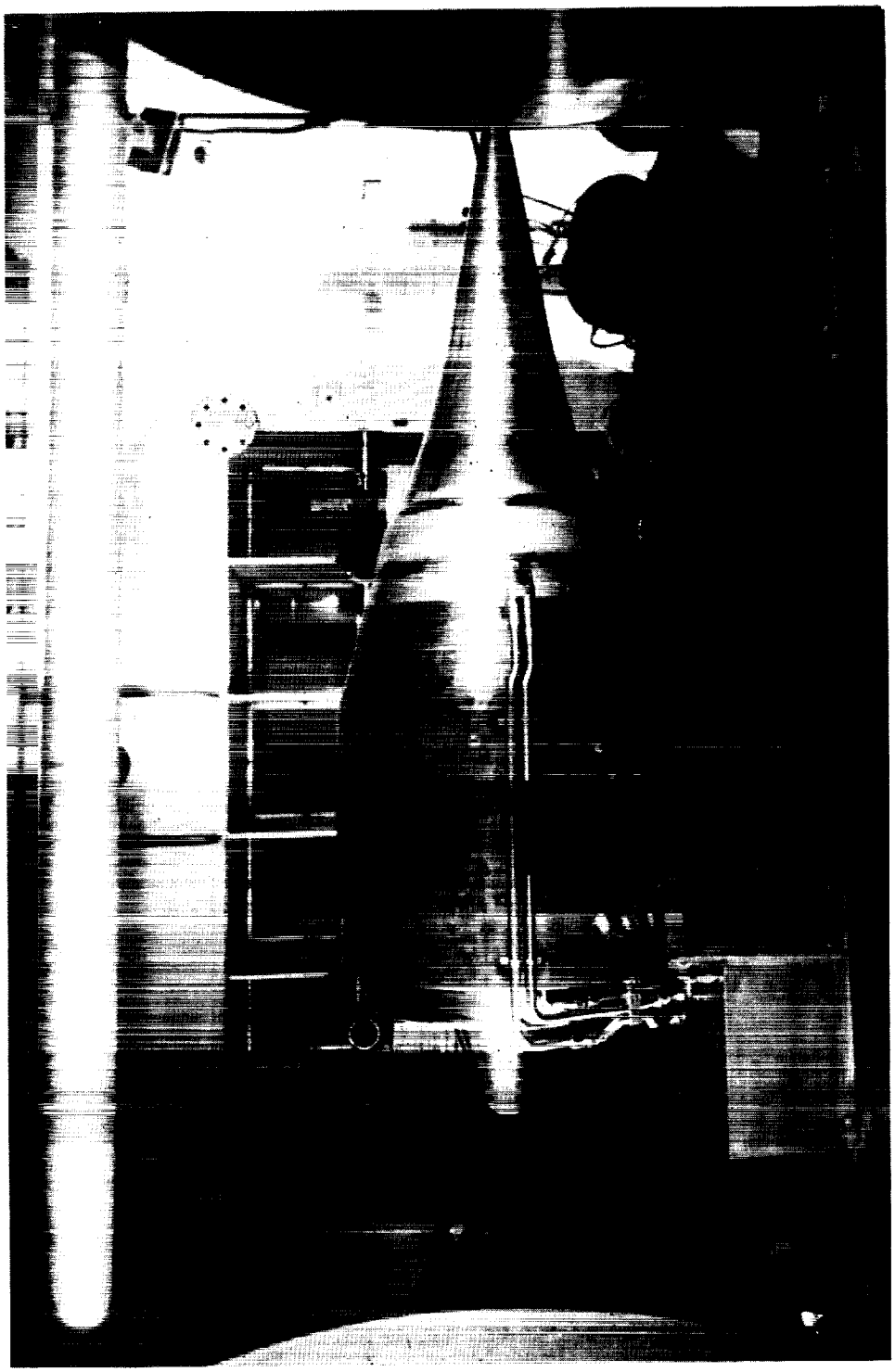

L-70-6938

Figure 2.- Hypersonic research (HRE) structural assembly model (SAM) installed in the Langley 8-foot high-temperature structures tunnel.

L-70-6345

Figure 3.- Fully assembled HRE structural assembly model before installation.

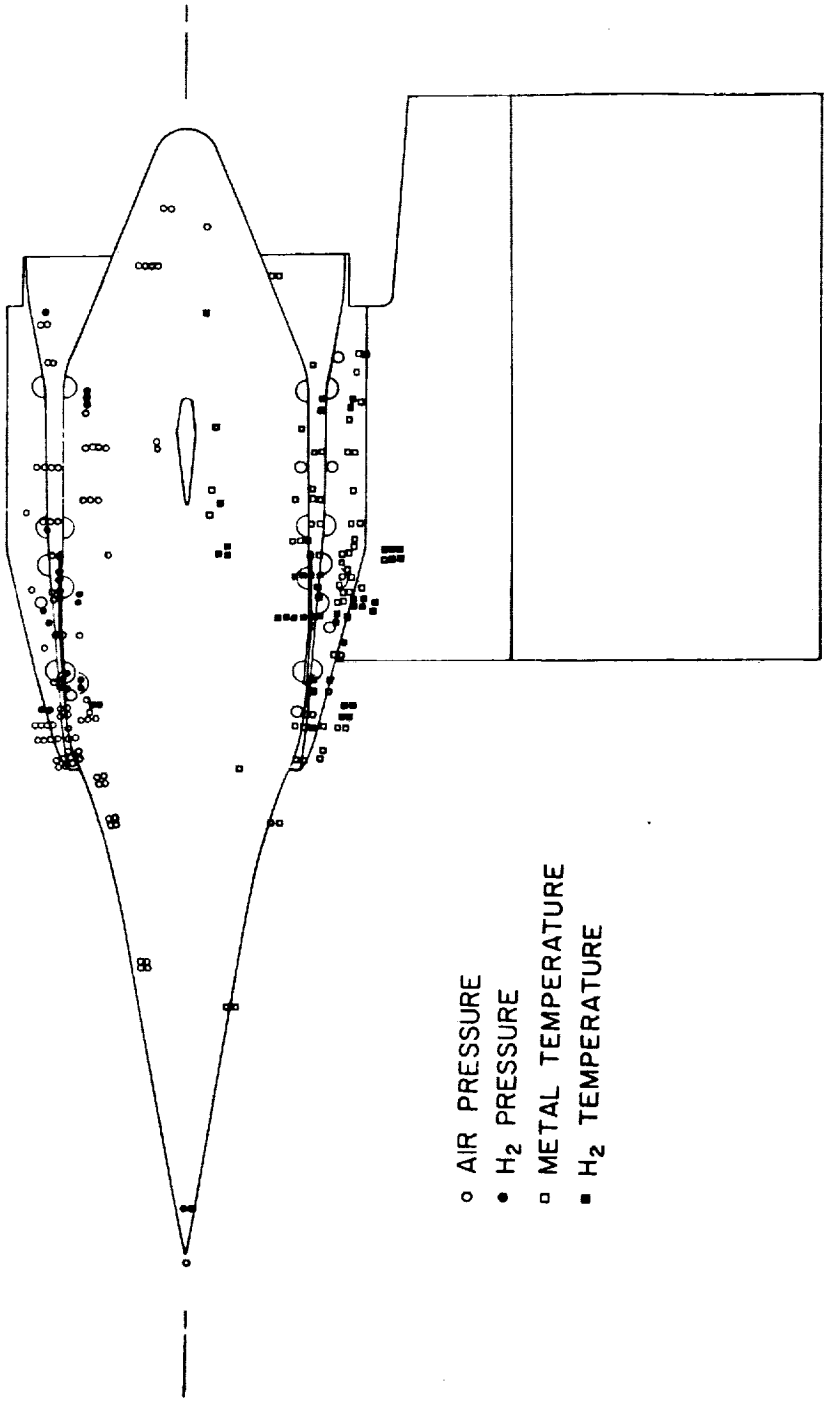

Figure 4.- HRE/SAM instrumentation locations.

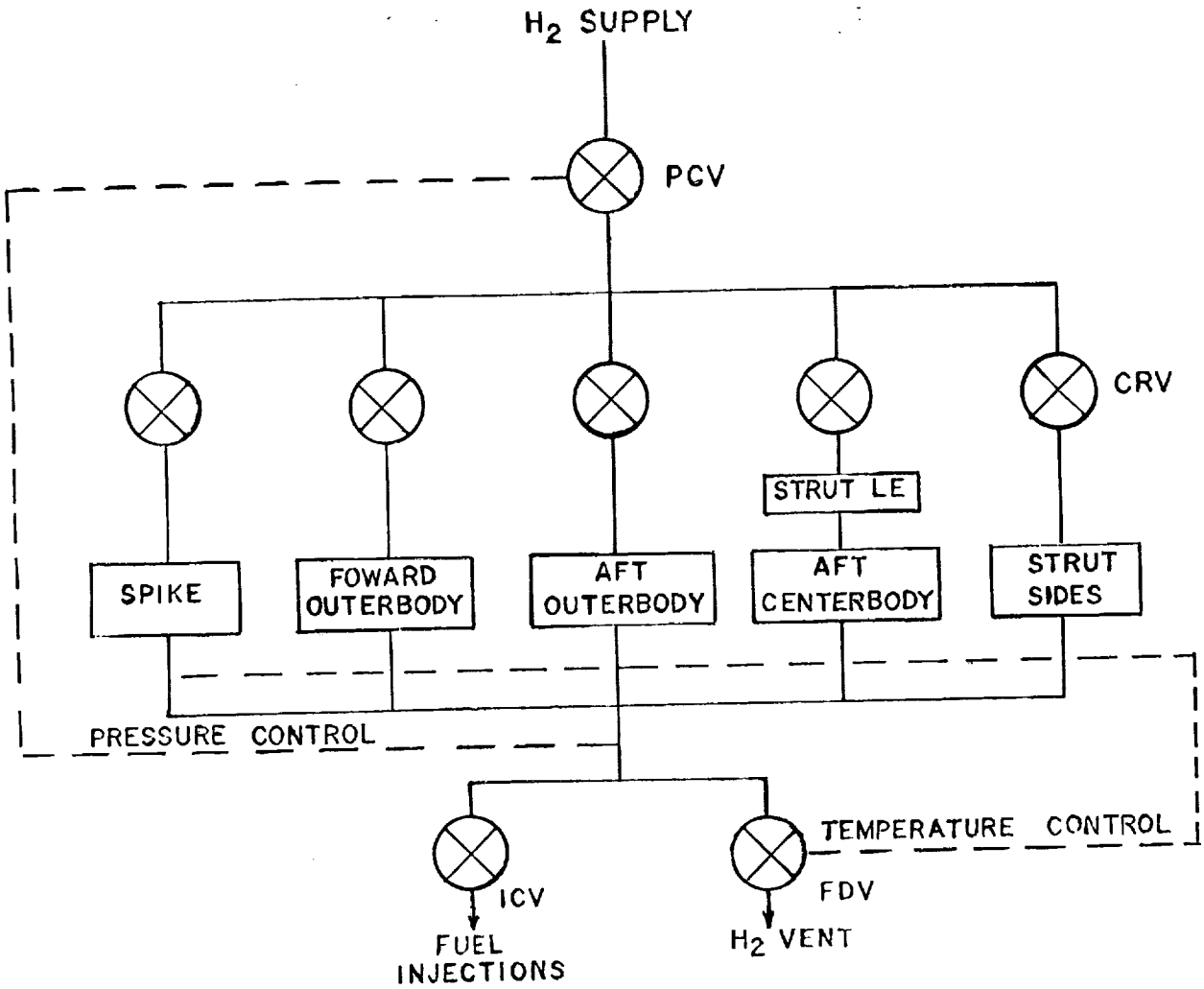

Figure 5.- HRE/SAM hydrogen system.

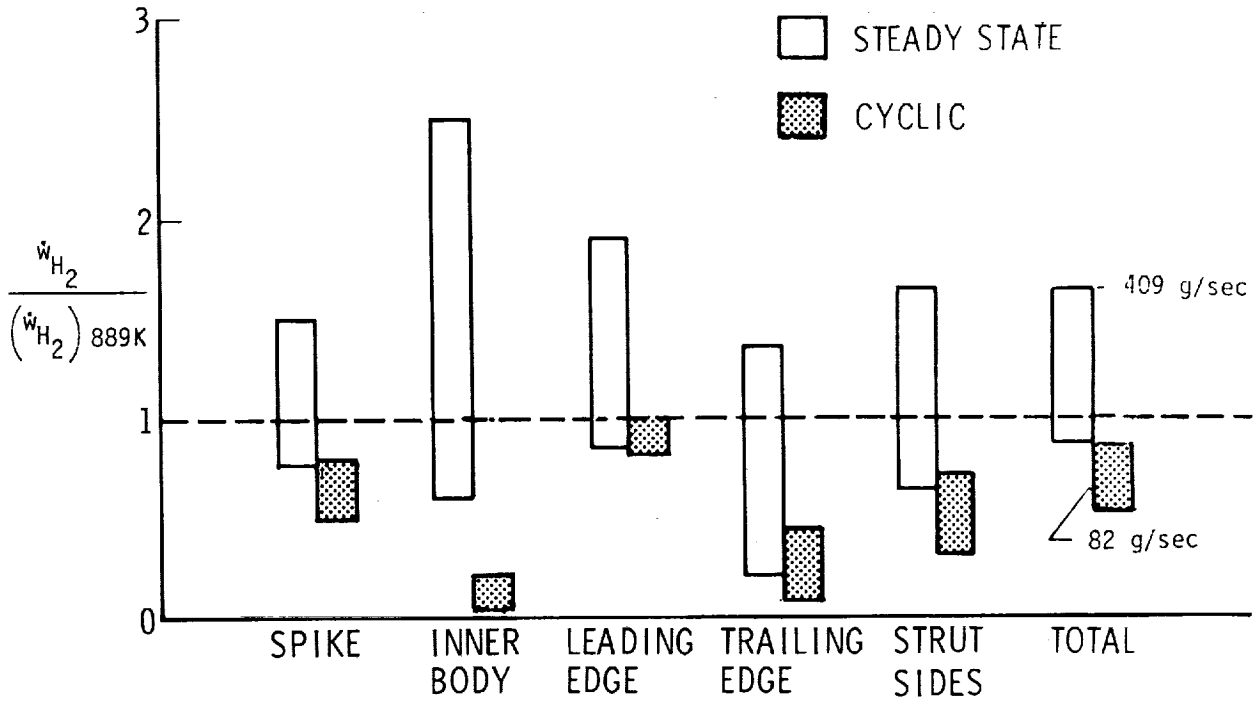

Figure 6.- SAM hydrogen flow rates.

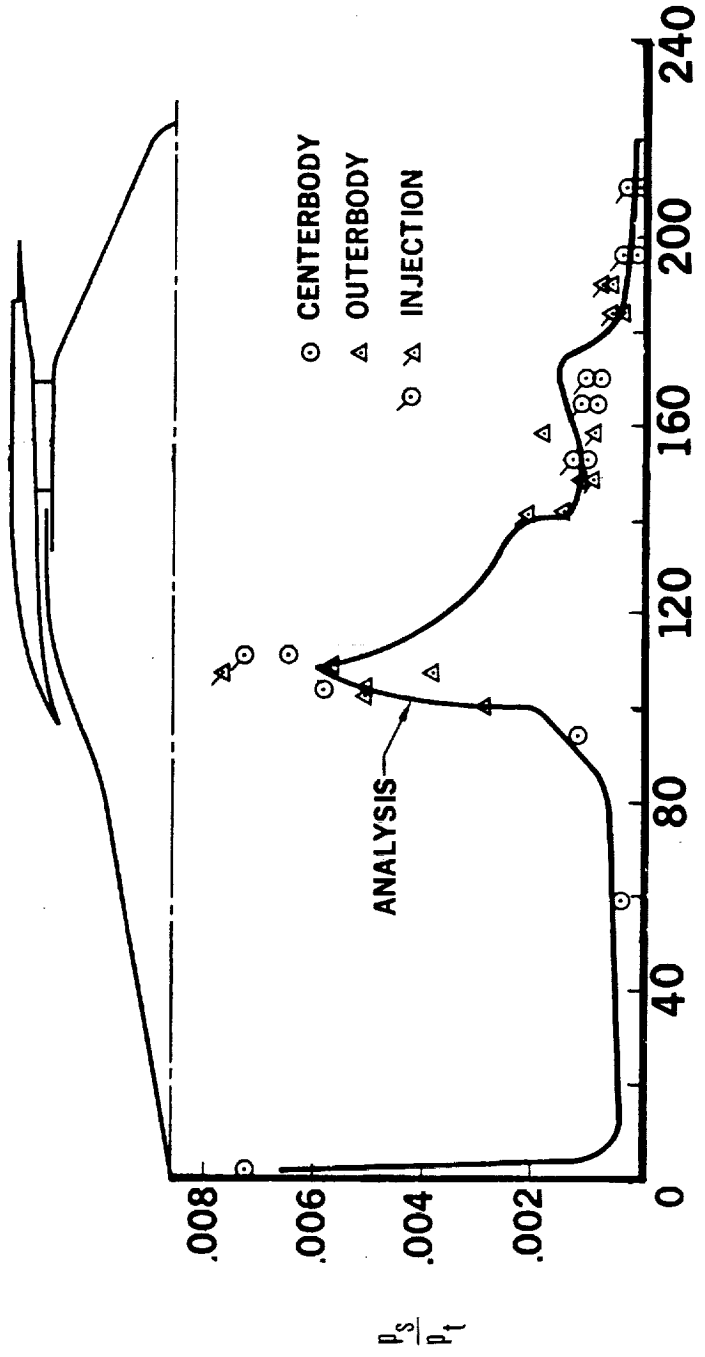

Figure 7.- HRE/SAM static-pressure distribution.

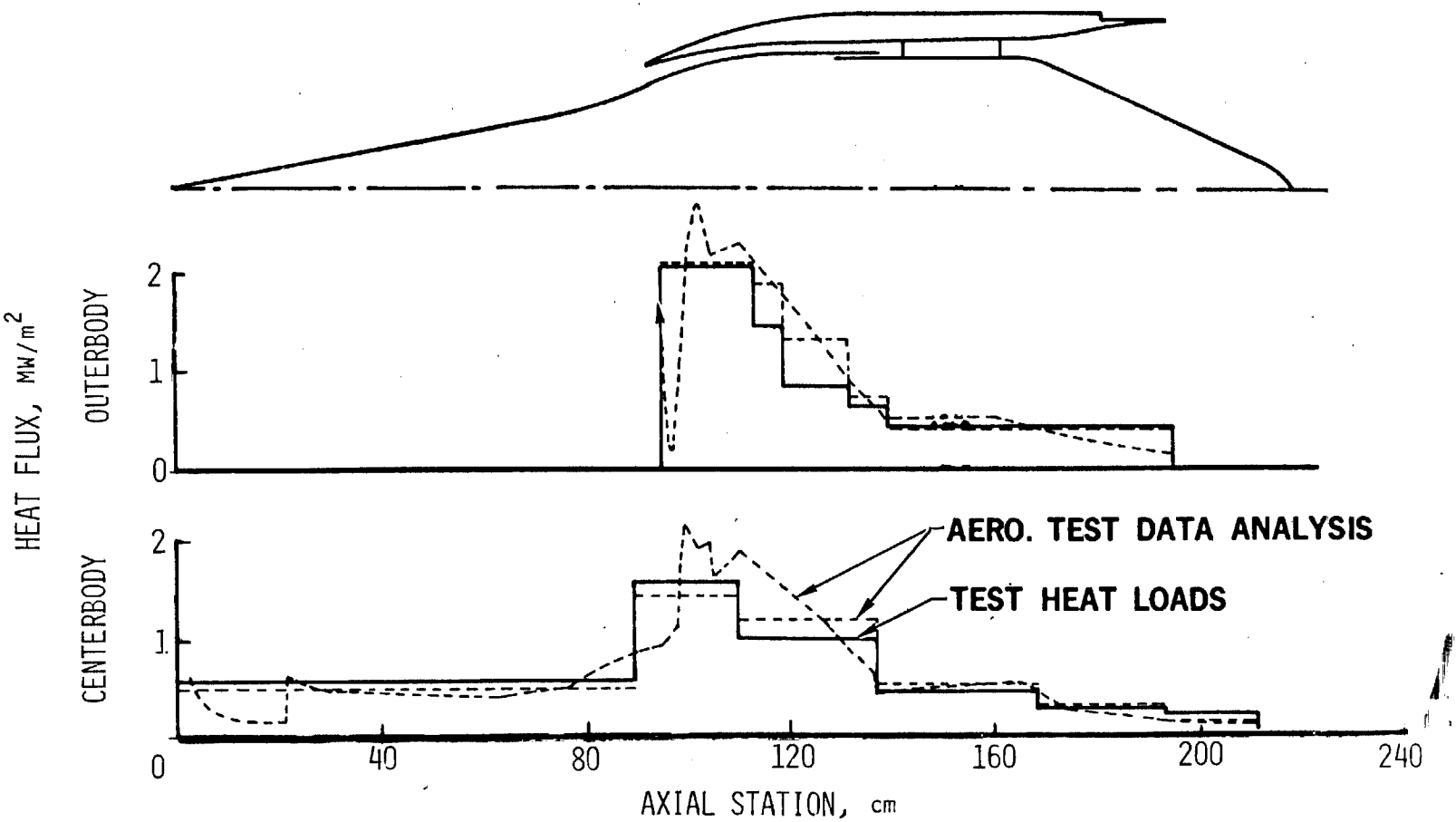

Figure 8.- HRE/SAM heat-flux distribution.

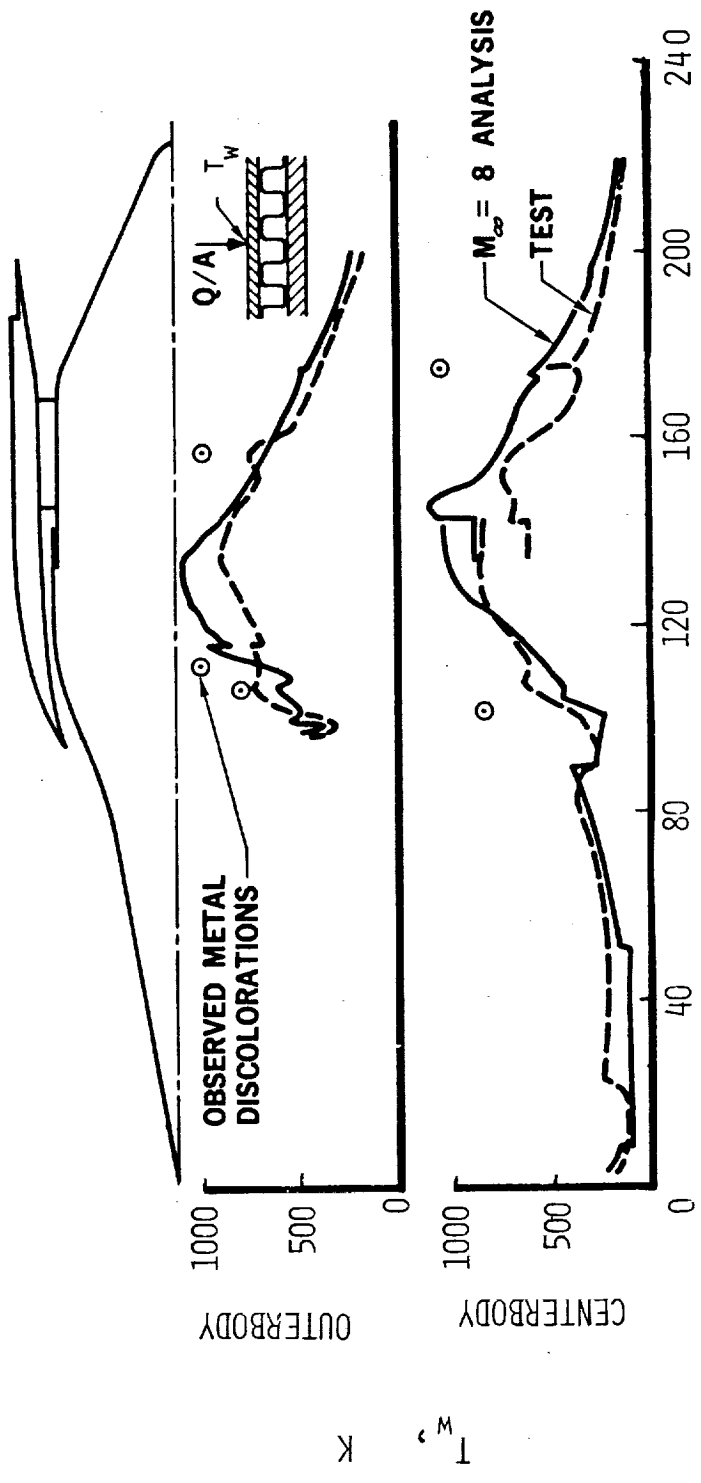

Figure 9.- HRE/SAM surface temperature distribution.

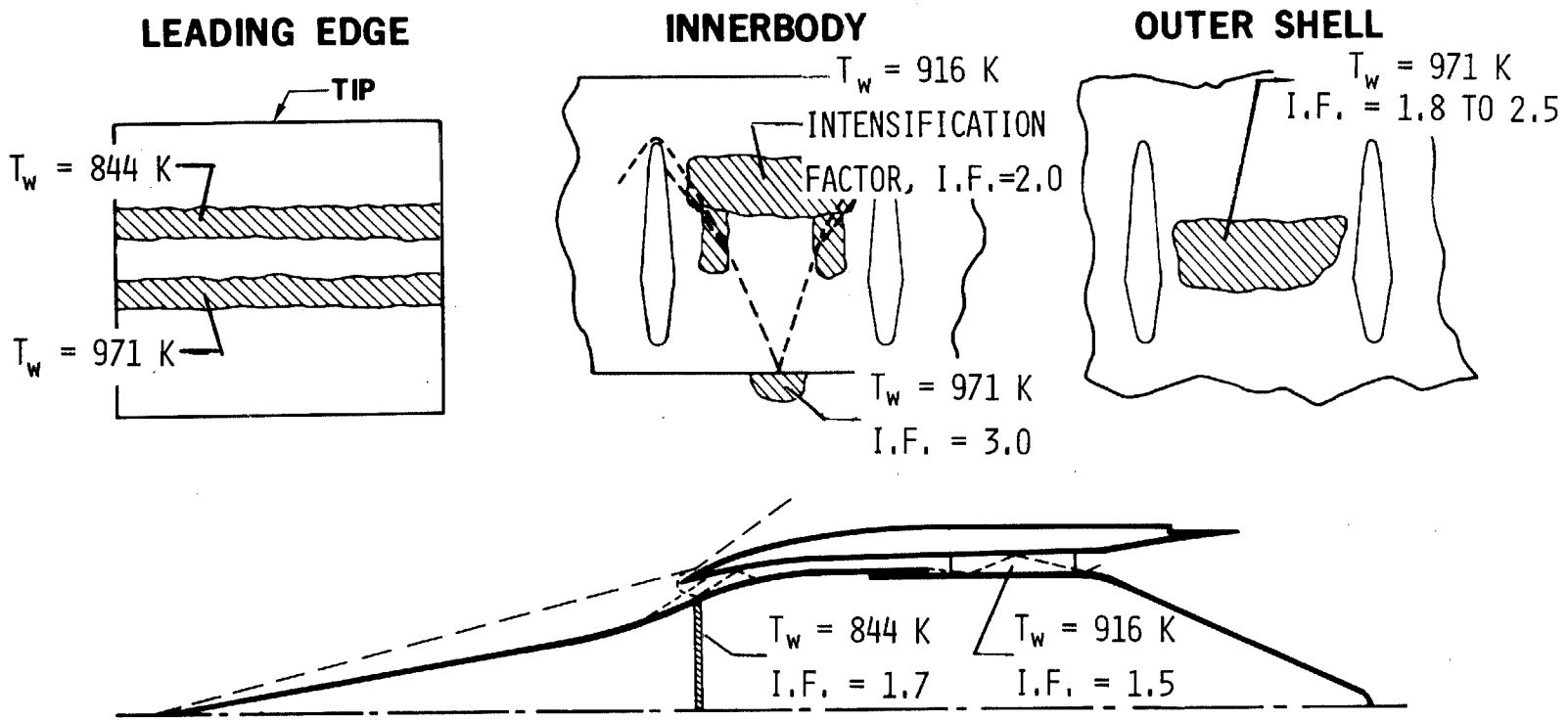

Figure 10.- Metal discoloration areas on internal surfaces.

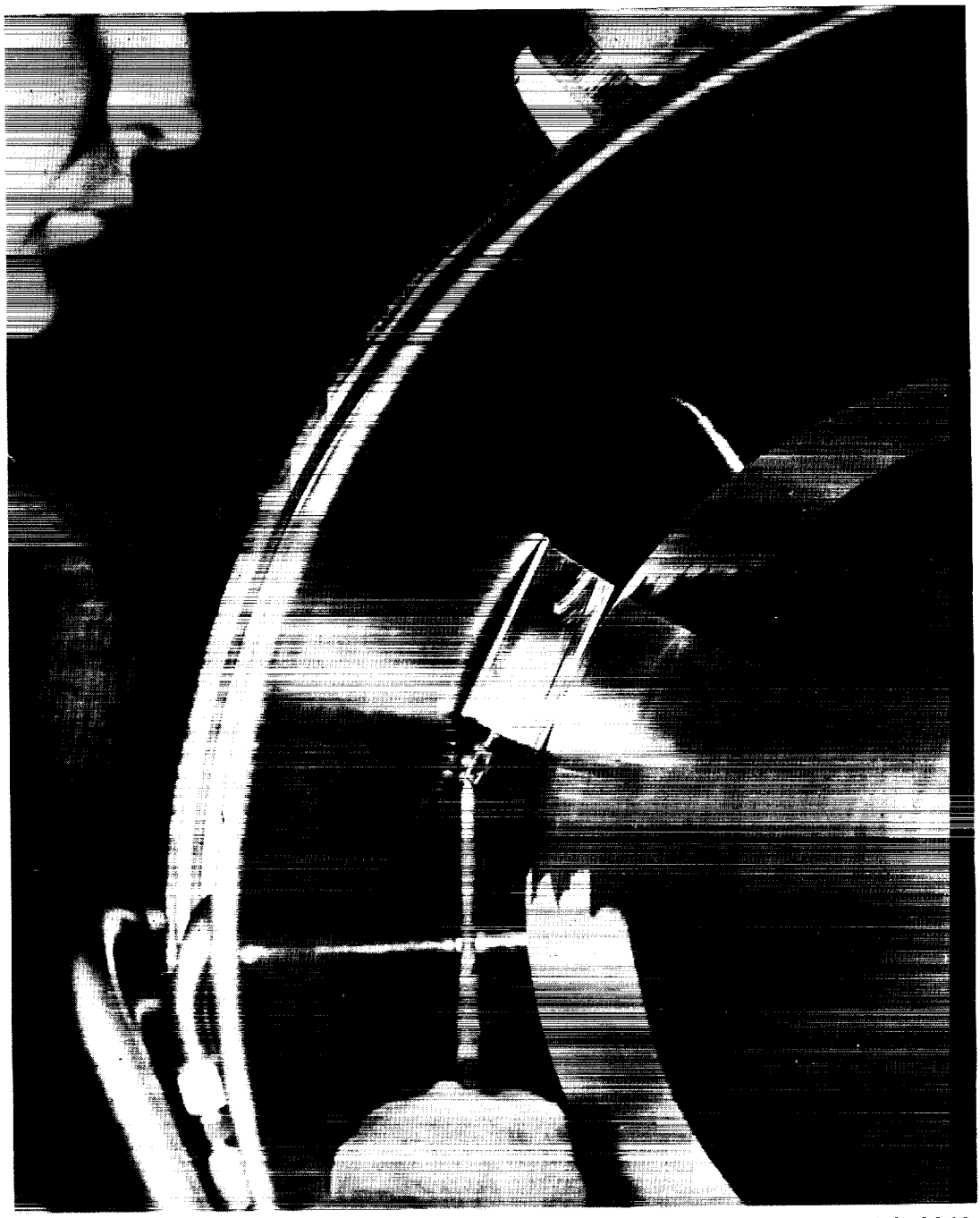

L-71-1842

Figure 11.- View of nozzle exit (top, port side) of HRE-SAM; mirror shows a discoloration because of heating in a region just downstream of the joint between the nozzle plug and the innerbody.

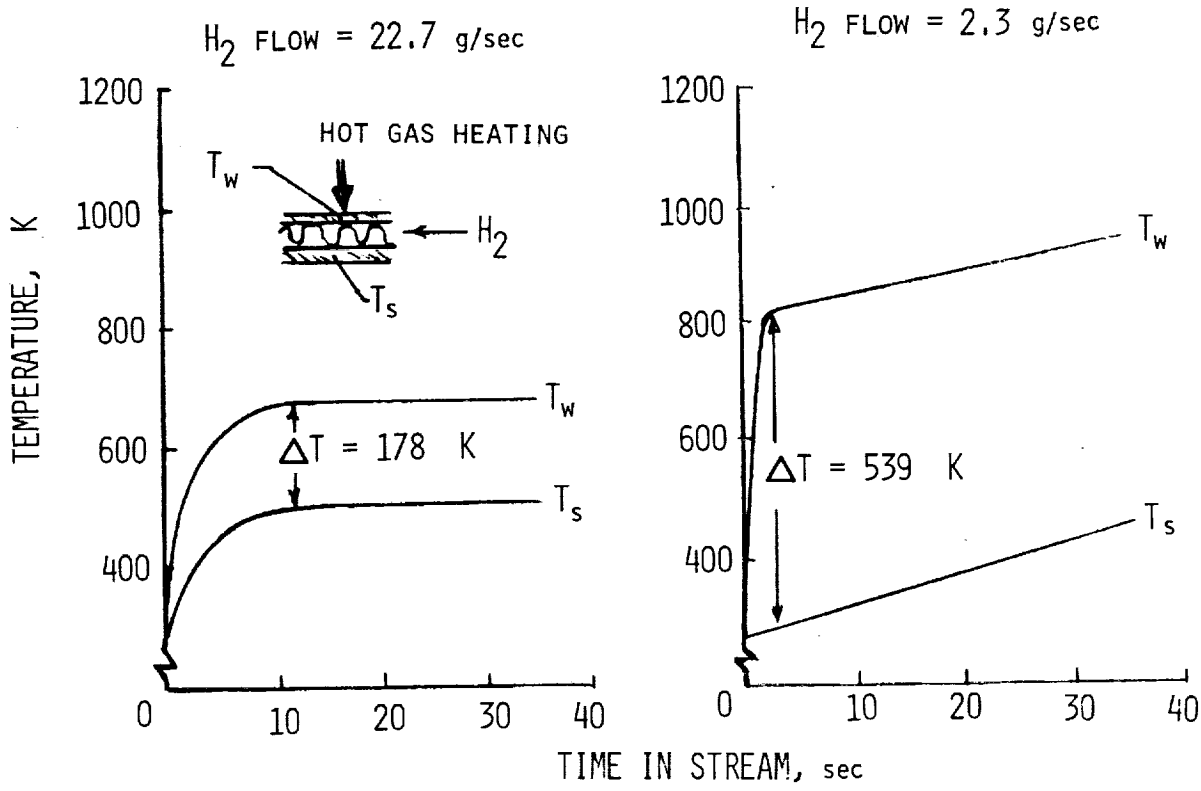

Figure 12.- Nozzle plate-fin transient temperature response. Station 178 cm.

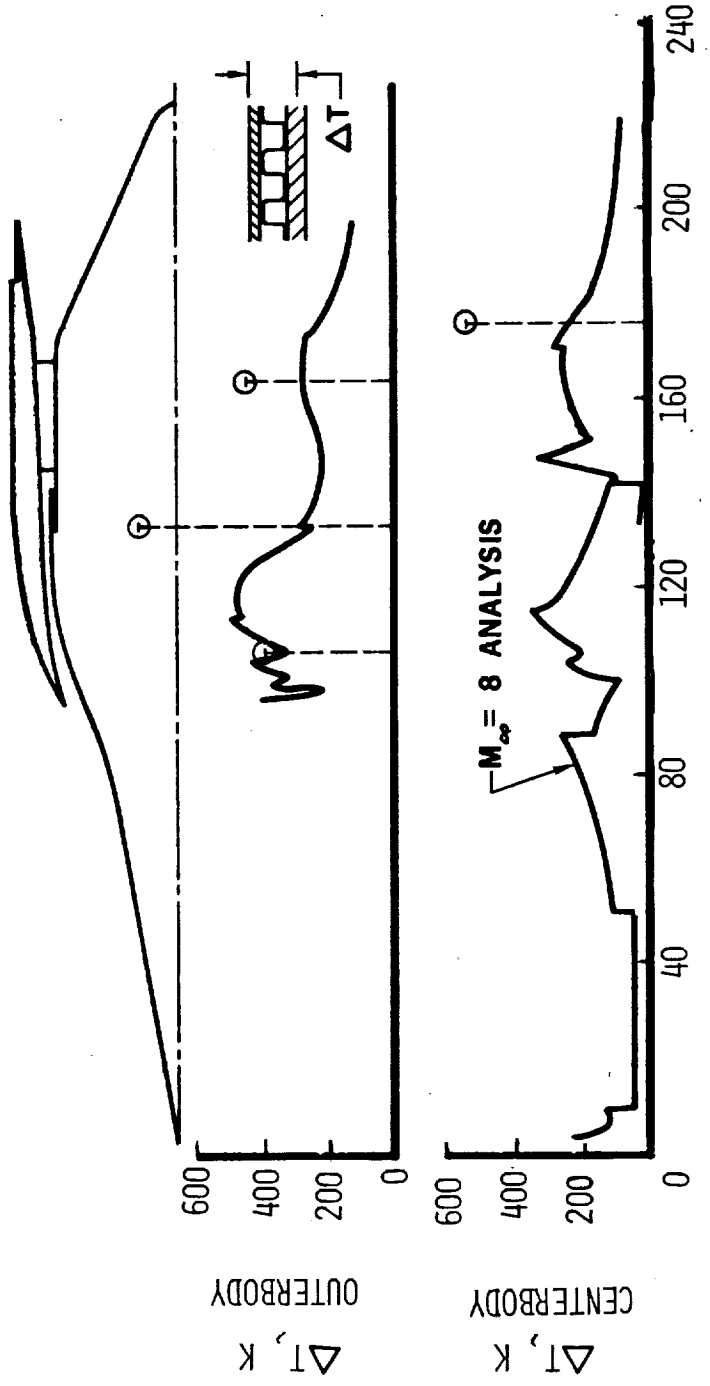

Figure 13.- HRE/SAM structural temperature differences as a function of axial station.

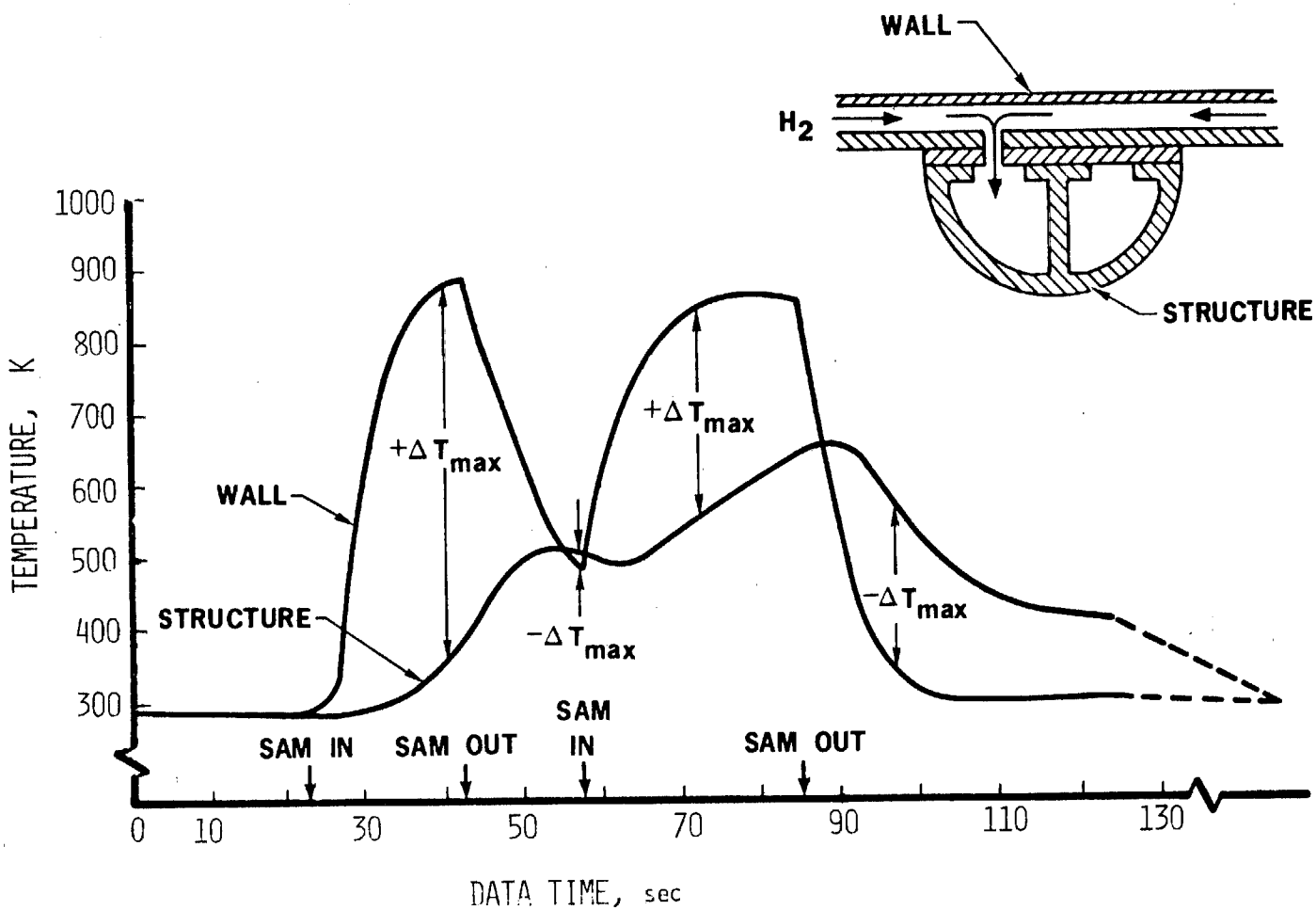

Figure 14.- HRE/SAM temperatures as a function of time for the hot surface and the cold structure at the outerbody outlet manifold.

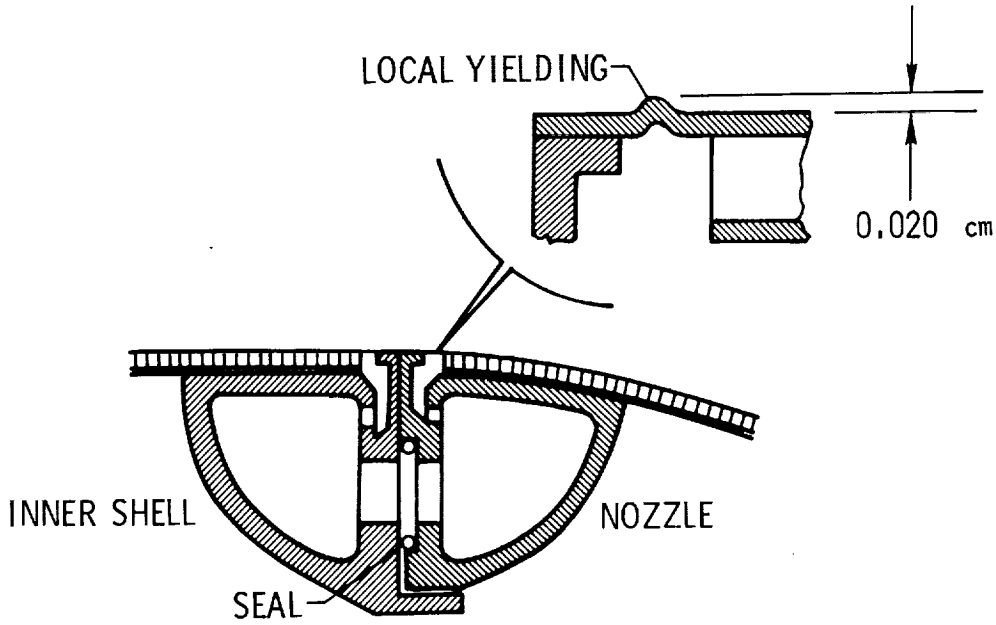

Figure 15.- Nozzle-innerbody joint.

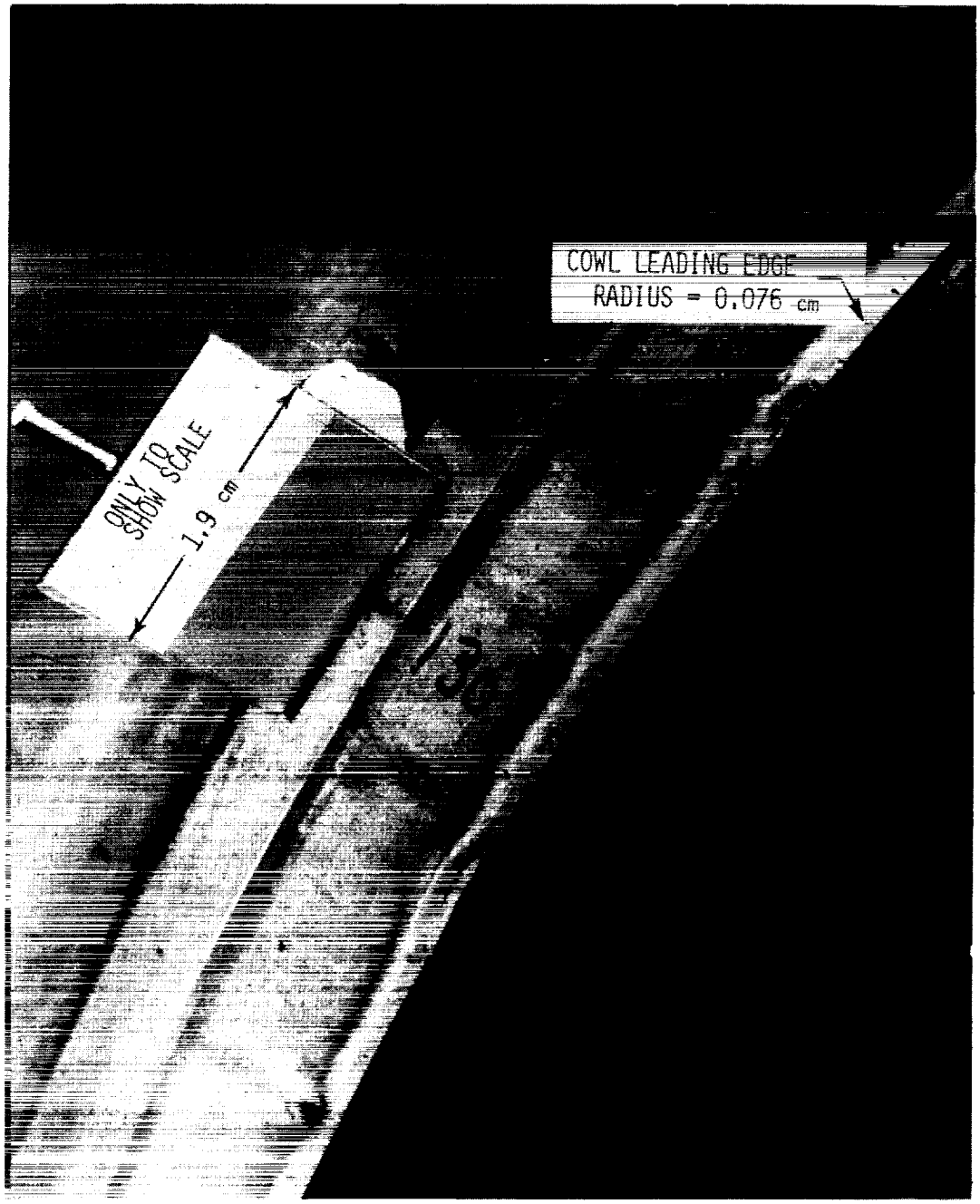

L-71-4199.1

Figure 16.- Closeup view (looking downstream) of cowl leading edge showing the effect of tunnel-stream foreign object impacts; area shown is near a radial station of 130° (top, starboard side).

NASA-Langley, 1972 — 28 L-8396